Mechanisms of Silver Nanoparticle Toxicity in Laboratory Suspensions and

Complex Environmental Media in *Caenorhabditis elegans*

by

Xinyu Yang

Environment
Duke University

Date:_____

Approved:

_____
Joel N. Meyer, Supervisor

_____
David E. Hinton

_____
Richard Di Giulio

_____
Heileen Hsu-Kim

_____
Mark Wiesner

Dissertation submitted in partial
fulfillment of the requirements for the degree
of Doctor of Philosophy in
Environment in the Graduate School
of Duke University

2014

ABSTRACT

Mechanisms of Silver Nanoparticle Toxicity in Laboratory Suspensions and Complex Environmental Media in *Caenorhabditis elegans*

by

Xinyu Yang

Environment
Duke University

Date:_____

Approved:

_____
Joel N. Meyer, Supervisor

_____
David E. Hinton

_____
Richard Di Giulio

_____
Heileen Hsu-Kim

_____
Mark Wiesner

An abstract of a dissertation submitted in partial
fulfillment of the requirements for the degree
of Doctor of Philosophy in
Environment in the Graduate School
Of Duke University
2012

Abstract

The rapidly increasing use of silver nanoparticles (Ag NPs) in consumer products and medical applications has raised ecological and human health concerns. Significant progress has been made in understanding the toxicity of silver nanoparticles (Ag NPs) under carefully controlled laboratory conditions. The goals of this dissertation were to investigate the mechanism of Ag NP toxicity under both laboratory conditions and environmental backgrounds, using *Caenorhabditis elegans* (*C. elegans*) as a model system. A key question for addressing these concerns is whether Ag NP toxicity is mechanistically unique to nanoparticulate silver or if it is a result of the release of silver ions. Ag NPs are produced in a large variety of monomer sizes and coatings, and since their physicochemical behavior depends on the media composition, it is important to understand how these variables modulate toxicity.

In order to test the hypothesis of a particle-specific effect, multiple techniques were used, including analytical chemistry, pharmacological rescue, and genetic analysis. Results suggested that dissolution was important for all tested Ag NPs and oxidative stress (a particle-specific effect) was important only for some Ag NPs, especially the citrate-coated Ag NPs (CIT-Ag NPs). The hypothesis of the particle-specific effect was further tested by investigating the cellular uptake and damage co-localization upon exposures to CIT-Ag NPs. I found that Ag NPs crossed all layers, including the pharynx,

gut, and also embryos through trans-generational transfer. Sites of damage were examined through transmission electron microscopy (TEM), and CIT-Ag NPs showed a more severe and deeper level of damage compared to ionic Ag. In addition, pharmacological inhibitors in parallel with genetic mutants (deficient in both endocytosis and lysosomal function) were used to explore the impact of those pathways on Ag NP uptake and associated toxicity. I found that endocytosis was important for CIT-Ag NP uptake and toxicity. Most intriguingly, one of the lysosomal deficient mutants was much more sensitive than wild type to reproductive inhibition after exposure to CIT-Ag NPs but not ionic Ag, constituting a clear nanoparticle-specific toxic effect.

These laboratory mechanistic studies, however, cannot be directly extrapolated to complicated environmental conditions, including variable amounts of natural organic matter (NOM), different temperatures and salinities, surface sulfidation, etc. My general hypothesis was that complex environmental medium would reduce Ag NP toxicity. In support of this, the environmental conditions present in mesocosms resulted in a loss of toxicity one week after dosing/spiking. In laboratory studies, I found that that increasing temperature and salinity tended to increase Ag NP toxicity, while sulfidation reduced Ag NP toxicity, acting as a "natural antidote." I studied two types of NOM, Suwannee River and Pony Lake fulvic acids (SRFA and PLFA respectively). PLFA rescued toxicity more effectively than SRFA. Therefore, CIT-Ag NP-NOM interactions were explored in

depth using PLFA. Using hyperspectral dark field microscopy, I was able to detect the formation of Ag NP-PLFA complexes and the limited tissue uptake of Ag NPs (with and without PLFA). Consistent with the reduced acute toxicity of Ag NPs by PLFA, I also found a rescue effect of PLFA on Ag NP-induced ultrastructural damage.

In conclusion, Ag NP toxicity resulted largely from dissolution and in some cases also from a particle-specific effect. However, Ag NP toxicity was strongly altered by environmental matrices. Continued in depth elucidation of Ag NP behavior, cellular uptake pathways and trafficking, and their interactions with other environmental factors will be invaluable in predicting, designing, and remediating the potential/existing environmental implications of silver-related nanotechnology.

Dedication

This work is dedicated to my family - my parents and husband Cesar whose love, support, friendship, and companionship have made every miracle happen.

Contents

List of Tables

List of Figures

Acknowledgements

I have been so grateful and blessed that my PhD experience has been accompanied by an amazing group of people whose support, guidance, patience, and encouragement have been invaluable to the success of my research and my personal development as a critical scientist.

First and foremost, I want to say thank you from the bottom of my heart to my great mentor, Dr. Joel Meyer, for all the guidance and support during the past five years. You gave me all sorts of training and practice as a future scientist. You never tried to restrain the way I formulated an idea and still valued it even when my ideas sounded ridiculous. I have always benefited from your wisdom, attitude, enthusiasm, kindness, patience, and the way you treat different people.

To my committee, Dr. Richard Di Guilio, Dr. David Hinton, Dr. Helen Hsu-Kim, and Dr. Mark Wiesner, thank you for all the guidance, suggestions, and challenges, which have made a huge contribution to the landscape and progression of my PhD research. Each of you has shaped a specific aspect of my research, and through collaborative work with you all, I have been provided the skills and power to investigate my research subject in various dimensions. Dr. Hsu-Kim, the collaboration with your research group has been a tremendous contribution to my dissertation project, and thank you for all the patience and guidance throughout! Dr. Hinton, I think a simple

"thank you" would not express my whole gratitude and appreciation of your guidance and kindness, and for going over manuscripts and research plans together with me! Last but not least, I will remember that concert evening with your family for my whole life!

I want to thank my dear former and current lab mates, who have indeed helped and encouraged me at all occasions, both in science and personal settings. Amanda Smith Bess, thank you for being such a sweet sister/friend/role model for me, you always give me great ideas and advices in my research and life, and the way you treated all sorts of issues and problems has truly shaped me as a person. Also I want to thank you for being such an advocate of my jokes, and I will not forget the tear responses after my "compressing fat story". Senyene Hunter, thank you for all the encouragement and support as a model of "rock science" in the lab; Maggie Gustafson, thank you for being such a wonderful lab manager and setting a really high bar for lab organizing and tidiness. The way you think and organize really influenced me a lot. Claudia Gonzales, thank you for all the joy, support, and encouragement you bring to my science and life, and you are such an angel!!! John Rooney, thank you for always being knowledgeable and nice, and all the great ideas coming from you! Tony Luz, thank you for being such a fun and smart person to be around, and I really enjoy all the happy times with you. Ian Ryde, thank you for being such a great support for all the work you have helped with in my dissertation research, which has been tremendous! Elena Turner, thank you for getting me started with the worm sorter and growth assay, and all the patience and

guidance during my PhD. Laura Macaulay, thank you for the mitosox work you have helped me do during your rotation in the lab and also your kindness and friendship during the past years; I also want to thank all the other lab members: Maxwell Leung, Alex Ji, Charu Anbalagan, Zhirui Zhu, and all the undergrads that have been directly or indirectly involved in my dissertation research; thank you so much for all the support and joy during our interactions.

I also want to thank all my collaborators outside the Nicholas School, Andreas Gondi, Chuangjia (CJ) Jiang, and Ross Taggart from Dr. Helen Hsu-Kim's lab, who have been tremendous and essential in my research projects. Dr. Helen Hsu-Kim, Andreas Gondi, and CJ Jiang have also contributed a lot to the development of research ideas and editing of manuscripts. The collaboration with Hsu-Kim lab has been amazing throughout my PhD years. Stella Marinakos, thank you for being so nice to me, and also all your hard work in synthesizing all the materials for the nanotechnology center. Raju Badireddy, thank you for being so supportive in helping me with the hyperspectral imaging and analysis, and your expertise was vital in my dissertation research. Kevin Kwok, thank you for all the great ideas that have inspired me during our discussions, which have made great contributions to the big picture of my dissertation.

I also want to say thank you to our collaborators in the Electron Microscopy Facility in NC State University, Dr. Michael Dykstra and Dr. Jeanette Shipley-Phillips, who have been super responsive, informative, and helpful during our collaborations.

Last but not least, I want to thank all the other collaborators, Ben Coleman and Adam Schindler from Duke Biology department, Joan Hudson, Steve Klaine from Clemson University, Jinhee Choi from University of Seoul, Jason Unrine, Olga Tsyusko from University of Kentucky, and Greg Lowry from Carnegie Mellon University.

I also want to thank Drew Day and Daniel Brown for a lot of help about my writing and editing in thesis and manuscripts, and Mariah Arnold, Audrey Bone, Simon Roberts, Mingliang (Thomas) Fang, Xiaoxing Cui, Chris Leonatti, and Nishad Jayasundara, who have given me an amazing time during my graduate school in the Toxicology Program.

I want to say thank you to all my great friends here in Duke, Cherrie Zhang (my great sister and best friend), Laifang Li (great roommate and best friend), Yang Yi (such a sweet sister), Manman Hu (we had so much fun time during the past 2 to 3 years that I will never forget), Hangjun Xu, Lihong Mo, Yifei Wang, Fangming (Kris) Ye, Kai Hu, Wenfeng (Winston) Gong, Jun Wang, Jiaoni Zhou, Yunfei Shen, Meng Li, Yun Jian, Jialu Sun, Jinxing Gan, Donghe Zhao, Wangzhi Zheng, Kai Peng, Shanshan Xiong, Daifang Wang, etc. I have indeed treasured all of your friendships (still a great number of names not listed) and thank you indeed for all of the great moments which make my life at Duke so meaningful.

I want to say special thanks to my family, my dear parents Gaoxiong Yang and Daoluan He, whose love, care, support, and everything else have shaped my personal

development and life. And also to my husband Chiehlun (Cesar) Yang, who entered my life in the last stage of my graduate school and has given me the faith of love and courage to carry on my dreams and all the adventurous endeavors in the near future. He has made me to believe in myself in all aspects.

Thank you all for the support, and I feel so blessed to have you in my education and life. I look forward to all the challenges and exciting explorations in my future.

1. Introduction

Nanotechnology has been increasing exponentially during the past decades (www.nanotechproject.org). As one of the most manufactured and fast-growing nanocompounds [1], silver nanoparticles (Ag NPs) have been extensively investigated for potential health effects on organisms and human populations [2-4].

1.1 Silver

Silver has been used since ancient times for multiple purposes including silverware, dental fillings, medicine, photography, jewelry, cosmetics, etc. [5, 6]. For medical purposes, it has been applied in combination with sulfadiazine as a topical antibacterial agent for the treatment of wounds [7, 8]. Due to the variety of silver uses, it has various routes of entry into the body, and ingestion has become the primary one, followed by dust/fume inhalation through occupational settings [4, 7]. Due to its high affinity to sulfhydryl groups, ionic silver (Ag^+) binds strongly to metallothionein, albumins, etc. and forms silver-protein complexes [6]. When Ag^+ is bound to other ions or proteins or deposited in tissue debris [9, 10], the bound ion is unavailable for antibiotic purposes but can lead to adverse health effects [11]. Chronic exposure to silver causes fatty degeneration of the liver and kidneys, alterations in blood cells [12], irritation in the respiratory and intestinal tract, and a permanent bluish-gray discoloration of the skin or eyes [8].

Silver is unusual in natural compartments; however, due to anthropogenic activities (smelting, manufacture, coal combustion, etc.), silver concentrations can be significantly increased [13].

1.2 Nanoparticles

Nanoparticles have been defined as structures with at least one dimension ranging from 1 to 100 nm [14, 15]. Due to the high surface area to volume ratio, quantum confinement, biomedical activities [16], etc., nano-sized particles can exhibit properties which substantially deviate from those of bulk forms [17]. The unique function of nanoparticles typically requires both the small (nano-) size of the particles and that they be present as well-dispersed particles without agglomeration [17]. Agglomeration is often prevented by various types of surface functionalizations (e.g., polymers) based on electrostatic or steric theories [18, 19]. Nanotechnology has been applied to medicine [20], cosmetics [21, 22], electronics [23], environmental engineering [24], energy [25], the food industry [26], etc. In the field of nanomedicine, efforts have been made in tailoring nanoparticle surfaces to be optimally commensurate with cellular and biomolecular systems [27]. The nano-sized particles can potentially cross the biological barriers, e.g., blood brain barrier, which opens new routes of drug delivery into the brain [28]. However, those particles can interact with sub-cellular structures and cause toxicities [29-31].

1.3 Silver Nanoparticles

1.3.1 Applications of silver nanoparticles

Silver nanoparticles (Ag NPs) have been used as antimicrobial agents, usually in the form of polymer nanocomposites [19], and their effectiveness is due to the release of germicidal silver ions [32]. This bactericidal effect of Ag NPs has resulted in their global application in various consumer products, e.g., deodorants, toys, humidifiers, filters and also the food and feed industry (packaging materials and nursing bottles), etc. [33, 34]. Due to the importance of emerging and re-emerging infectious diseases, e.g., influenza (A/H5N1), cholera, etc., advanced antimicrobial nanomaterials have been suggested to prevent those outbreaks [16, 35]. The broad range of targets within the virus makes metal nanoparticles a novel substitute for traditional antiviral drugs [35]. Due to the significantly lower skin absorption and internal organ deposition and their relatively lower toxicity compared to silver sulfadiazine, Ag NPs have become highly used as a topical antibiotic in burn patients [36]. Additionally, Ag NPs have been applied widely in solar cells [37], clinical medicine [16], cosmetics [38], nano-scale sensors [39], etc.

1.3.2 Physicochemical characteristics of silver nanoparticles

Ag NP size has been controlled through multiple factors during the synthesis procedure, e.g., handling of the Ar and Hg gas flow, length of the aggregation zone, and the magnetron power [40]. Ag NPs have various shapes, e.g., nanoparticles, nanowires, nanoplates, nanocoatings, nanofilms, etc. [4]. Ag nanoplates and nanowires were more

toxic and eliminated less readily in comparison with spherical Ag NPs [41, 42]. Surface functionalizations were used to achieve the required stability, and the particle colloidal stability can change when suspended in other aquatic conditions [43]. Functionalized Ag NPs can be further dispersed into polymer matrices, resulting in the formation of polymer/Ag nanocomposite films with significantly higher stability [44].

The surface charge of Ag NPs has been controlled during the synthesis process to achieve specific application purposes [45], e.g., surface-enhanced Raman scattering [46], contaminant remediation [47], etc. The dissolution rate of Ag NPs, a major driver of Ag NP toxicity, was correlated with both the characteristics of Ag NPs [48] and the surrounding environmental factors [49]. These physicochemical properties of Ag NPs can affect their interactions with organisms and the environment [42, 50-52]. Crystal defects contributed to Ag NP toxicity, in addition to toxic effects resulting from Ag ions dissolving from nanoparticles [41].

1.3.3 Fate and transport of silver nanoparticles

In order to characterize the fate and transport of Ag NPs in the environment, it is essential to understand their use, potential pathways, and sinks (Fig. 1). Surface functionalizations of Ag NPs and environmental factors (pH, salinity, hardness, and dissolved organic matter) can affect Ag NP aggregation and dissolution [53-55], which further alter their fate and transport in the environment. Nanosilver products, including disinfectants, clothing, toothpaste, etc., are disposed into wastewater treatment plants or

directly into landfills with Ag NPs reaching sewage sludge, natural water, atmosphere, etc. Those particles may potentially enter agriculture soil/crops, sediment, oceans, etc. [56]. Transformations of Ag NPs have been investigated within wastewater treatment plants to better predict their potential risks to the environment. Those studies indicated that most of the Ag NPs were in the form of Ag_2S [57], and sulfidation was shown to be an important natural detoxification process of Ag NPs [58].

To date, most fate studies focused on the chemical and compositional alterations of Ag NPs in laboratory-simulated conditions [59-61], and transport models used in further predicting their fate in a riverine environment. This dissertation will examine the effect of various environmental factors on Ag NP physicochemical characteristics and subsequent toxicity, with the effect of natural organic matter (NOM) explored in more depth.

1.3.4 Environmental implications and concerns

The accelerating incorporation of Ag NPs into commercial products has increased their likelihood of release into the environment [62], and uncertainty remains in evaluating the positive and negative impacts of Ag NPs [63, 64]. Silver nanoparticles were shown to come off from the fabrics in which they are embedded during the wash cycle [65]. Most of the nanotoxicity is associated with the "nano-scale" [3], although synthesis of silver nanoparticles can also incorporate toxic metals or other substances adsorbed onto them [66]. Smaller Ag NPs (20 nm in diameter) penetrated pear skin and

pulp after pears were exposed to Ag NP suspensions for 96 hrs while larger nanoparticles (70 nm) did not [67], raising great concern regarding the safety of smaller Ag NPs in food. The environmental toxicology of Ag NPs was intensively studied in aquatic ecosystems [68-71] and relatively less studied in the atmosphere [72, 73]. Environmental transformations of Ag NPs, e.g., sulfidation, aggregation, oxidative dissolution, etc., were essential in predicting the fate, transport and risk of Ag NPs in the environment [58, 74]. Predicted environmental concentrations of Ag NPs have been generated, which were shown to have a significant potential risk to environmental organisms [68]. Mechanistic toxicological studies have been conducted to improve the current understanding and prediction of the environment implications of Ag NPs [51, 75, 76].

1.4 Caenorhabditis elegans (C. elegans)

1.4.1 General biology and advantages as a model organism

C. elegans, a free-living nematode distributed globally in nutrient and bacteria-rich decaying materials [77], was first established as a model organism by Sydney Brenner in 1974 and became extensively studied in fields of cell signaling [78], molecular biology [79], apoptosis [80], neurobiology [81], etc. There are several major features of this species that makes it a powerful model organism. *C. elegans* is grown on agar plates or in liquid culture with *Escherichia coli* as its food source [82, 83]; therefore, the maintenance become easier and cheaper compared to other species, e.g., rats, fish, etc. *C.*

elegans has short, hermaphroditic lifecycle and each adult nematode can have approximately 300 offspring, which makes medium to high-throughput studies more feasible [84]. With the whole genome sequenced [85] and 60-80% of the genes homologous to human genome [86], *C. elegans* has the potential to reveal the molecular mechanisms of stress responses and complicated human genetic disorders [87, 88].

1.4.2 Model organism for nanoparticle uptake and mechanism of toxicity

The uptake of nanoparticles has been examined both *in vitro* [89, 90] and *in vivo* [91], with the mechanism of uptake investigated using multiple approaches: molecular genetics, confocal/fluorescent microscopy, spectroelectrochemistry [92, 93], etc. The transparency of *C. elegans* allows direct examination of *in vivo* nanoparticle uptake using fluorescent or high-spectra dark field microscope [94, 95]. The availability of mutant strains makes it possible to explore the molecular mechanisms of nanoparticle uptake and associated toxicity [51, 94]. Table 1 summarizes the advantages and limitations of *C. elegans* in nanotoxicological studies in comparison with other model organisms.

1.5 Dissertation Objectives and Outline

The primary goals of this dissertation are to identify the mechanisms of silver nanoparticle toxicity in both laboratory conditions and complicated environmental matrices using multiple techniques, including collaborative works (analytical chemistry work) with researchers in the Center of Environmental Implications of Nanotechnology

(CEINT) and the Electron Microscope facility at NC State and Clemson University with details described in the following chapters.

This dissertation is divided into the following five research chapters which address the mechanisms of silver nanoparticle toxicity:

Chapter 1: Introduction

Chapter 2: Investigating the mechanisms of silver nanoparticle toxicity using multidisciplinary techniques in *Caenorhabditis elegans* (published in Environmental Science and Technology, Yang et al., 2012)

A key question for addressing the concerns raised by increasing silver nanotechnology is whether Ag NP toxicity is mechanistically unique to nanoparticulate silver, or if it is a result of the release of silver ions. Furthermore, since Ag NPs are produced in a large variety of monomer sizes and coatings and since their physicochemical behavior depends on the media composition, it is important to understand how these variables modulate toxicity. I found a linear correlation between Ag NP toxicity and dissolved silver, but no correlation between size and toxicity, suggesting that the toxicity of most Ag NPs resulted from dissolution. I also found evidence that some Ag NPs (typically less soluble due to size or coating) acted via oxidative stress, an effect specific to nanoparticulate silver. However, in no case studied here was the toxicity of a Ag NP greater than would be predicted by complete dissolution of the same mass of silver as silver ions.

Chapter 3: *In vivo* study of the role of endocytosis and lysosomal function in silver nanoparticle uptake and toxicity in *Caenorhabditis elegans*

This aim of this chapter was to study the roles of endocytosis and lysosomal function in the uptake and subsequent toxicity of silver nanoparticles (Ag NPs). Both pharmacological and genetic tools were used to understand how endocytosis and lysosomal function correlates to subsequent Ag NP toxicity. I found that the clathrin-mediated endocytosis inhibitor chlorpromazine reduced the toxicity of CIT-Ag NPs, but not $AgNO_3$. One of the endocytosis-deficient mutants (*rme-6*) took up less silver and was resistant to the acute toxicity of CIT-Ag NPs as compared to N2, and none of those mutants showed altered sensitivity to $AgNO_3$. Interestingly, the lysosomal mutants were more sensitive to the growth-inhibiting effects of CIT-Ag NPs and were in fact more sensitive to CIT-Ag NP-mediated inhibition of reproduction. Most intriguingly, the *glo-1* mutants were much more sensitive than wild type to inhibition of reproduction after exposure to CIT-Ag NPs but not $AgNO_3$, constituting a clear nanoparticle-specific toxic effect. Microscopic examination of the reproduction-impaired *glo-1* mutants revealed a phenotype of bagging (retention of developing eggs in the adult), resulting from both insufficient yolk in the embryo and blockage of embryo transport to the vulval opening by excess yolk accumulation. This severe phenotype in lysosomal deficient mutants has demonstrated gene-environment interactions that can potentially affect specific human populations with deficiencies in lysosomal pathways.

Chapter 4: Silver nanoparticle behavior, uptake, and toxicity in *Caenorhabditis elegans*: Effects of natural organic matter, temperature, sulfidation, and mesocosm conditions (Published in Environmental Science and Technology, Yang et al., 2014)

Natural organic matter (NOM) is omnipresent in complex environmental systems where it may alter the behavior of nanoparticles in these systems. This chapter describes multiple techniques in addressing the mechanisms of NOM effect on Ag NP toxicity. I found that the majority of the CIT-Ag NP uptake was limited to the digestive tract. Limited tissue uptake was detected by hyperspectral microscopy, but not by transmission electron microscopy. Co-exposure to PLFA rescued $AgNO_3$ and CIT-Ag NP-induced cellular damage, and also resulted in formation of NOM-Ag NP composites (both in medium and nematodes). Toxicity of Ag NPs was also affected by temperature, with increasing toxicity at a higher temperature for Ag NPs but not $AgNO_3$.

Chapter 5: Conclusion

To conclude, the results of this dissertation, their broader implications and future directions are described in Chapter 5.

Appendices

The appendices describe experiments I have done during my PhD aside from the main chapters: Appendix A - the quantification of production of the superoxide anion using mitosox (aims to provide parallel biomarker evidence of oxidative stress resulting from particle effects), Appendix B - DNA damage using Q-PCR (aims to explore the

genotoxicity of Ag NPs or oxidative damage to DNA as parallel biomarkers), and Appendix C - the role of ER stress-related genes in silver toxicity (aims to investigate whether deficiency in the immune system of *C. elegans* modulate Ag NP toxicity or if Ag NP toxicity is related to the immune oxidative burst).

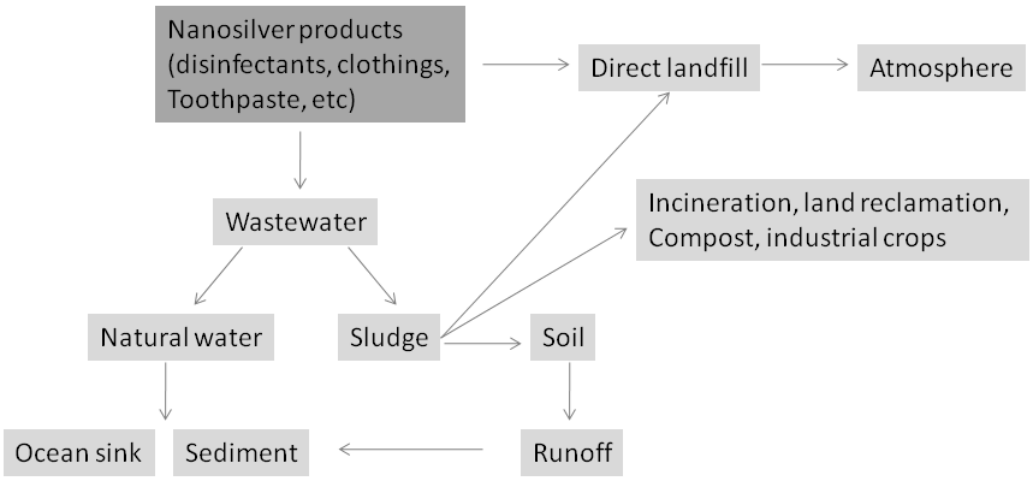

adapted from Whiteley et al., 2013 [56].

Figure 1: Life cycle and possible fate and transport pathway analysis of silver nanoparticles in the environment.

Table 1: Advantages and limitations of *Caenorhabditis elegans* as a model system in nanotoxicological studies.

***C. elegans* features**	**Advantages of *C. elegans* in nanotoxicological studies**	**Limitations of *C. elegans* in nanotoxicological studies**	**If limitations, any compensatory method suggested?**
Short generation time, ease of culturing, small size, large brood sizes	Permits medium- to high-throughput laboratory experiments and long-term studies (2+ generations)	May be a poor model for chronic toxicities that require a long life (e.g., cancer)	
Fully sequenced genome and large variety of mutant strains	Improved analysis of molecular mechanisms of NP toxicity [96]		
Conventional culture medium (K medium or M9 buffer) contains high levels of chloride [97]		Interferes with NP physicochemical behavior and results in increased agglomeration or precipitation; meanwhile the culture medium cannot represent the complicated environmental conditions	Use a new medium with low ionic strength and chloride concentration
Body transparency	Microscopic detection of NP uptake and distribution [94]		
Genetic similarity to higher eukaryotes (e.g., humans)	Potentially provide guidance for human studies if nematodes with a specific genetic background are more susceptible to NPs		

Whole organism examination	This model provides a simple but efficient and physiologically relevant platform for systematic investigation in growth, reproduction, etc. [98], bridging the gap between *in vitro* and *in vivo* studies [99]	Simplified model for extrapolating to more complicated biological system	
Well-studied cell and developmental biology	Allowing analysis at single cell level	The small size of *C. elegans* makes it more difficult to target specific organ systems during sample fixation and sectioning, compared to rodents and other vertebrates	Include a larger number of nematode during sample fixation processes to get a better representation of different body systems
Availability of green fluorescence protein tagging and transfections [100]	Makes it possible to examine fluorescent NPs' behavior and fate in living organisms using optical microscopy		
Feeding behavior of *C. elegans*- Pharyngeal pumping	To model an important exposure route of NPs- dietary ingestion		

2. Investigating the mechanisms of silver nanoparticle toxicity using multidisciplinary techniques in *Caenorhabditis elegans*

2.1 Introduction

The increased use of silver nanoparticles (Ag NPs) as antimicrobial agents in commercial and medical products has led to elevated human and environmental exposures [5, 101, 102]. In addition to being bactericidal [103-106], Ag NPs are toxic to other taxa. Documented effects include developmental deformities in zebrafish [107-109], altered stress-related gene expression in Japanese medaka [110], respiratory stress in Eurasian perch [111], mitochondrial toxicity in human cells [112], inflammatory responses in rats [113], neurotoxicity in mice [114], and decreased growth and reproductive capacity in *Caenorhabditis elegans* [115, 116].

2.1.1 General mechanisms of Silver Nanoparticle toxicity

Despite many recent publications on Ag NP toxicity, the mechanism of Ag NP toxicity remains unclear [63]. Understanding this mechanism is critical for risk assessment; if Ag NP toxicity is driven by release of dissolved silver, our current knowledge relating dissolved silver speciation and toxicity may be highly informative for risk assessment. If on the other hand Ag NPs have unique toxicities deriving from their nanoparticulate form, additional studies will be required. Release of metal ion from nanoparticle dissolution is an important mechanism for toxicity of some NPs [117], and recent work has suggested that oxidative dissolution rates of Ag NPs may be quite high

under some circumstances [118]. Several studies suggest that the mechanism of Ag NP toxicity is largely explained by Ag ions (Ag^+). For example, no toxicity was observed when Ag^+ was complexed by a thiol ligand [107, 119-123], and dietary exposure to Ag NPs resulted in similar toxicity to Ag^+ [124]. Using genetic analysis, I also found evidence that Ag NP toxicity was mediated by ionic silver release [116]. However, other studies suggest that ion release does not explain all toxicity, and some support a role for generation of reactive oxygen species (ROS), which might occur at the surface of Ag NPs [125-129] but is not expected to result from silver ion dissolution alone. One study reported that cysteine, a strong Ag^+ ligand, only partially rescued Ag NP toxicity [130], while another found that Ag NP cytotoxicity was independent of Ag^+ concentration and resulted primarily from oxidative stress [127, 131]. It has also been found that Ag+ can form Ag NPs *in vivo* [124], which added more uncertainties in distinguishing between the ionic and NP effect. Thus, the reported mechanism of Ag NP toxicity has been variable depending on the Ag NP and system in question and needs further elucidation, preferably using multiple different Ag NPs that might have different mechanisms of action, but all measured in the same system.

2.1.2 Physicochemical characteristics of Ag NPs in suspensions

Ag NPs have a high tendency to aggregate, and are typically synthesized with surface coatings to stabilize them in suspension [132, 133]. Both aggregation and surface coatings can alter Ag NP toxicity [134]. For example, biogenic Ag NPs (coated with

protein) were more toxic than chemically synthesized Ag NPs, and citrate-coated Ag NPs were more toxic than PVP-coated Ag NPs [135]. However, more information on the impact of surface coatings on the mechanisms of Ag NP toxicity is needed, especially in conjunction with characterization of the physicochemical state of the particles at the time of exposure, which is critical but relatively rarely done [118, 136-139].

2.1.3 Study goals

The goal of this study, therefore, was to investigate the factors determining Ag NP toxicity in the model organism *C. elegans*. I compared the toxicity of several sizes of Ag NPs (from 5 to 75 nm mean diameter) coated in different ways and suspended in two different culture media chosen on the basis of differing ionic strengths. I used pharmacological rescue (trolox and N-acetylcysteine), genetic knockouts (analysis of metal- sensitive and oxidative stress-sensitive mutants), and physicochemical characterization (analysis of aggregation, surface charge, crystalline structure, and dissolution of Ag NPs) to test for the importance of dissolved silver vs Ag NP-mediated oxidative stress. The use of differentially coated Ag NPs of similar size permitted insight into the role of coating.

2.1.1 Use multiple tools to address the mechanism of Silver Nanoparticle toxicity

2.1.1.1 Analytical chemistry tools

Measurement of dissolution from each type of Ag NPs was used to directly correlate dissolution with toxicity. Meanwhile other physicochemical characteristics of

Ag NPs were analyzed, including surface charge, NP monomer size, and hydrodynamic diameter, etc.

2.1.1.2 Genetic tools

Both oxidative stress- and metal- sensitive mutant *C. elegans* were used to see if they showed increased sensitivity to Ag NPs. For example, increased sensitivity of the metal-sensitive mutant indicated that ion dissolution was important in Ag NP toxicity.

2.1.1.3 Pharmacological tools

To explore whether the major driver of Ag NP toxicity was dissolution or reactive oxygen species (ROS) generation, we used two types of chemicals, trolox (water soluble version of Vitamin E) and N-acetyl-cysteine (NAC). We used trolox as a ROS scavenger and NAC as both a ROS scavenger and an ion chelator. The ion effect on Ag NP toxicity can be revealed by comparing the pharmacological rescue from both chemicals.

2.2 Materials and Methods

2.2.1 *C. elegans* strains and culture

C. elegans were cultured in petri dishes on K-agar seeded with OP50 strain Escherichia coli [140] to prepare nematodes for liquid medium exposure, which was carried out in 96 well plates as previously described [116] except as detailed below. In addition to wild-type, mutant strains were chosen based on their known sensitivity to certain mechanisms of toxicity. Strains N2 (wild-type Bristol), VC433 (*sod-3* deletion),

TM1748 (*pcs-1* deletion, outcrossed 6 times), and TK22 (*mev-1*, mutation uncertain, outcrossed 5 times) were obtained from the Caenorhabditis Genetics Center (CGC; Minneapolis, MN, USA). Strain JF23 (*mtl-2* deletion, outcrossed 4 times from the VC128 strain) was a generous gift from J. Freedman and W. Boyd (NIEHS).

2.2.2 Ag NP synthesis and characterization in stock solution

I used 5 types of previously-characterized Ag NPs: citrate-coated Ag NPs (herein referred to as "CIT-Ag NPs", where the subscript indicates monomer diameter in nanometers) [116], small and large polyvinylpyrrolidone (PVP) -coated Ag NPs ("PVP_S-Ag NPs" and "PVP_L-Ag NPs") acquired from NanoAmor [116], and gum arabic (GA)-coated Ag NPs ("GA_5-Ag NPs", "GA_{22}- Ag NPs") [141]. Also two additional PVP-coated particles ("PVP_8-Ag NPs", and "PVP_{38}-Ag NPs") were manufactured. Silver nitrate and sodium borohydride were purchased from Sigma-Aldrich. PVP with molecular weights (MW) 10,000 and 55,000, and ethylene glycol were acquired from Fisher Scientific. Ultrapure water (Barnstead Nanopure Diamond) was used in all syntheses. To synthesize the PVP-coated 8 nm Ag NPs (PVP_8-Ag NPs), 1.5 g of PVP (MW 10,000) was dissolved in 280 mL of water in an Erlenmeyer flask. 9 mL of 0.1 M silver nitrate was added, and the solution was stirred for 5 min before adding 11 mL of ice-cold sodium borohydride (0.08 M) all at once. The PVP-stabilized silver nanoparticles were centrifuged for 3 h at 112,000x g (Beckman Optima L-100XP equipped with a Type 45 Ti rotor). The precipitate, containing the 8 nm Ag nanoparticles, was resuspended in

water. There was no detectable effect of the molecular weight of PVP on toxicity when comparing 8 nm PVP-coated Ag NPs with either 10K or 55K PVP (data not shown).

To synthesize the PVP-coated 38 nm Ag NPs (PVP_{38}-Ag NPs), 20 g of PVP (MW 55,000) was dissolved in 50 mL of ethylene glycol. The solution was transferred to a round-bottom flask equipped with a condenser, 1.5 g of silver nitrate was added, and the mixture was stirred at room temperature. Once silver nitrate was dissolved, the solution was heated in an oil bath to 120°C for 24 h. The PVP-stabilized silver nanoparticles were then removed from heat, diluted 1:10 with water, and purified by dialysis (Optiflux F200NR Fresenius Polysulfone Dialyzer, Fresenius Medical Care) [142, 143].

The syntheses of GA_5 and GA_{22} were described by Yin et al [141]. The morphology and particle size distributions of PVP and GA-coated Ag NPs were determined using a Tecnai G2 Twin transmission electron microscopy (FEI, Hillsboro, OR) at acceleration voltages of 160 kV and 200kV, respectively. Samples were prepared by placing a drop of the nanoparticle suspension on a standard copper grid and drying at room temperature. The UV-Vis absorbance spectra of nanoparticles were acquired using a Cary 500 scan UV-Vis-NIR spectrophotometer (Varian, CA). Hydrodynamic diameters of the particles were quantified by dynamic light scattering (DLS) conducted with an ALV-CGS 3 compact goniometer system (ALV-GmbH, Germany) using a helium-neon laser (λ = 632.8 nm) scattered at 90°.

2.2.3 COPAS Biosort flow sorting system and growth assay

All of the experiments described in this chapter used L1 stage larvae ("L1s") obtained via bleaching and overnight hatch of embryos in the absence of food to obtain age-matched individuals [144, 145]. Starved L1s were manually transferred into the sample cup of a COPAS Biosort (Union Biometrica Inc., Somerville, MA, USA) and diluted to ~1 nematode/μL [146, 147] in Moderately Hard Reconstituted H_2O ("EPA water") [148]. Fifty L1s individuals were dispensed into each well of a 96-well plate with dosing solution and UVC-inactivated bacteria, as previously described [116]. All COPAS Biosort measurements were made with the following parameters: EXT signal gain=4, EXT integral gain = 1.6, EXT threshold=20, and TOF minimum 18.

Silver nitrate (Sigma) was used as a positive control for ionic silver toxicity. In the growth assay, I also co-exposed with either trolox (a water soluble vitamin E analogue, Aldrich Chemical Co., Milwaukee, WI) or N-Acetylcysteine (NAC) (Sigma Chemical Company, St. Louis, MO). Target concentrations of each Ag NP and $AgNO_3$ were achieved by dilution of stock solution (prepared in ddH_2O), using EPA water. The volume of stock solution added was balanced by addition of the same volume of 2X EPA water to ensure a final ionic strength equivalent to EPA water (1X). From day 0-2, 50 μL of Ag NP dosing solution was added to each well (i.e., the dosing solution was only 2-fold higher than the final exposure solution when it was added to an equal volume of growth medium with nematodes). On Day 0, the dosing solution was twice the desired

concentration to account for the 50 μL that was added to each well with dispensed worms. Before dosing solution was added to the wells, I added 30 μL UVC-inactivated bacteria to the 1.5 ml dosing solution on day 1, 60 μL on day 2, and 120 μL on day 3. Every day, plates with exposed nematodes were aspirated using the COPAS Biosort [149]. Time of flight (TOF) and extinction (EXT) measurements were acquired for each individual when dispensing and aspirating. However, since previous work has demonstrated that nematode curling during their passage through the flow cell of the COPAS Biosort results in higher variability of TOF than EXT values [146], EXT values were used for our analyses.

2.2.4 Quantification of Ag NP properties and dissolved silver in exposure medium

Barnstead Nanopure-grade water (>17.8 MΩ-cm, Sigma Aldrich) was used to prepare all reagents and samples for measurements of Ag NP hydrodynamic diameter, electrophoretic mobility (and ζ-potential), and dissolved silver and N-acetyl cysteine (NAC). Trace-metal grade HNO_3 was used to adjust the pH of solutions. Ultrahigh purity nitrogen was utilized to degas reagent water for the NAC stock solutions. Borosilicate glass containers for reagents were acid cleaned by an overnight soak in 1 N HCl followed by three rinses with Nanopure water.

The hydrodynamic diameter of the Ag NPs was quantified by diluting an aliquot of the Ag NP stock suspension in EPA water to reach a final silver concentration ranging from 20 to 46 μM Ag. A subset of the solutions contained 123 μM NAC. This NAC

concentration was 2 times higher than that used in the toxicity test exposure, due to the fact that most Ag NP concentrations in this characterization were higher than the dosing concentrations. Size and ζ potential of Ag NPs were analyzed by dynamic light scattering (DLS) (Malvern Zetasizer). Experiments with PVP-coated nanoparticles were prepared in glass containers and transferred to a 1-cm glass cuvette before analysis with DLS. The intensity-weighted average hydrodynamic diameter of the colloids was quantified over time using incident light (λ= 633 nm) scattered at 173°. Electrophoretic mobility at 25°C (Malvern Zetasizer) was measured in triplicate after one h in suspension. Zeta potential was calculated from the electrophoretic mobility based on the Smoluchowski equation [150].

Dissolution of silver and adsorption of NAC on Ag NPs were quantified to investigate how toxicity might be related to silver ion release from the NPs, and whether NAC was sorbing to the particles and influencing aggregation. Batch experiments were carried out by suspending Ag NPs in EPA water with or without NAC under ambient laboratory conditions. Replicates of the suspensions were incubated at room temperature for 1, 5, and 24 hr. At each time point, a sample replicate was sacrificed for filtration using a 0.025 μm membrane filter (VSWP Millipore) inserted in a glass vacuum filtration apparatus. The filtered samples were acidified with 2% v/v HNO_3 and 0.5 v/v % HCl and allowed to digest at room temperature for at least one day prior to silver concentration quantification by ICP-MS. NAC concentration was measured in the filtrate

by derivatization with DTNP and quantification by reverse phase high performance liquid chromatography (Varian ProStar) [151, 152]. In all Ag NP solutions, at least 65% of the initial NAC was observed in the water after filtration (Fig. 2), and in all cases, the nominally dissolved NAC concentration (i.e. in filtered water) was greater than the nominally dissolved Ag concentration.

Control experiments were performed to confirm that free NAC, Ag^+, and Ag-NAC complexes were not sorbing to the filters. In these experiments, two solutions comprising 123 μM NAC and 37 μM $AgNO_3$+123 μM NAC in EPA water were filtered with the 0.025 μm membrane filters. A third solution consisting of 1.85 μM $AgNO_3$ in a $NaHCO_3$ (pH 8.3) was also prepared as the Ag+ control. The percentage of total NAC quantified in the filtrate was 96.9% in the NAC-only mixture and 92.3% in the $AgNO_3$+NAC mixture. The recovery of total silver in the $AgNO_3$-bicarbonate mixture and $AgNO_3$+NAC mixture were 94.1% and 96.1%, respectively. The efficiency of the filtration system to remove particles was also tested by quantifying the retention of silver after filtration of Ag NP stock solutions. Filtration of the stocks resulted in removal of 99.7%, 79.5%, 99.4%, 89.7%, and 95.6% of total silver from CIT-Ag NPs, GA_5-, GA_{22}-, PVP_8-, and PVP_{38}-Ag NP stock suspensions, respectively. Although the monomer diameters for some of our stock suspensions were below the nominal filter pore size, particles were probably aggregated to some extent since hydrodynamic diameters (quantified by DLS) were greater than monomer diameter (quantified by TEM) for all

particles. Hydrophobic or electrostatic interactions between particles and the mixed cellulose esters hydrophilic membrane may have also contributed to retention of particles during filtration.

2.2.5 Quantification of NAC, borate, PVP, and citrate concentrations in exposure medium

A stock solution of 15 mM N-acetyl-L-cysteine (NAC) was prepared in degassed water and stored at 4°C. The NAC stock solution was utilized within three weeks of preparation. Reagents for NAC quantification included 2,2′-dithiobis(5-nitropyridine) (DTNP) dissolved in acetonitrile and 0.5 M sodium acetate buffer dissolved in water and adjusted to pH 6. HPLC-grade solvents were utilized for all reagents. Citrate was measured in 10 mM NaOH eluent with a DIONEX DX-120 ion chromatographer equipped with an AS11 column and AG11 guard column (refer to the next section for more details). Borate was measured in digestions of centrifugation-purified PVP8 stock (4081 ppm) suspension diluted to 10 and 50 ppm Ag, using inductively coupled plasma atomic emission spectroscopy (Teledyne Leeman Labs Prism High Dispersion ICP Spectrometer) and sodium tetraborate decahydrate as a standard. The limit of detection was 0.1 ppm (9.2 μM). Boron was undetectable in the 10 ppm Ag preparations, and detectable but unquantifiable (< 0.1 ppm) in the 50 ppm samples. This corresponds to a molar ratio of at least 50:1 of Ag to B in the stock and dosing solutions. PVP concentrations in stock solutions were measured via total organic carbon analysis (Shimadzu TOC-5050A Total Organic Carbon Analyzer), and were 11%

by mass in the PVP38 stock vs 23% by mass in the PVP8 stock. It has been previously shown that these levels of PVP do not inhibit nematode growth [116].

Dissolved citrate in the CIT-Ag NP suspensions was quantified by diluting the stock solution to approximately 30 μM total silver in pH 7.5 water (buffered with 7 mM $NaHCO_3$). Replicates of this solution were sacrificed for total silver measurements by acidifying with 50% HNO_3. For ICP-MS analysis, the acidified sample was further diluted in 2% HNO_3 and 0.5% % HCl before injection into the instrument. For citrate analysis, filtered samples were not modified and were directly measured by ion chromatography (Dionex) fitted with an anion exchange column (Dionex AS11 and AG11 guard column), conductivity detector, and a mobile phase comprising of 10 mM NaOH degassed with helium.

2.2.6 Equilibrium speciation calculations

Dissolved Ag(I) speciation in the experimental matrices was calculated using MINEQL+ (v. 4.5) [153]. Calculations were performed for total silver Ag(I) concentrations between 0.01 and 10 μM dissolved in EPA water at pH 7.6 and 25°C. Cerargyrite AgCl(s) was supersaturated at the highest silver concentration (>5 μM), but precipitation was not considered in the calculation. Thermodynamic equilibrium constants in the MINEQL+ database and NIST database [154] were used for the calculations. The constant for the dissolved silver-citrate complex was estimated based on correlations between Ag^+- and Hg^{2+}-carboxylate complexes (Fig. 3). Formation

constants for the Ag-NAC complex were estimated based on published values for other Ag-thiolate complexes [155].

2.2.7 Equilibrium calculations of dissolved silver speciation

Silver(+I) speciation in the culture media was estimated using MINEQL+ (v. 4.5) [156] . All thermodynamic equilibrium constants used in the calculation were those listed in the MINEQL+ database. Protonation constants for citrate were obtained from the Smith and Martell reference database [157]. The formation constant for the silver-citrate complex was not found in the literature. Thus, the constant for this complex was calculated based on correlations between the Ag^{+}-carboxylate and Hg^{2+}-carboxylate complexes (Fig. 3). Assuming the formation equation for the Hg-citrate complex [9]:

$$Hg^{2+} + citrate^{3-} \Leftrightarrow Hg(citrate)^{-} \qquad K = 1012.2 \tag{1}$$

We estimated that the equilibrium constant for the $Ag(citrate)^{2-}$ complex is approximately 104 (Fig. S12).

The following stability constant was used for the formation of the Ag-NAC complex:

$$Ag^{+} + R\text{-}S^{-} \Leftrightarrow Ag\text{-}S\text{-}R \qquad K \cong 1012 \tag{2}$$

where in Eq. 2, R-S- is the deprotonated thiolate group of NAC. The stability constant K was estimated based on K values ranging from 1011.9 to 1012.4 for other

deprotonated thiolate ligands including cysteine, penicillamine, glutathione, and mercaptoproprionate [158, 159].

2.2.6 Silver speciation by X-ray absorption spectroscopy

Silver K-edge (25.514 KeV) XANES experiments (X-ray absorption near edge structure) were acquired at the European Synchrotron Radiation Facility (ESRF, France) on the FAME beamline (BM30b) with Si(220) monochromator crystals [160, 161]. Samples were cooled to a temperature close to that of liquid Helium (around 10 K) during spectra acquisition into fluorescence mode using a multichannel fluorescence detector. Two samples were analyzed: bacteria alone and C. elegans (age-synchronized L1s) incubated with bacteria, both exposed to 1.2 μM $AgNO_3$ in EPA water. After 48 hrs, both bacteria and nematodes were rinsed 3 times with EPA water and centrifuged at 2200 and 5000 rpm for nematodes and bacteria, respectively. Samples were freeze-dried, homogenized, mixed with boron nitride, and pressed into thin pellets for XANES analysis. 4 scans were collected for each sample. The XANES data were obtained after performing standard procedures for pre-edge subtraction and normalization using the iFEFFit software package [162].

2.2.6 Statistical analysis

Data from the Biosort for each aspiration time was graphed as a scatterplot between TOF and EXT, which are highly correlated values (Fig. 4). As other COPAS toxicology researchers suggested, EXT values are preferable because nematode curling

leads to greater variability in TOF values [146, 163]. Therefore, we used EXT values for graphical presentation and statistical analysis. To exclude measurements of objects other than nematodes (e.g., Ag NP aggregates), values were deleted if they deviated by >one standard deviation at that EXT value from the TOF vs EXT plots for an entire dataset (all doses and strains) on a given day. As an additional quality-control criterion, measurements that were less than the mean measurement of the previous day minus one standard deviation (which would represent negative growth) were deleted. EXT values were normalized to the control nematodes of a given strain since some strains grow more slowly than N2. We used R (SAS institute) to carry out data plotting and the non-parametric Wilcoxon rank sum test, with $p < 0.05$ considered statistically significant.

2.3 Results

2.3.1 Characterization of Ag NPs

Toxicity experiments were performed for 7 different Ag NPs. Except for PVP_S and PVP_L, all nanomaterials were synthesized in our laboratory. All of the tested Ag NPs were composed of Ag^0, roughly spherical and polydisperse in purified water (Fig. 5). Monomer diameters (mean particle size ± standard deviation; median with 10th and 90th percentiles) were measured by ImageJ from TEM images (n>=100) and are shown in Table 1.

2.3.2 Dependence of toxicity on medium type

As indicated in Table 2, Ag NP toxicity in the moderately hard reconstituted water ("EPA water") was higher than in K^+ medium, which has a much higher ionic strength. Control measurements were made in EPA water and K^+ medium, and when the two control groups are observed at the same experimental trial, there is no detectable difference between them. Toxicity was measured as growth inhibition over a 3-day period, with size on each day quantified as the optical density (extinction, "EXT") of the nematodes, using a COPAS BioSort. We calculated the dose of Ag NPs causing 50% growth inhibition (EC_{50}) compared to the control with no silver treatment (Fig. 6), and the "threshold lethal dose" corresponding to the lowest observed concentration of Ag NPs leading to 100% mortality of nematodes within 24 hrs. The EC_{50} values and threshold lethal doses for each nanomaterial were 1.5 to 12 times greater in K^+ medium than in EPA water. For the dissolved $AgNO_3$ treatment, the EC_{50} value and threshold lethal dose were 100 times greater in K^+ medium than in EPA water. K^+ medium has 1600 times more chloride content than EPA water and 10 and 3.5 times the level of Ca^{2+} and Mg^{2+}, respectively. Differences in Cl^-, $Ca^{2+,}$ Mg^{2+} and HCO_3^{2-} levels can affect dissolution and alter the electrostatic surface properties of Ag NPs, which can affect the aggregation state of the particles in suspension [116, 136, 164]. Furthermore, counter ions such as chloride are capable of binding Ag+ to form aqueous Ag-chloride complexes, some of which are less bioavailable to the organisms [165]. These differences likely

explain the fact that Ag NP toxicity was significantly higher in EPA water than K^+ medium for all Ag NPs. The subsequent mechanistic analyses described in this chapter were carried out in EPA water.

2.3.3 Dependence of toxicity on dissolved Ag and independence from size or surface charge

Particle size may affect not only oxidative release of dissolved silver from Ag NPs [166, 167], but also Ag NP reactivity due to a higher mass-normalized rate constant of surface ROS generation in nano-size than micro-size particles [125, 126, 168]. These effects result from the increase of the specific surface area of the particles when their sizes decrease [169, 170]. Other researchers have reported that smaller particles (measured by TEM) were more toxic on a mass basis than larger particles that were otherwise similar [33, 125], a generalization that did not hold entirely in our experiments, even with particles of the same coating (Fig. 7A). For instance, PVP_8-Ag NPs had a smaller monomer size and lower ζ-potential than PVP_{38}-Ag NPs, characteristics that, based on work with microbes, would point to higher toxicity for PVP8 [50]. However, we found that PVP38 was twice as toxic as PVP_8-Ag NPs in EPA water. Overall, while ζ-potentials were all negative with the different particle sizes and coatings (Fig. 8), there was no obvious correlation between ζ-potential and toxicity. Rather, our data suggested that other factors contributed to toxicity, particularly fraction dissolved silver (defined as the amount of silver in solution after filtration with a 0.025

μm filter) (Figs. 7B and 7C). There was a clear inverse linear relationship ($r^2 = 0.89$) between dissolved silver and toxicity (Fig. 7C), with GA_5-Ag NPs being the most toxic Ag NP with the highest dissolved silver concentration (comparable to $AgNO_3$), and CIT-Ag NPs being the least toxic with the lowest dissolved silver. The same relationship was observed when dissolved silver concentration rather than fraction dissolved silver after 24 h was plotted on the x axis ($r^2 = 0.81$). The dissolved silver associated with PVP_{38}-Ag NPs in EPA water was twice that of PVP_8-Ag NPs (with the same initial total silver concentration) (Fig.7B). Therefore, smaller particle size was not necessarily correlated with more dissolved silver, but the dissolved silver concentration at 24 hr was directly linked to differences in toxicity (Fig. 7C). For GA-coated Ag NPs, suspensions with the smaller particles had much higher dissolved silver concentration (25.7% of the total silver) than the suspensions with the larger GA-coated Ag NPs (2.7% of the total silver was dissolved) (Fig.7B). Moreover, the fraction of dissolved silver in the $AgNO_3$ treatment was similar to the GA_5-Ag NP suspension possibly due to supersaturation and precipitation of cerargyrite AgCl(s) when $AgNO_3$ was added to EPA water at concentrations greater than 5 μM (Fig. 9). PVP_8-Ag NPs and CIT-Ag NPs contained only 1.6% and 0.1% dissolved silver, respectively, and were less toxic than the other silver treatments.

The average hydrodynamic diameters measured in all Ag NP suspensions were larger than the monomer diameters recorded by TEM, indicating that the Ag NPs were

aggregated when they were suspended in EPA water. There was some correlation between aggregation and toxicity, with the least toxic Ag NP (CIT-Ag NPs) also aggregating during the course of the exposure period (Fig.7D). Thus the reduced toxicity of CIT- Ag NP may be attributable to the formation of aggregates and a subsequent decrease of available surface area for dissolution. However, since there was no measureable aggregation of the other particles, it was not possible to formally correlate the aggregation state with toxicity. In addition, there is uncertainty regarding the importance of aggregation and settling in determining exposure in the context of an organism such as *C. elegans* that feeds on bacteria and large particles that have settled to the bottom of the water column, and processes food by pharyngeal grinding.

2.3.4 Coating effects on dissolution and toxicity

The smallest Ag NPs (CIT-, PVP_8- and GA_5-Ag NPs) were similar in size, with mean monomer diameters of < 10 nm, yet were not similar in degree of toxicity: GA_5-Ag NPs was ~9-fold more toxic than PVP_8-Ag NPs, which in turn was ~3-fold more toxic than CIT-Ag NPs. Because the sizes were so similar, we attribute the difference in toxicity to surface coating. As discussed previously, this may relate in part to dissolution (Fig. 7B). In addition, we hypothesized that the citrate used as a coating in the CIT-Ag NPs might be protective via chelation that might reduce availability of dissolved silver. We assessed this possibility via speciation modeling and toxicity testing.

First, we measured the amount of free citrate present in a filtered CIT-Ag NP stock and found that it comprised up to 10.8 ± 0.7 mmol free citrate per mmol of total Ag. Next, we modeled the effect that this amount of citrate would have on silver speciation (Fig. 9), and found that citrate significantly altered dissolved Ag(I) speciation, depending on relative proportions of dissolved Ag and citrate in EPA water.

To empirically test the importance of Ag ion and citrate in CIT-Ag NP toxicity, we co-exposed CIT-Ag NPs (37.04 μM) with $AgNO_3$ (1.18 μM). If the toxicity of CIT-Ag NP were only driven by Ag ion, we would expect that the addition of $AgNO_3$ would increase toxicity. However, the combined toxicity was not statistically distinguishable from CIT-Ag NPs alone (data not shown). Based on our measurements of silver solubility of CIT-Ag NPs in EPA water (Fig. 7B) and free citrate, we estimated that the mixture contained 1.2 μM dissolved Ag and 400 μM dissolved citrate. Our speciation calculations supported the notion that free citrate complexed a large portion (42%) of dissolved Ag (Fig.9), which would partly explain the reduction of toxicity. Another reaction that could play a role but was not captured by our equilibrium calculations is sorption of Ag ions on citrate-coated particles, which might also lead to reduced bioavailability.

2.3.5 Pharmacological rescue of Ag NP toxicity

Our dissolved silver measurements supported a dominant role for ionic silver release as the mechanism for toxicity for many Ag NPs. Next we tested whether

pharmacological rescue experiments would support that result. Bioavailability of ionic silver can be reduced by binding to glutathione (GSH) or other thiol-containing proteins such as metallothionein [171]. We tested the ability of a chelating chemical (N-acetyl cysteine, NAC) and an ROS-scavenging chemical (trolox) to rescue the toxicity of Ag NPs. In addition to its role as a Ag+ chelator, NAC can also serve as an antioxidant. The concentrations of the rescue agents (61.3 μM NAC and 23 μM trolox) were chosen based on pilot studies that identified concentrations that were effective but showed no adverse effect when administered alone. The NAC molar concentration was in excess of the molar concentration of the silver, even assuming complete dissolution.

Rescue was tested in wild-type (N2 strain) nematodes, using the EC_{50} of each Ag NP. NAC completely rescued the growth inhibition of all the tested Ag NPs and $AgNO_3$. In contrast, partial rescue by trolox was observed in the following order of effect: CIT-Ag NPs > PVP_{38}-Ag NPs > GA_{22}-Ag NPs, and no rescue by trolox was observed for PVP_8-Ag NPs, GA_5-Ag NPs or $AgNO_3$ (Figs. 10A, B, E). The trolox-mediated rescue of CIT-Ag NP toxicity was only slightly less than that of NAC. Trolox or NAC alone had no effect on nematode growth compared to controls.

2.3.6 Physicochemical identification of an effect of NAC and trolox on dissolution, aggregation, and ion chelation but not surface properties

The addition of NAC to NP suspensions increased the dissolved silver concentrations, by more than 10-fold in some cases (compare Fig. 11 to Fig. 7B). However, chemical equilibrium calculations of Ag(+I) speciation in the EPA water

matrix indicated that in a mixture of 30 μM NAC and dissolved Ag(+I) (ranging from 0.01 to 10 μM), Ag-NAC complexes dominated dissolved Ag(+I) speciation (Fig. 9). We believe that the dominance of Ag-NAC species is applicable to our filtered Ag NP suspensions amended with NAC, in which the measured dissolved NAC concentrations were 91 to 120 μM and exceeded the silver concentrations (Fig. 2 and 11A). One potential confounding factor for our NAC rescue experiments would be sorption of NAC to the Ag nanoparticles. To explore the potential for NAC-Ag NP interaction, we measured both the hydrodynamic diameter (Fig. 11B) and ζ-potential of all Ag NPs with and without NAC (Fig. 8). No significant changes in electrophoretic mobility (and ζ-potential) were detected (Figs. 8A and 8B). Furthermore, the addition of NAC did not change the average hydrodynamic diameter of most Ag NPs. The exceptions were CIT-Ag NPs and PVP_8-Ag NPs. NAC reduced the aggregation rate of CIT-Ag NPs (compare Fig. 11B to Fig. 7D), possibly due to adsorption of NAC on Ag NP surfaces, based on the fact that less dissolved NAC was measured in the CIT-Ag NP suspensions compared to other Ag NPs (Fig. 2). The addition of NAC to the PVP_8-Ag NPs suspensions resulted in the opposite effect, causing aggregation of the nanoparticles (compare Figure 11B to Fig. 7D), although the reasons for this are not clear. Overall, the effects of NAC on toxicity were best explained by chelation of Ag+ and the reduction of bioavailable forms of silver. This interpretation is supported empirically by the fact that NAC completely rescued $AgNO_3$ toxicity (Fig. 10).

Trolox is a polycarboxylate compound that can potentially bind Ag+ ions in solution. Binding constants were not found in the literature or thermodynamic databases, so we could not directly calculate the potential for silver binding by trolox. However, if another polycarboxylate ligand, citrate, was used to estimate potential binding of Ag+ by trolox, then the presence of 23 μM citrate (the concentration of trolox in rescue experiments) was not sufficient to alter dissolved silver speciation (Fig. 9). Our model predicted that the trolox added in our rescue experiments did not affect silver speciation and only served as a ROS scavenger. This prediction was consistent with our result that trolox could not rescue $AgNO_3$ toxicity (Fig. 10).

2.3.7 Analysis of the mechanism of Ag NP toxicity via genetic approaches

We further tested mechanisms of Ag NP toxicity with a third set of experiments comparing the effects of different Ag NPs on mutant and wild-type (N2) nematodes. This genetic approach was based on the toxicological importance of specific genes in mediating the vulnerability to Ag NPs. For example, nematodes lacking DNA repair capacity are more vulnerable than N2 nematodes to exposures that cause DNA damage [147, 172] . Since we wished to test the roles of oxidative stress and metal ions in mediating toxicity, we chose two oxidant-sensitive (*sod-3* and *mev-1*) and two metal-sensitive (*mtl-2* and *pcs-1*) mutants. The *mev-1* mutant carries a mutation in a succinate dehydrogenase subunit that renders it highly susceptible to oxidative stress [173, 174]. The *sod-3* nematodes are deficient in one of the two *C. elegans* mitochondrial superoxide

dismutases and are oxidative stress-sensitive [175]. The *mtl-2* strain lacks one of the two metallothionein genes and is sensitive to multiple metals [176-178]. The *pcs-1* nematodes lack phytochelatin synthase, an enzyme that synthesizes a poly-glutathione cysteine-rich peptide with strong metal-chelating capacity, and are more sensitive than mtl-2 mutants to many metals [179].

We selected doses for the more toxic Ag NPs (PVP_8-, PVP_{38}-, CIT-, GA_5- and GA_{22}-Ag NPs) at which an intermediate level of growth inhibition (30-50%) was induced in N2s, such that increased susceptibility in mutant strains would be detectable if present. Metal-chelating mutants were more sensitive to ionic silver and all Ag NPs (Table 3), while oxidative stress-sensitive mutants were more sensitive only to PVP_{38}-, CIT-, and GA_{22}-Ag NPs (Fig. 12).

2.3.8 Combined mutant and pharmacological rescue analysis confirms the role of Ag^+ in CIT-Ag NP toxicity

While our mutant experiments supported a role for Ag ions in CIT-Ag NP toxicity, our pharmacological rescue results were equivocal: the difference in rescue by trolox and NAC was small and statistically marginal ($p=0.044$, compared to $p<0.001$ for all other Ag NPs). To further confirm the Ag ion-mediated effect in CIT-Ag NP toxicity, we used the metal ion-sensitive mutant *pcs-1* to test its pharmacological rescue. Since *pcs-1* was the most susceptible strain tested, we reduced the dosing concentration of CIT-Ag NPs to 18.5μM (compared to 37 μM in N2s). Most nematodes died by 24 h post exposure, while no mortality was observed when nematodes were co-exposed with

either trolox (23 μM) or NAC (61.3 μM). However, trolox only rescued mortality but not growth, so the nematodes arrested at the L2 stage, while NAC not only rescued mortality but also restored nematode growth to control levels (Fig. 13). Thus, CIT-Ag NPs do exert toxicity via release of ions, although this effect is less important than for PVP_8-, PVP_{38}-, GA_5- and GA_{22}-Ag NPs.

2.3.9 Complexation of silver ions in our experimental conditions

All of the experiments described so far suggest that the most toxic Ag NPs were also the most soluble and therefore likely acted largely by releasing silver ions that bind to sulfhydryl groups associated with proteins and low molecular weight antioxidants such as glutathione. In contrast, the less-soluble Ag NPs also caused toxicity via oxidative stress. This pattern predicts that we should see a great deal of thiol binding of silver inside the *C. elegans* upon incubation of $AgNO_3$. To test this hypothesis, we measured silver speciation through Ag K-edge XANES analysis on washed *C. elegans* individuals (or their bacterial food source) after they were incubated with $AgNO_3$. The shape of the XANES spectra and the position of the edge are distinguishable for AgCl, Ag_2O, $AgNO_3$ or Ag_2S compounds. Consequently, a change in the silver ions speciation after incubation with the nematodes or their food can be quantified using linear combination (LCF) of reference compounds. Obvious differences (a strong decrease of the white line intensity) are observed in the XANES spectra of the $AgNO_3$ after interaction with the organisms. Using LCF, we conclude that 89 to 96% of the silver is

complexed with sulfur atoms in vivo while silver atoms are only surrounded by oxygen atoms before incubation (Fig. 14).

2.4 Discussion

The mechanism of Ag NP toxicity was dependent in these experiments on dissolved silver and surface coating. Three independent lines of evidence demonstrated that release of Ag^+ contributed to the toxicity for all the tested Ag NPs, and was a major driver for the toxicity of many, including the most toxic (GA_5-Ag NPs). A role for oxidative stress, presumably "nano-specific" generation of reactive oxygen species, was also supported, but only in the cases of larger or less toxic Ag NPs (PVP_{38}-, CIT- and GA_{22}-Ag NPs; Table 2), which were generally less soluble. These results demonstrated that both mechanisms of toxicity (dissolved Ag^+ and oxidative stress) can occur with Ag NPs; however, in our experiments, the ROS mechanism was apparent only when dissolved silver is minimal. Our findings may explain the differing literature reports on the role of oxidative stress in Ag NP toxicity. Of note, while silver ion could in principal cause indirect oxidative stress via depletion of biological thiols such as glutathione [180], this was not a major mode of toxicity of silver ion in our experiments, as demonstrated both by the inability of trolox to rescue $AgNO_3$ toxicity (Fig. 10), and by the lack of sensitivity to $AgNO_3$ of the *mev-1* and *sod-3* strains (Table 3). Based on our EPA water results, the toxicity of Ag NPs could be conservatively estimated as no greater than the toxicity of an equivalent mass of dissolved silver. However, there were exceptions to this

in K^+ medium (where overall toxicity was less), and other reports have identified greater toxicity associated with nanoparticulate Ag [125-129, 139, 178, 181]. It will be important to elucidate the reason for these differences. It is interesting to note that most studies that report that Ag NPs are more toxic than the equivalent mass of dissolved silver, or that generation of reactive oxygen species is a major driver for toxicity, are carried out in single-cell systems (either microbial or cell culture experiments) [125-129, 182], with some exceptions [141, 183]. On the other hand, most studies that report that Ag NPs cause toxicity largely via dissolution have been carried out in multicellular organisms [107, 111, 116].

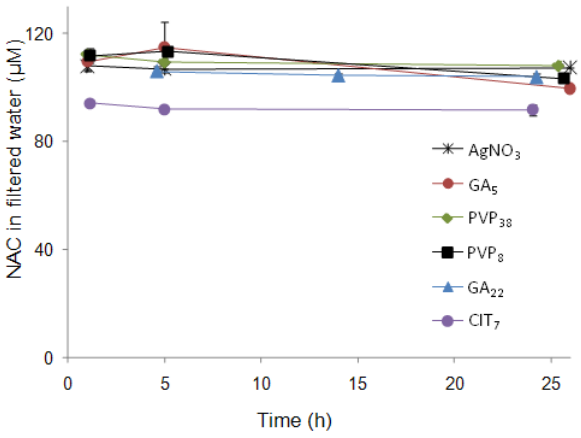

Figure 2: Concentration of N-acetylcysteine (NAC) passing through a 0.025 mm filter in suspensions containing $AgNO_3$ or Ag NPs (20 - 46 mM total silver) and 123 mM NAC added to EPA water.

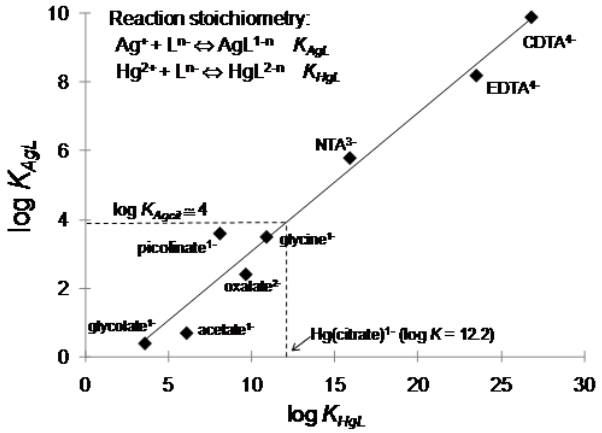

Figure 3: Correlation between the formation constants of Ag^{+}-carboxylate and Hg^{2+}-carboxylate complexes.

Equilibrium constants were obtained from the Smith and Martell database (National Institute of Standards and Technology, 1993). Linear least-squares regression (denoted by solid line) of the data points was the following: $log\ K_{AgL} = 0.40 \times log\ K_{HgL} + 0.96$ (R^2 = 0.96).

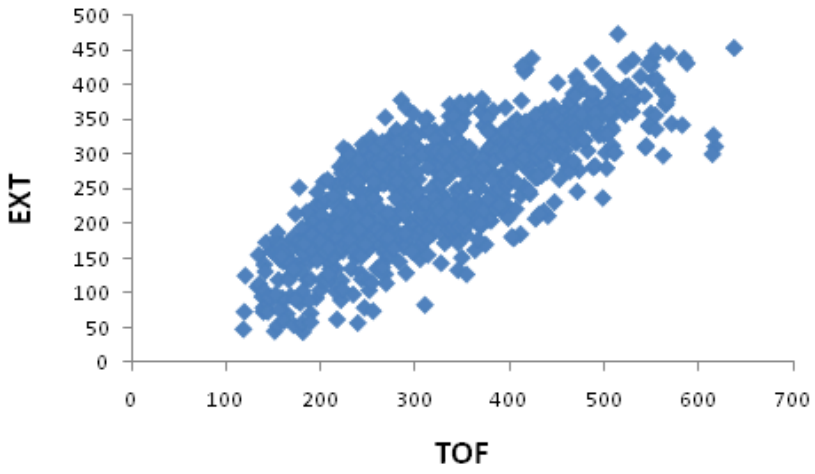

Figure 4: EXT (extinction, which measures nematode optical density, a combination of width and opacity) and TOF (time of flight, a measurement of nematode length) were highly correlated in these experiments.

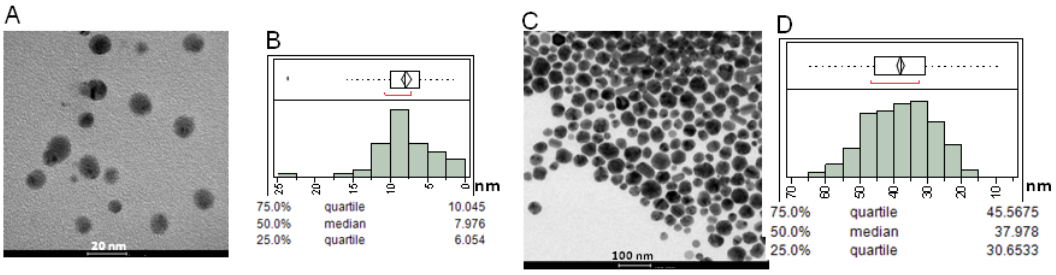

Figure 5: Shape and size distribution of silver nanoparticles.

A-B) PVP_8-Ag NPs; C-D) PVP_{38}-Ag NPs; Sample images were obtained from transmission electron microscopy, and size distributions are based on the TEM pictures.

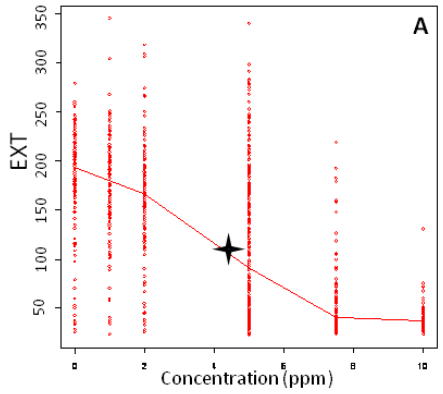

EC_{50} = 4.30 ppm

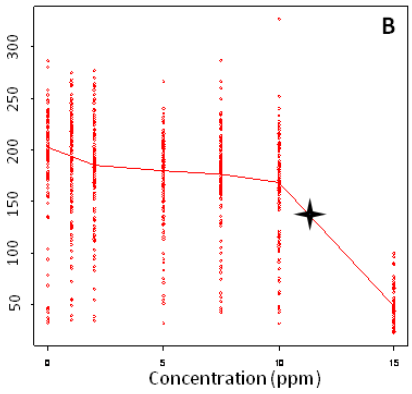

EC_{50} = 11.69 ppm

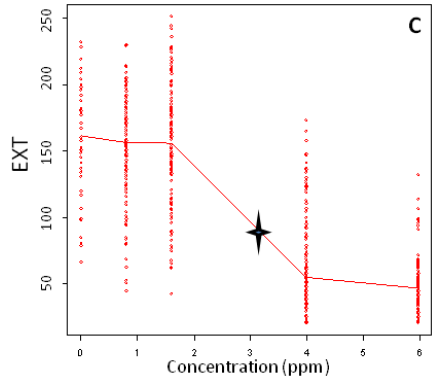

EC_{50} = 3.29 ppm

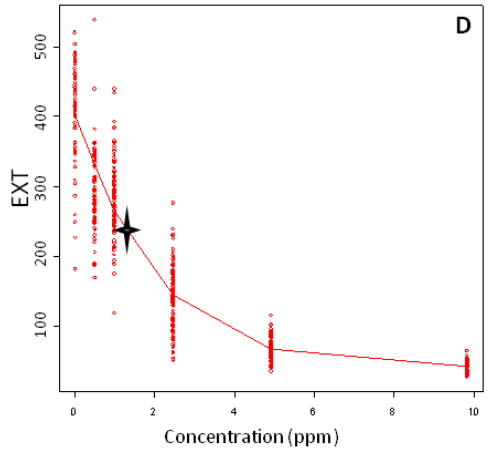

EC_{50} = 1.37 ppm

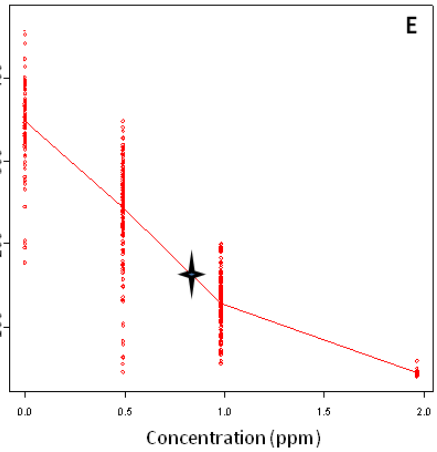

EC_{50} = 0.87 ppm

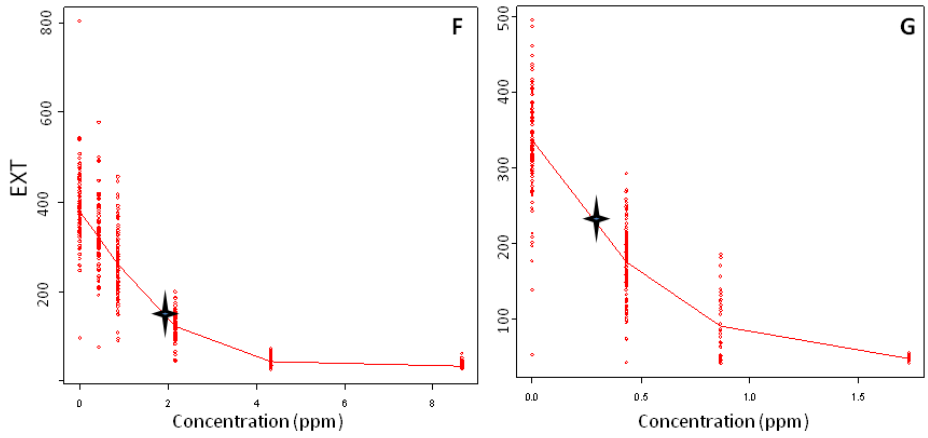

EC_{50} = 1.81 ppm

EC_{50} = 0.38 ppm

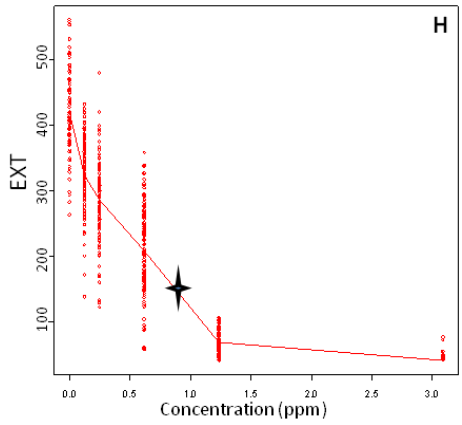

EC_{50} = 0.88 ppm

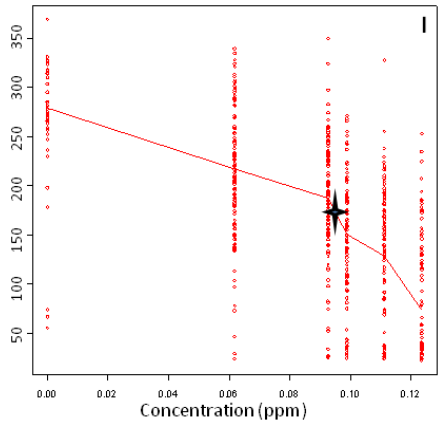

EC_{50} = 0.093 ppm

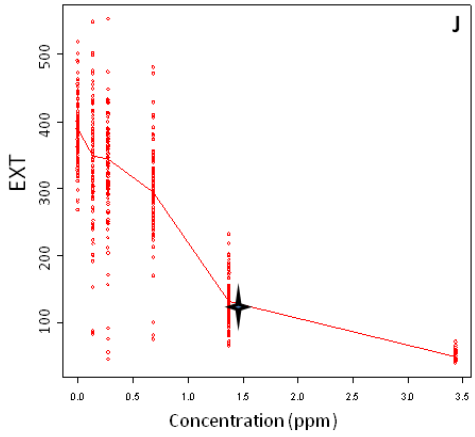

EC_{50} = 1.48 ppm

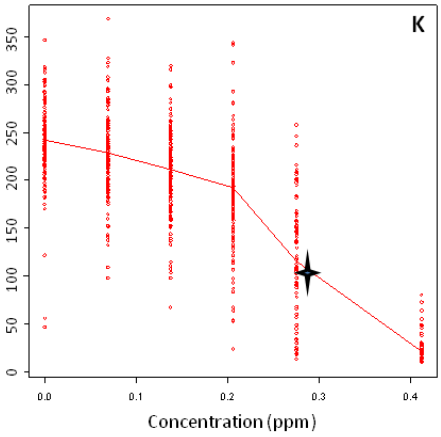

EC_{50} = 0.29 ppm

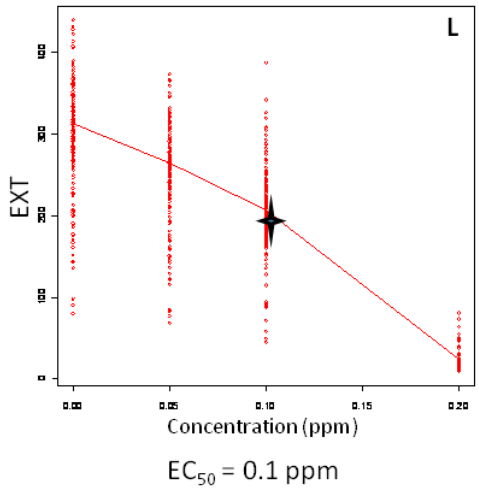

Figure 6: Comparison of dose-response relationships for all Ag NPs between K^+ medium and EPA water.

A) PVP_S-Ag NPs (NanoAmor) in EPA water; B) PVP_L-Ag NPs (NanoAmor) in EPA water; C) CIT-Ag NPs in EPA water; D) PVP_8-Ag NPs in K^+ medium; E) PVP_8-Ag NPs in EPA water; F) PVP_{38}-Ag NPs in K^+ medium; G) PVP_{38}-Ag NPs in EPA water; H) GA_5-Ag NPs in K^+ medium; I) GA_5-Ag NPs in EPA water; J) GA_{22}-Ag NPs in K^+ medium; K) GA_{22}-Ag NPs in EPA water. L) $AgNO_3$ in EPA water. The asterisks indicate the 50% growth inhibition dose (EC_{50}).

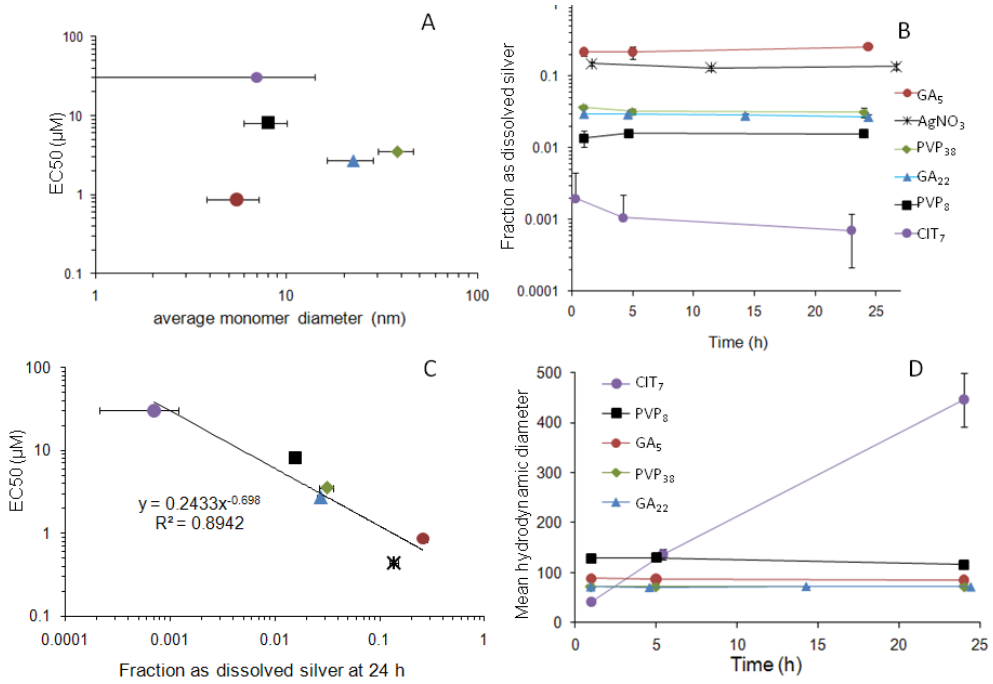

Figure 7: Physicochemical characteristics of various types of Ag NPs in EPA water and their correlation to toxicity profiles.

(A) No relationship observed between the 50% effect concentration (EC_{50}) and the diameter of the Ag NP monomers. (B) Fraction of total silver passing through a 0.025 μm filter after the silver nanoparticles and $AgNO_3$ were mixed in EPA water for up to one day. The total silver concentration was different for each type of silver and ranged from 30 to 50 μM. (C) Correlation between EC_{50} values of the silver treatments and the fraction of the total silver that was dissolved at 24 h. D) Average light intensity-weighted hydrodynamic diameters of silver nanoparticles in EPA water. Data points represent the average ± 1 standard deviation of replicates (n = 3). The error bars corresponding to the EC50 values are smaller than the symbols.

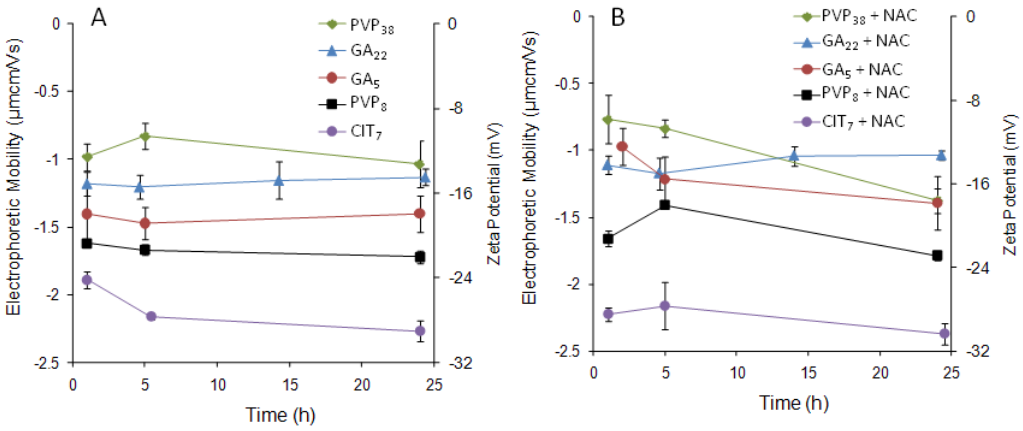

Figure 8: Electrophoretic mobility of Ag NP suspensions in EPA water

(A) without NAC; and (B) with 123 µM NAC.

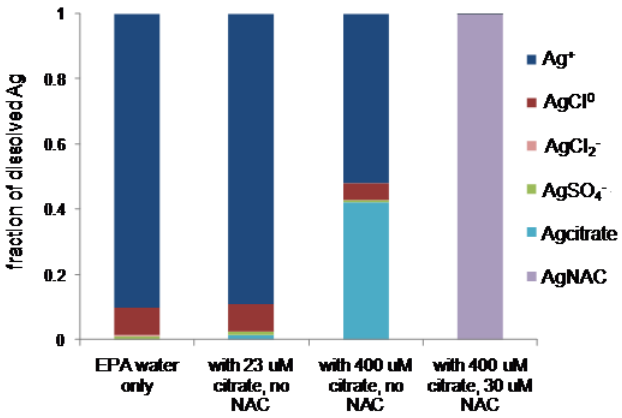

Figure 9: Effect of citrate and NAC on dissolved Ag(I) speciation, based on equilibrium speciation models.

Calculations were performed for 10^{-8} to 10^{-5} M total dissolved silver and resulted in the same proportions of dissolved silver speciation for each case tested: EPA water only, EPA water with 23 mM citrate, with 400 mM citrate, and with 400 mM citrate + 30 mM NAC. The speciation modeling suggests that $AgCl_{(s)}$ ceragyrite was supersaturated at total silver concentrations exceeding 5 mM. Moreover, toxicity rescue experiments with the addition of 30 mM NAC resulted in chelation of dissolved Ag(I) while the addition of 23 mM trolox did not significantly change silver speciation (assuming that trolox binds to Ag^+ with an affinity similar to other polycarboxylates such as citrate).

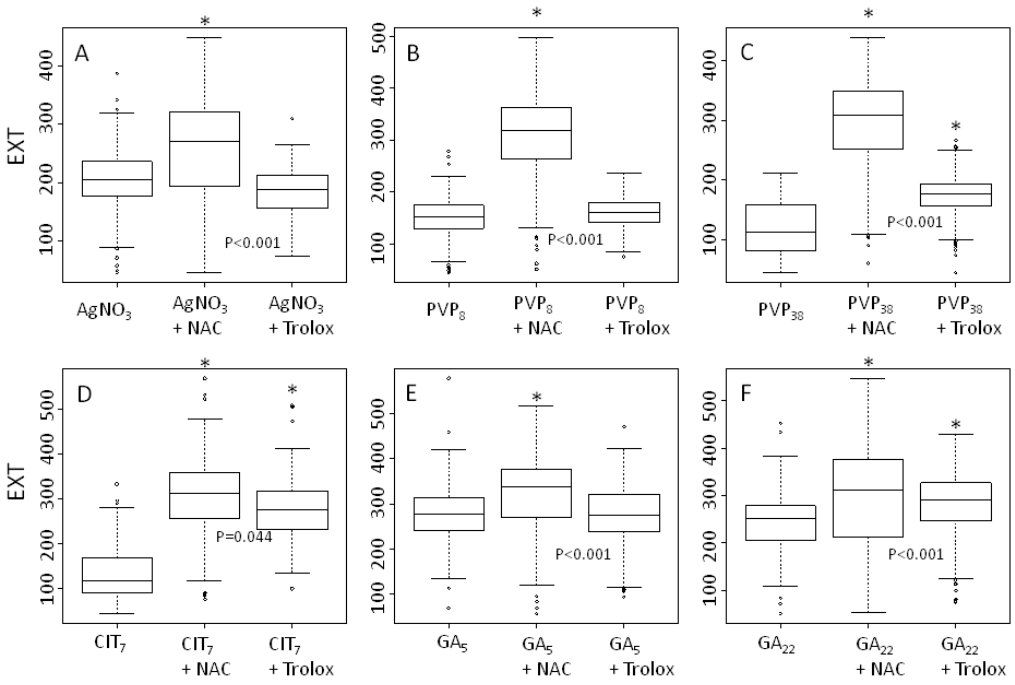

Figure 10: Pharmacological rescue of Ag NP toxicity

A) 0.6 μM $AgNO_3$ as a positive control; B) 37 μM (total silver) citrate-coated Ag NPs; C) 4.6 μM PVP8; D) 4.6 μM PVP38; E) 0.8 μM GA5; F) 2.8 μM GA22. Rescue by trolox is an indicator of the biological effects caused by reactive oxygen species (ROS), while rescue by NAC indicates the effects were caused by ROS and/or ionic silver. This figure showed the Effect from the addition of 61.5 μM NAC and 23 μM trolox to suspensions that contained total silver corresponding to EC_{50} values. Boxplots show the 10%, 25%, median, 75% and 90% quantiles of EXT (extinction; a proxy for nematode size) values 72 h post exposure. Asterisks indicate statistically significant differences compared to the Ag NPs alone. The data points are combined from 3 to 4 replicate experiments.

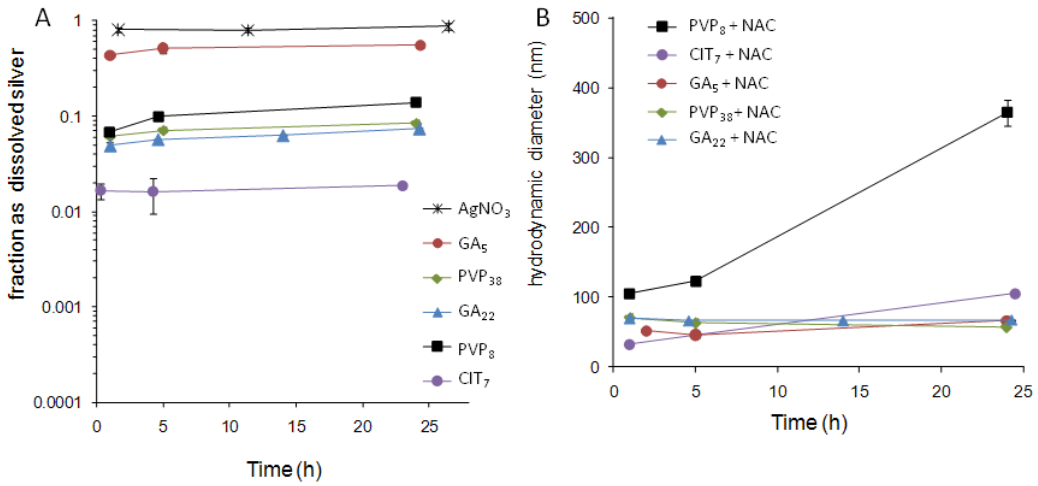

Figure 11: Effect of NAC on physicochemical properties of Ag NPs.

(A) Dissolved silver concentration; (B) Light intensity-weighted hydrodynamic diameter as quantified by dynamic light scattering. All suspensions consisted of 20 - 46 mM silver in EPA water and 123 mM NAC.

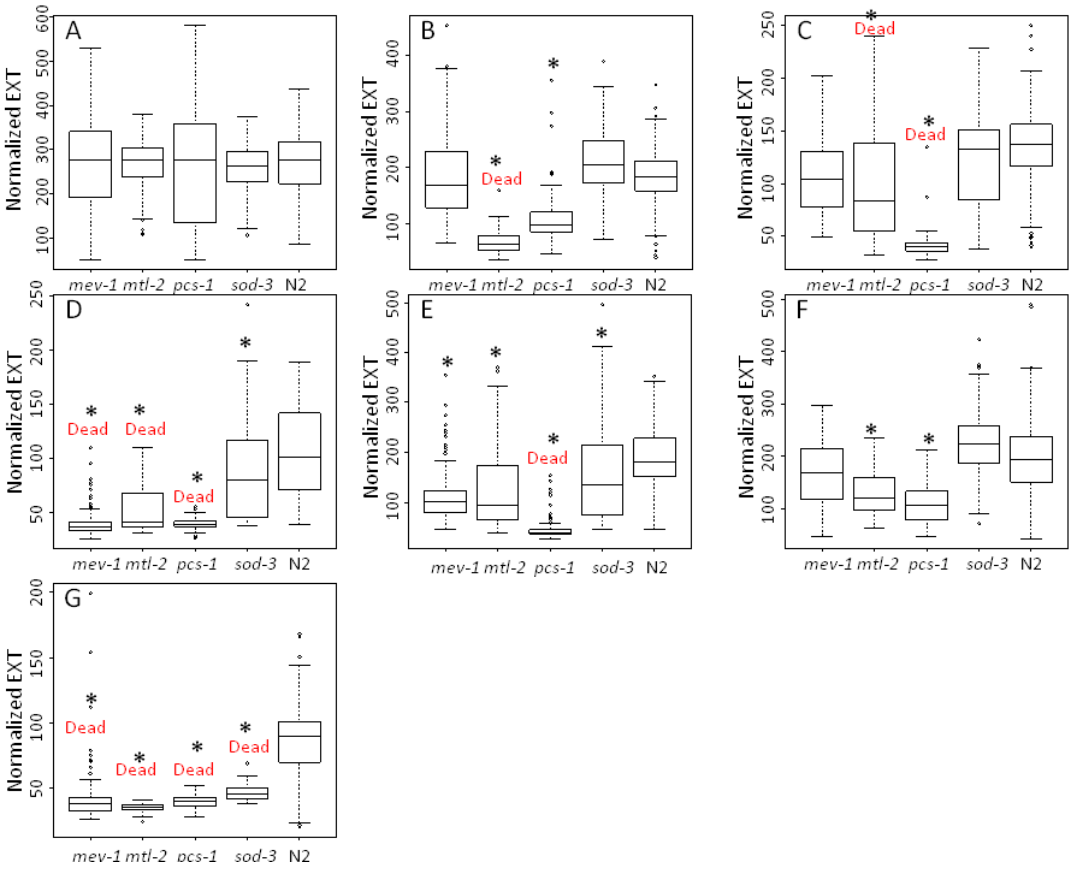

Figure 12: Toxicity of all Ag NPs in metal and oxidant-sensitive mutants.

A) Control; B) $AgNO_3$ (positive control); C) PVP_8-Ag NPs; D) PVP_{38}-Ag NPs; E) CIT-Ag NPs; F) GA_5-Ag NPs; G) GA_{22}-Ag NPs. Data presented as the EXT values (a proxy for size) 72 h post exposure.

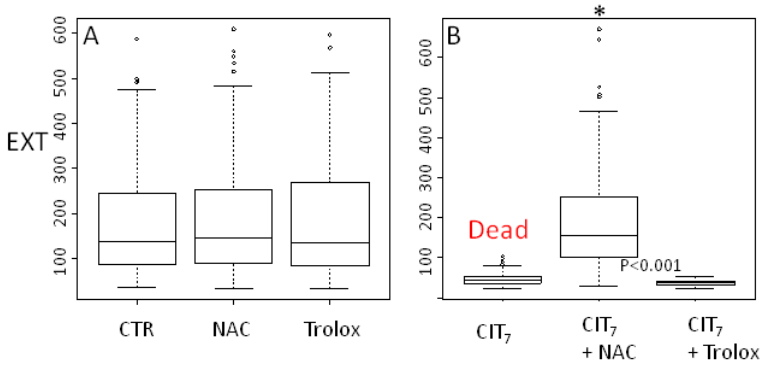

Figure 13: Pharmacological rescue by trolox and NAC in the *pcs-1* mutant (metal-sensitive). NAC was more effective than trolox at rescuing toxicity mediated by CIT-Ag NPs. A) Control, trolox only and NAC only; B) CIT-Ag NPs rescued by trolox and NAC.

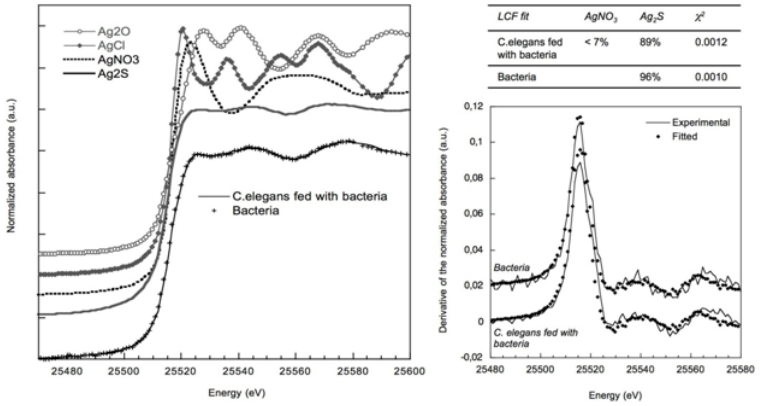

Figure 14: Experimental XANES spectra at the Ag K-edge of $AgNO_3$ incubated in EPA water with *C. elegans* (fed with bacteria) and the bacteria alone (left).

The experimental data were fitted using linear combination (LCF) of XANES spectra of $AgNO_3$, Ag_2S, Ag_2O, and AgCl reference compounds. The results of the LCF are presented in the table and the curve showing the derivative of the fitted and experimental normalized absorbance (right). [$AgNO_3$] = 1.2μM.

Table 2: Mean size of Ag NP monomers as determined by transmission electron microscopy and 50% growth inhibition doses (EC_{50}) (in wild type) and threshold lethal dose (minimum observed dose causing 100% lethality within 24 hrs) of tested Ag NPs and $AgNO_3$ in K^+ medium and EPA water.

Surface coatings	Mean particle size ± SD （nm)	Median particle size (10^{th}, 90^{th} percentile) (nm)	EC_{50} /μM (ppm±SD)		Threshold lethal dose /μM (ppm)	
			K^+	EPA	K^+	EPA
$AgNO_3$	N/A	N/A	59 (10)	0.6 (0.1±0.02)	> 59 (10)	0.9 (0.15)
PVP_8	8 ± 2	8 (2.6, 12)	13 (1.4±0.3)	8 (0.9±0.2)	111 (12)	9.3 (1)
PVP_{38}	38 ± 8	38 (25, 51)	17 (1.8±0.5)	3.5 (0.4±0.1)	111 (12)	9.3 (1)
PVP_S (NanoAmor)	21 ± 17	13 (6, 40)	463 (50)	40 (4.3)	> 463 (50)	93 (10)
PVP_L (NanoAmor)	75 ± 21	76 (48, 102)	417 (45)	108 (11.7)	> 463 (50)	186 (20)
CIT_7	7 ± 11	3 (1.5, 21.5)	369 (40)	31 (3.3±0.7)	> 463 (50)	74 (8)
GA_5	5 ± 2	5 (3.4, 7.6)	8 (0.9±0.1)	0.9 (0.09±0.02)	33 (3.6)	1.1 (0.1)
GA_{22}	22 ± 6	22 (15, 31)	14 (1.5±0.2)	2.7 (0.3±0.1)	38 (4.1)	3.9 (0.4)

Table 3: Mutant sensitivity analysis of all Ag NPs and $AgNO_3$. "+" indicates basal sensitivity of N2s, and "++" indicates increased sensitivity.

Strain Sensitivity	N2	mtl-2	pcs-1	mev-1	sod-3
$AgNO_3$	+	++	++	+	+
PVP_8	+	++	++	+	+
PVP_{38}	+	++	++	++	++
CIT_7	+	++	++	++	++
GA_5	+	++	++	+	+
GA_{22}	+	++	++	++	++

3. *In vivo* study of the role of endocytosis and lysosomal function in silver nanoparticle uptake and toxicity in *Caenorhabditis elegans*

3.1 Introduction

As one of the most commonly used metal nanoparticles (www.nanotechproject.org), silver nanoparticle (Ag NP) uptake [76, 184-186] and toxicity have been explored extensively both *in vitro* and *in vivo* [76, 187-189], and intracellular uptake of NPs is important to NP toxicity [76, 94]. NPs are internalized into cells [190-192] and subsequently sorted into lysosomes [193, 194]. NPs have been widely used as drug delivery vehicles, e.g., Poly (Glycerol-Adipate), specifically targeting brain tumor cells, instead of normal brain cells [195]. Ag NPs crossed both the blood-brain barrier and blood-testis barrier in rats with low clearance rate, resulting in brain and testis retention of Ag NPs [196]. Mechanisms and kinetics of NP uptake are dependent on NP surface chemistry [185, 197, 198] and shape [199], as well as cell type [192].

3.1.1 Intracellular trafficking in *Caenorhabditis elegans*

Recent studies suggested that endocytosis was an important mechanism for intracellular NP uptake [199-202]. There are two major types of endocytosis, receptor-mediated (clathrin-mediated [203] and caveolae-mediated [204]) and non-receptor-mediated (macropinocytosis [205] and phagocytosis [206]). Receptor-mediated endocytosis begins with bud formation, followed by activities of protein adaptors

(linking formed vesicles to the membrane) and ending with the scission of endocytic vesicles from the interior aspect of the membrane [207].

3.1.2 Endocytosis as the mechanism of *in vitro* Ag NP uptake

Extensive *in vitro* studies showed that endocytosis was the major mechanism underlying the cellular uptake of Ag NPs [202, 208, 209], which was directly associated with cytotoxicity [210]. Ag NP uptake was altered through modification of surface functionalizations [210]. Uptake of gold nanoparticles has been visualized inside endocytic vesicles within a range of liver cell types [211]. Supporting the role of endocytosis in NP internalization, electron-dense Ag NPs (confirmed by EDX for the Ag peak) were associated with endocytic pits proximal to the apical membrane [212]. Cellular uptake of quantum dots was detected in a progression from early endosomes to late endosomes or lysosomes [90]. Endothelial cell uptake of iron oxide, titanium dioxide and silica NPs was confirmed via detection in both endosomes and lysosomes [194], and accumulation in lysosomes can cause impairment of lysosomal degradation capacity [129, 213].

In vitro studies of Ag NP uptake showed that their toxicity was dependent on both clathrin-mediated endocytosis and macropinocytosis [214]. However, *in vivo* investigations of endocytosis in Ag NP uptake were quite limited, and the majority of uptake studies were focused on biodistribution (mostly through visualization and quantification) [215].

3.1.3 Lysosomal function and nanoparticle toxicity

Lysosomes are the cellular sites where fluid flow converges intracellularly for degradation. There are two routes of lysosomal pathway: the first route is from early to late endosomes culminating in fusion with lysosomes, and the second is through autophagy [216]. Lysosomes have been shown to be an important sink of NPs and several types of NPs were found to result in alterations of lysosomal function, e.g., lysosomal membrane integrity, lysosomal pH, activity of lysosomal sulfatases, etc. [217]. Acidic NPs were trafficked to lysosomes, and could lower lysosomal pH and restore the normal lysosomal function [193]. The acidic environment within lysosomal compartments may result in enhanced oxidation and ion release from NP cores [210].

3.1.4 Study goal

To explore the role of endocytosis and lysosomal function in Ag NP uptake and toxicity in a multicellular organism *in vivo*, we used pharmacological inhibition and genetic manipulation of endocytosis and lysosomal function in *C. elegans*. *C. elegans* is a particularly useful model for these studies due to the availability of mutants and due to its well-differentiated, transparent body [98] which facilitates studies of uptake and tissue-specific effects [218]. We used both endocytosis inhibitors and endocytosis- and lysosome-related mutants to investigate the role of endocytosis and lysosomes in regulating *in vivo* responses to Ag NPs. Our results supported the hypothesis that endocytosis was important for Ag NP uptake in *C. elegans*, but also revealed a surprising

sensitivity to Ag NPs in lysosomal function mutants. This sensitivity was not observed after exposure to $AgNO_3$, and thus constitutes a nanoparticle-specific effect.

3.2 Materials and Methods

3.2.1 *C. elegans* culture conditions

C. elegans were cultured in petri dishes on K-agar seeded with OP50 strain *Escherichia coli* [140] to prepare the nematodes for liquid medium exposure, which was carried out in 96 well plates as previously described [116] except as detailed below. Strains N2 (wild-type Bristol), DH1201 (*rme-1* deletion, outcrossed 2 times), DH1370 (*rme-6*, point mutation, outcrossed 3 times), DH1206 (*rme-8*, point mutation, outcrossed 3 times), GS2477 (*cup-5*, point mutation, outcrossed 3 times), JJ1271 (*glo-1*, point mutation) and RB950 (*cup-4* deletion) were obtained from the Caenorhabditis Genetics Center (CGC; Minneapolis, MN, USA).

3.2.2 Nanoparticles and chemicals

The citrate-functionalized Ag NPs (herein referred to as CIT-Ag NPs) were prepared using the same method as in our previous paper, with size distribution of 25 nm ± 9 nm [219]. Chlorpromazine and phenothiazine were both purchased from Sigma Aldrich Co. (St. Louis, USA).

3.2.3 *C. elegans* 24-h Lethality Test

Young adult nematodes (46 hrs on OP50 plate at 20°C after L1 synchronization, defined as fully developed and mature nematode with no eggs in the uterus yet) were

treated with Ag NPs in this assay. Nematodes were dispensed into a 96-well plate using the COPAS Biosort with EPA moderately hard reconstituted water ("EPA water" hereafter) as the exposure medium (details previously described) [187]. No bacterial food was added to the dosing suspension. After 24 hrs, nematodes were examined for lethality. The criterion for lethality was a lack of movement for 15 sec after poking with a worm picker. Nematodes were scored blindly.

3.2.3 *C. elegans* 96-h reproduction assay

This assay was modified from a high-throughput reproduction assay protocol [220]. Synchronized L4 nematodes were dispensed in a 96-well plate, with 5 nematodes in each replicate well. On the day of dispensing, 120 μL (with bacteria cells concentrated to approximately $1* 10^{10}$ cells/ml) of UV-inactivated bacteria (UVRA strain) were added to the dosing solution (with a total volume of 1.5 ml) to ensure enough food for 48 h (details of dosing solution preparation in [51]). After 48 h, 10 μL of the UVRA was added to each dosing well to ensure enough food for another 48 h. After 96 h (assay duration), each dosing plate with exposed nematodes was aspirated using the COPAS Biosort, and offspring were counted.

3.2.4 Total silver measurements

For nematode silver content measurement, the exposed *C. elegans* (N2, *rme-1*, *rme-6* and *rme-8*) were transferred to clean EPA water with food to allow the gut to clear for 2 h, and then centrifuged at 2200 rpm for 2 min, rinsed with EPA 3 times, and freeze-

dried (Labconco, US) for 2 d. The freeze-dried samples were digested with concentrated nitric acid (70%, Fisher Scientific, US) at ~ 90 °C for 4 h. The digest was diluted with ultrapure water, held overnight at room temperature, and further diluted with mixed acid (2% HNO_3 and 0.5% HCl) prior to ICP-MS analysis.

3.2.4 Transmission Electron Microscopy

We exposed nematodes in 24-well plates to ensure sufficient nematodes for fixation. Exposures used 24-well plates to ensure sufficient nematodes for fixation. Nematodes were from 24 h LC_{75}'s exposure groups of $AgNO_3$ or CIT-Ag NPs. High doses were chosen to increase probability of detecting Ag NPs using TEM and because lower doses, from earlier experiments failed to induce tissue damage, precluding possibility of identifying target tissues. After exposure, nematodes were initially fixed in osmium tetroxide (2% osmium tetroxide in 0.1 M sodium cacodylate buffer, pH 7.4) for 5 min in an appropriate hood. This treatment resulted in death and fixation of all nematodes. Following 3X washes in sodium cacodylate buffer (0.1 M), nematodes were placed in secondary, aldehyde fixative, 4F: 1G [221] at 4 ºC. After 2 rinses in 0.1 M sodium phosphate buffer (pH 7.2-7.4), samples were placed in 1% osmium tetroxide in the same buffer for 1 h at room temperature. Samples were rinsed 2 times in distilled water, dehydrated in a series of increasing ethanol solutions followed by two changes of 100% acetone. Tissues were then placed in a mixture of Spurr (2) resin and acetone (1:1) for 30 min, followed by 2 h in 2 changes of 100% resin. Finally, samples were placed in

fresh 100% resin in molds and polymerized at 70 ºC for 8 h to 3 d.[222] Semi-thin (0.5 μm) sections were cut with glass knives and stained with 1% toluidine blue-O in 1% sodium borate. Ultrathin (70-90 nm) sections were cut with a diamond knife and initially examined with and without post-staining. After analysis showed sufficient detail without post-staining, all subsequent analyses were on non- stained sections.

3.2.5 DIC Nomarski imaging

In order to examine the effect of CIT-Ag NPs on vulval formation and reproductive apparatus, nematodes were dosed from L3 for 48 h (dosing as for the reproduction assay). DIC examination was focused on the reproductive apparatus especially the vulva area.

3.2.6 Statistical analysis

We used Microsoft Excel to carry out all the data plotting and R (SAS institute) to do the Kruskal-Wallis test and ANOVA, with $p < 0.05$ considered statistically significant. Processing of COPAS output (time of flight and extinction analysis) was previously described [51].

3.3 Results and Discussions

3.3.1 Uptake of Ag NPs in *C. elegans*

Silver toxicity has been extensively investigated in multiple organisms, suggesting that Ag NP toxicity could mainly be explained by oxidative dissolution and subsequent silver ion toxicity. Previous studies showed that AgNPs can be taken up by

bacteria [33] and multicellular organisms (e.g., gill, liver and kidney in rainbow trout) [223-225]. Uptake of other nanoparticles (not Ag NPs) has also been detected in *C. elegans* [226]. The purpose of examining Ag NP internalization in *C. elegans* was to assess the possibility that Ag NPs might exert a NP-specific effect. In specific, if Ag NP uptake was observed at a specific site or tissue type, and if this site of uptake co-localized with damage, a NP-specific effect would be supported. Cytoviva-based examination of hyperspectral images of *C. elegans* treated with Ag NPs detected intracellular uptake and intergenerational transfer of Ag NPs, mainly through ingestion and internalization by *C. elegans*. Intergenerational transfer was only observed after CIT-Ag NP exposure, and was detected in combination with a "bagging" effect (Fig. 15A, B), while PVP-functionalized Ag NPs did not detectably induce either of the two effects. Metal nanoparticle formation from dissolved metal ions was indicated in some organisms [227], but we detected minimal Ag NP signal in $AgNO_3$-exposed nematodes, at least under the conditions of our experiments.

3.3.2 Effect of an endocytosis inhibitor on $AgNO_3$ and Ag NP toxicity

Chlorpromazine is an inhibitor of clathrin-mediated endocytosis [228]. At the dose we used, chlorpromazine alone did not cause worm mortality. $AgNO_3$ was used as a positive control for ion effect. Chlorpromazine did not significantly alter $AgNO_3$ toxicity, but almost eliminated CIT-Ag NP-induced toxicity (Fig. 16A, B). This selective rescue of CIT-Ag NP toxicity, in combination with our previous results demonstrating

that CIT-Ag NPs caused NP-specific toxicity [51], supported the hypothesis that CIT-Ag NPs are taken up by endocytosis. We attempted similar experiments with phenothiazine, which is also an inhibitor of clathrin-mediated endocytosis. However, after mixing phenothiazine into the dosing solutions, white aggregates were formed, which confounded our ability to interpret the rescue effect that we observed in both Ag^{+} (lower concentrations) and CIT-Ag NP exposures (Fig. 17), since the rescue could have resulted from reduced exposure due to precipitation. Chlorpromazine did not cause precipitation in either $AgNO_3$ or CIT-Ag NP dosing suspensions.

3.3.3 Silver toxicity in endocytic trafficking and biogenesis deficient mutants

In order to further understand the importance of endocytosis-related pathways in Ag NP uptake and associated toxicity, we used three endocytosis-deficient mutants (*rme-1*, *rme-6*, and *rme-8*) to complement the pharmacological inhibitor results. Ag NPs or small aggregates enter the cell through receptor-mediated endocytosis [229] resulting in incorporation into early endosomes, which become late endosomes and eventually fuse with lysosomes. *rme-6* is required in endocytic trafficking from plasma membrane to endosomes, while both *rme-1* and *rme-8* modulate endocytic trafficking from early endosomes to late endosomes. *cup-4* functions in fluid endocytosis by coelomocytes, *cup-5* is essential for late endosome-lysosome fusion and normal lysosomal degradation, and *glo-1* is required in lysosome-related gut granules, lysosome biogenesis and regeneration. The roles of the mutants we used are presented schematically in Figure 18.

The acute toxicities (measured as mortality) of $AgNO_3$ and CIT-Ag NPs were previously tested [219]. *rme-1*, *rme-6* and *rme-8* mutants were similar to N2 (wild-type strain) in sensitivity to $AgNO_3$ (Fig. 19A): there were no significant differences among strains in $AgNO_3$ toxicity (one-way ANOVA, $p= 0.57$). However, the *rme-1* and *rme-6* strains were more and less sensitive than N2 to $AgNO_3$, respectively ($p<0.05$ in both cases, Kruskal-Wallis test). *rme-8* nematodes were not significantly different from N2 ($p>0.05$, Kruskal-Wallis test) (Fig. 19B). We detected statistically indistinguishable amounts of total silver in all strains of $AgNO_3$-exposed nematodes, consistent with the mortality results. However, in CIT-Ag NP treated nematodes, we found increased and decreased total silver uptake in *rme-1* and *rme-6* respectively, but no significant difference in *rme-8* compared to N2 (Fig. 19C). We also correlated total silver uptake with CIT-Ag NP toxicity, and found a positive relationship between the two variables ($R^2 = 0.74$) (Fig. 19D).

Our results indicated that *rme-6* was more resistant to CIT-Ag NP toxicity, and accumulated less total silver, further supporting a role for endocytosis in CIT-Ag NP toxicity. We also compared the growth inhibition of the mutants to N2s, and found that *rme-6* also showed increased resistance (Fig. 20). We tested across all types of Ag NPs, and *rme-6* was the only one that showed increased sensitivity to CIT-Ag NPs, not to other Ag NPs (Table 4). Others have reported that another endocytosis mutant strain, *rme-2*, was more resistant to gold nanoparticle toxicity than wild type [230]. However,

due to the severe growth retardation of *rme-2* compared to N2, we chose not to use it. The increased uptake and toxicity in *rme-1* mutants was surprising, and may result from either a role for *rme-1* in CIT-Ag NP detoxification pathways, or a generally compromised physiological state that resulted in greater uptake and sensitivity.

3.3.4 Silver toxicity in lysosomal function mutants

cup-5 mutants have excess lysosomes [231] and defective proteolytic degradation in autolysosomes, which leads to inefficient lysosomal regeneration [232]. CUP-5 protein localizes to lysosomes [233], while *glo-1* colocalizes with lysosome-related gut granules (gut granules are intestine specific lysosome-related sites) and encodes a GTPase specific to the intestine [234]. GLO-1 protein is associated with lysosomal biogenesis [235] and gut granule formation [236]. *glo-1* mutants lack autofluorescent gut granules and the acidified endocytic compartment [237]. *cup-4* encodes a putative orphan receptor in *C. elegans* [238] and *cup-4* mutants display severely defective coelomocyte endocytosis [239]. Considering that both *cup-5* and *glo-1* have been shown to be involved in coelomocyte endocytosis as well as deficient lysosomal function, we used *cup-4* mutant as a control to test the effect of coelomocyte endocytosis deficiency only. The two lysosomal mutants (*cup-5* and *glo-1*) and *cup-4* were not significantly more sensitive than N2 to the lethal effects of either $AgNO_3$ or CIT-Ag NPs (Fig. 21A, B) (one-way ANOVA, $p = 0.23$).

Lysosomes are not only associated with cellular degradation processes, but also relate to energy metabolism, cellular signaling and homeostasis [240, 241]. Lysosomal deficient mutants showed more growth inhibition than wild-type upon both $AgNO_3$ and CIT-Ag NP exposures (Fig. 22), suggesting that normal lysosomal function was involved in nematode growth under silver-related stress conditions. There were no statistically significant differences in growth between the mutant strains (two-way ANOVA strain effect for the three mutant not significant, p=0.26; Fig. 21A, B). We next examined reproduction. The four strains (N2, *cup-5*, *glo-1* and *cup-4*) produced similar numbers of offspring under control conditions (EPA water). Dose-dependent reductions in reproduction were observed after exposure to both $AgNO_3$ and CIT-Ag NPs (Fig. 21C, D), which was consistent with other researchers' work on Ag NP toxicity on *C. elegans* reproduction [242]. $AgNO_3$ reduced reproduction capacity at a higher magnitude in the *cup-5*, *cup-4*, and *glo-1* mutants compared to N2; the degree of decrease was comparable in all of the mutant strains (one-way ANOVA, p>0.01 for all pair-wise comparison between *cup-4*, *cup-5* and *glo-1*; two-way ANOVA strain effect for the three mutant not significant, p=0.13). In contrast, while all mutants were also more sensitive than N2 to reproductive impairment by CIT-Ag NPs, the *glo-1* mutants were exceptionally sensitive, almost unable to produce any offspring at all tested concentrations (Fig. 21D). Since *glo-1* mutants were no more sensitive than *cup-5* and *cup-4* to $AgNO_3$, their

sensitivity to CIT-Ag NP-induced reproductive impairment was likely to be derived from a nanoparticle-specific effect.

3.3.5 CIT-Ag NPs but not $AgNO_3$ causes yolk accumulation- mediated inhibition of egg laying in *glo-1* mutants

In order to understand the mechanisms of the impaired reproductive capacity in *glo-1* mutants, we examined nematodes exposed for 96 h from the L4 stage (the same as described in the reproduction assay) using light microscopy. The *glo-1* mutants showed complete egg retention after CIT-Ag NP exposure, with a number of internally hatched offspring irregularly placed in the adult, while *cup-4* and *cup-5* showed regular embryonic developmental progression compared to wild type nematodes (Fig. 23). Considering that *cup-4* produced similar number of offspring compared to *cup-5* after both $AgNO_3$ and CIT-Ag NP exposure and both mutants showed less offspring compared to N2, it was likely that fluid endocytosis to coelomocytes or other coelomocyte-related functions (e.g., roles in innate immune response, detoxification pathways) was important in long-term nematode fitness in stress conditions [243]. However, the control nematodes of those 4 strains (N2, *cup-4*, *cup-5* and *glo-1*) showed similar rate of growth, which was consistent with other studies that these coelomocyte endocytosis and lysosomal deficient genes were not required for growth or survival of nematodes under normal laboratory conditions [243, 244]. Interestingly, the high reproductive toxicity observed in *glo-1* mutants indicated that normal functioning of gut granules was critical in reproductive capacity upon exposure to CIT-Ag NPs.

To examine in more detail the impact of CIT-Ag NP exposure on reproductive abnormalities, we examined the exposed nematodes using Nomarski microscopy. The major difference in *glo-1* mutants due to CIT-Ag NP exposure was the significant amount of yolk present close to the vulva opening (Fig. 24J-L), while N2, *cup-4* and *cup-5* showed similar level of yolk residue compared to controls. There has been a lack of research on the yolk protein accumulation for *glo-1* mutants; however, *sand-1* mutants, which are deficient in the transport of yolk to the yolk granules [245], displayed a similar yolk accumulation phenotype to that which we observed in *glo-1* control (Fig. 24I). Therefore, CIT-Ag NP exposure caused yolk accumulation close to the vulva only in the *glo-1* mutant, and this accumulation likely blocked the transport of embryos through the vulval opening, leading to a severe "egg-retention" phenotype and blocking egg laying in the timecourse of our experiment in the exposed nematodes. Excess yolk accumulation was not observed in nematodes exposed to equi-toxic levels (concentrations between two treatments leading to similar toxicities) of $AgNO_3$ (Fig. 24E-H). Therefore, the reproductive toxicity resulted from CIT-Ag NP exposure resulted from a different mechanism compared to ion-induced reduction in reproductive capacity, indicating a NP-specific effect on the yolk trafficking within the nematodes. The eggs retained in the exposed *glo-1* nematodes were physically dissolved from the adult, with 10% and 0% hatchability observed at 0.5 and 0.75 mg-Ag L^{-1}, respectively.

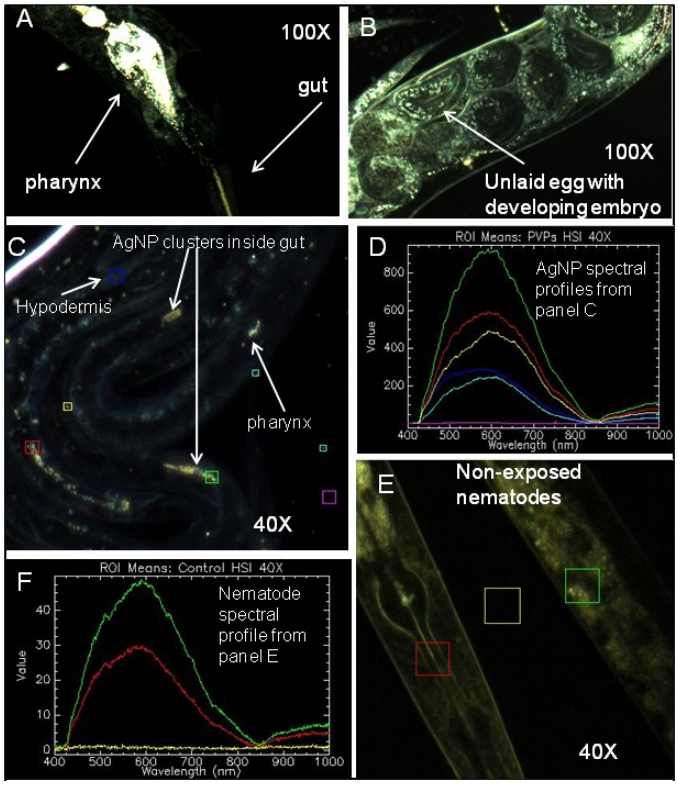

Figure 15. Ag NPs are ingested and internalized into the cells of *C. elegans*.

A) CIT-AgNPs are taken up along with food by *C. elegans*; B) Some CIT-Ag NPs are also taken up into the cells of the nematodes, and are transferred to the offspring. Ag NP identity was confirmed by hyperspectral analysis: C) Hyperspectral image (HSI) showing the presence of PVPs Ag NPs inside and outside *C. elegans* after exposure; colored rectangles correspond to the pixel areas (regions of interest (ROI)) in HSI where spectral profiles are collected; D) The spectral profiles of Ag NPs and hypodermis region of *C. elegans*: green, red, and cyan colored profiles are Ag NPs clusters, white and yellow profiles are hypodermis and background (no silver and no worm). The cyan colored ROI corresponds to a small Ag NP cluster outside the nematode. E) and F) Very little signal is detected in non-exposed nematodes; note that y-axis values are much lower in F) than D); higher contrast was used in E) than C) for visualization. Images taken using

CytoViva hyperspectral imaging technology with darkfield microscopy at 100× (panels A B and E) or 40× (panel E) total magnification.

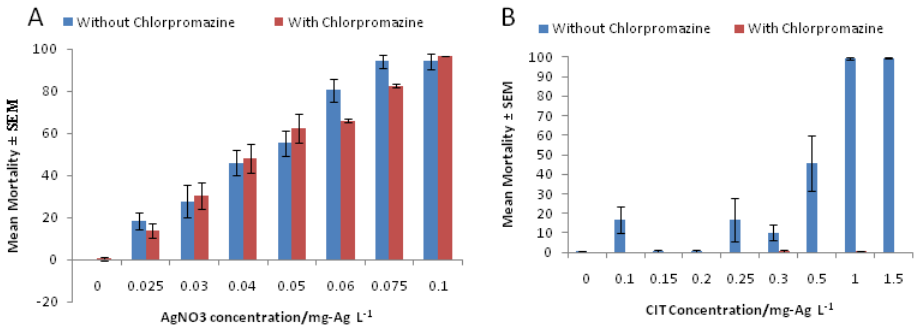

Figure 16: Dose response curves for ionic silver and Ag NP toxicity with and without chlorpromazine.

A) $AgNO_3$ (0.025-0.1 mg-Ag L^{-1}); B) CIT-Ag NPs (0.1-1.5 mg-Ag L^{-1}). Chlorpromazine concentration was 10 mg L^{-1}.

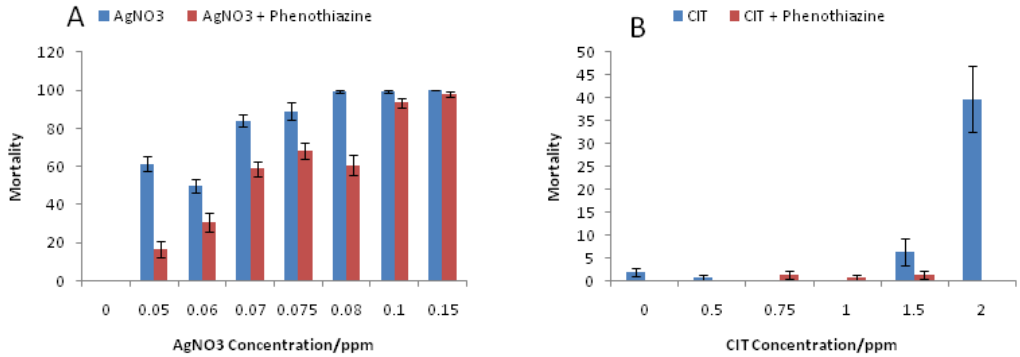

Figure 17: Dose response curves for ionic silver and Ag NP toxicity with and without phenothiazine.

A) $AgNO_3$ (0.05-0.15 mg-Ag L^{-1}); B) CIT-Ag NPs (0.5-2 mg-Ag L^{-1}). Phenothiazine concentration was 10 mg L^{-1}.

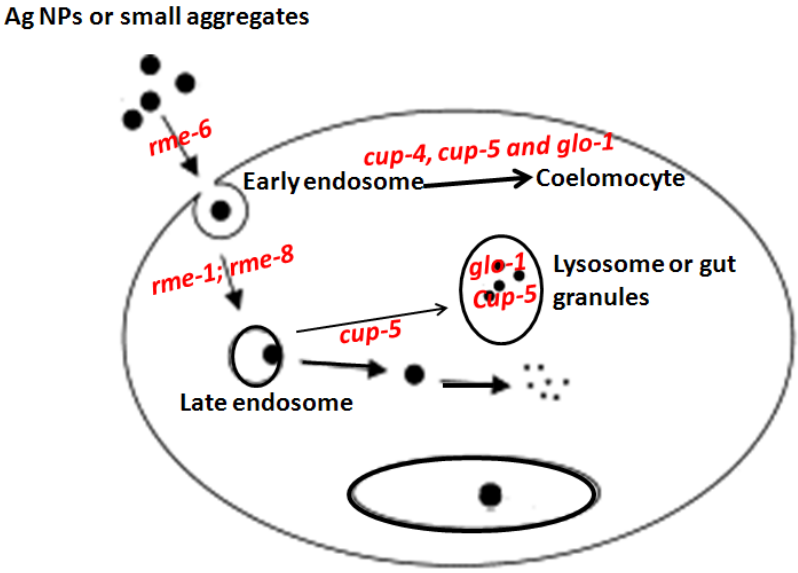

Figure 18: Schematic illustration of endocytosis-related uptake pathways for NPs and all the mutants utilized in this study.

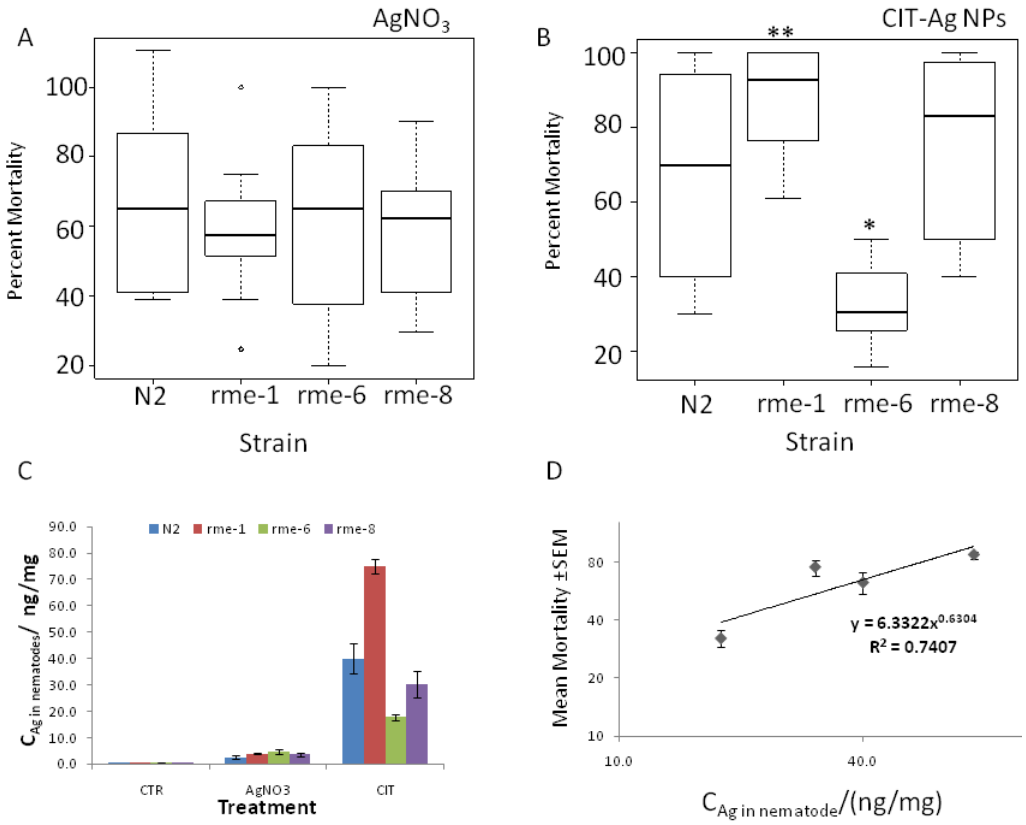

Figure 19: Mutant sensitivity in silver nanoparticle toxicity and nematode total silver uptake.

(A-B) Percent mortality of N2 and endocytosis mutants 24 hrs post exposure to (A) $AgNO_3$ (0.05 mg-Ag L^{-1}) and (B) citrate-coated Ag NP (CIT-Ag NPs) (1 mg-Ag L^{-1}). *indicated that the strain was significantly different from N2. For $AgNO_3$ exposure, N= 18 for each strain ("N" was defined as independent dosing well for acute toxicity tests), with data pooled from 3 separate experiments. For CIT-Ag NPs exposure, N= 12 for each strain, with data pooled from 2 separate experiments. Statistics were done with one-way ANOVA. C) ICP-MS measurements of total silver contents in all strains upon exposure to both $AgNO_3$ and CIT-Ag NPs. For each strain, N=5 for $AgNO_3$ and N=6 for CIT-Ag NPs, and data were pooled from 2 separate batches of nematode samples; D) Correlation

between mean mortality 24 hrs after the silver treatments and total silver concentration in nematodes based on nematode dry weight.

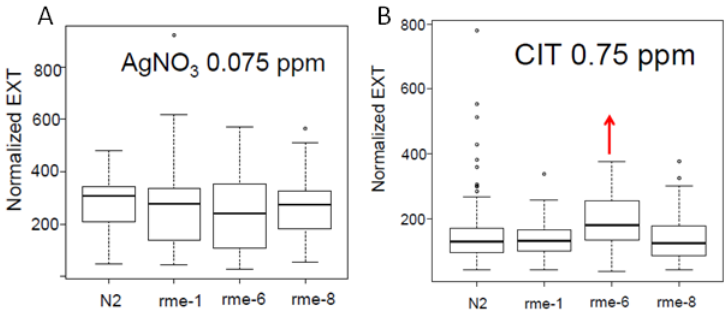

Figure 20: Extinction values (represent growth) of N2 and endocytosis mutants to $AgNO_3$ and CIT-Ag NP exposure.

A) $AgNO_3$ 0.075 mg-Ag L^{-1}; B) CIT-Ag NPs 0.75 mg-Ag L^{-1}. Red arrow indicates increased resistance and asterisk for statistical significance. Boxplots show the 10%, 25%, median, 75% and 90% quantiles of EXT (extinction; a proxy for nematode size) values 72 h post exposure. Asterisks indicate statistically significant differences compared to the Ag NPs alone. The data points are combined from 3 to 4 replicate experiments.

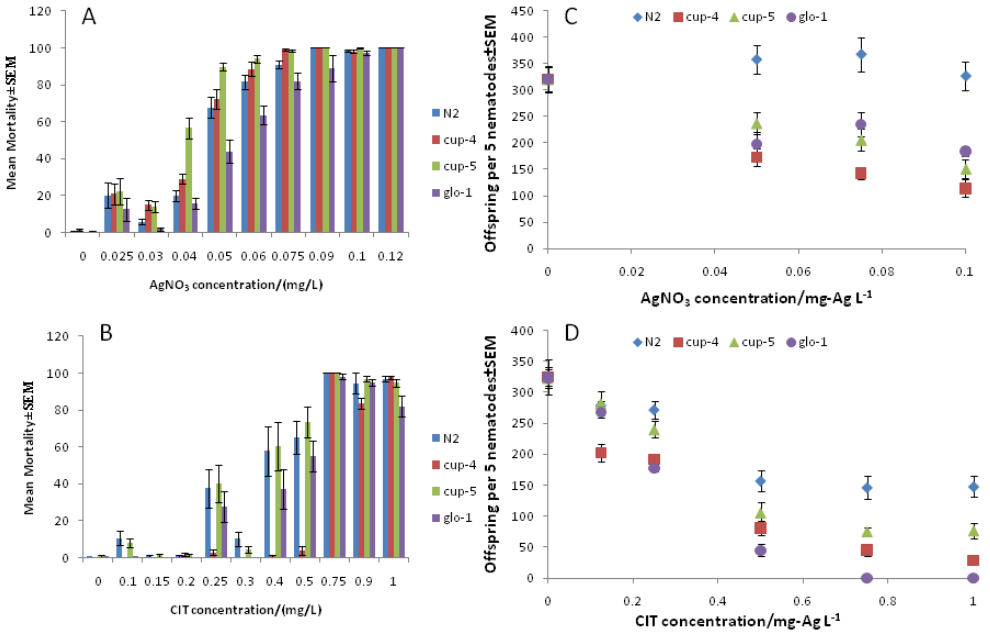

Figure 21: 96 h reproductive capacity (per 5 adult nematodes) of N2 and lysosomal deficient mutants 24 hrs after exposure to $AgNO_3$ and CIT-Ag NPs.

A) $AgNO_3$ (0-0.12 mg-Ag L^{-1}); B) citrate-coated Ag NP (CIT-Ag NPs) (0-1 mg-Ag L^{-1}). *cup-4* mutants were used here as a positive control for deficient uptake into coelomocyte, other than lysosomal dysfunction. Data included 4 replicate experiments, within each experiment, each dosing concentration N=6. Statistical significance was tested using one way ANOVA, and comparisons were performed in pairs at each concentration. We used $p<0.01$ to determine statistical significance.

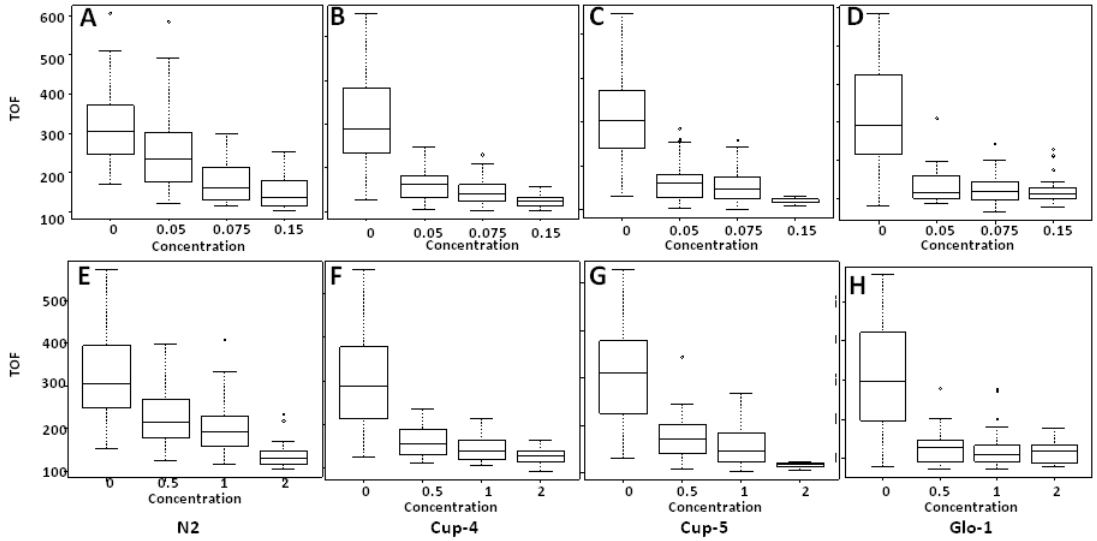

Figure 22: Extinction values (represent growth) of N2 and lysosomal mutants to $AgNO_3$ and CIT-Ag NP exposure.

A) $AgNO_3$ 0.075 mg-Ag L^{-1}; B) CIT-Ag NPs 0.75 mg-Ag L^{-1}. Red arrow indicates increased resistance and asterisk for statistical significance. Boxplots show the 10%, 25%, median, 75% and 90% quantiles of EXT (extinction; a proxy for nematode size) values 72 h post exposure. Asterisks indicate statistically significant differences compared to the Ag NPs alone. The data points are combined from 3 to 4 replicate experiments.

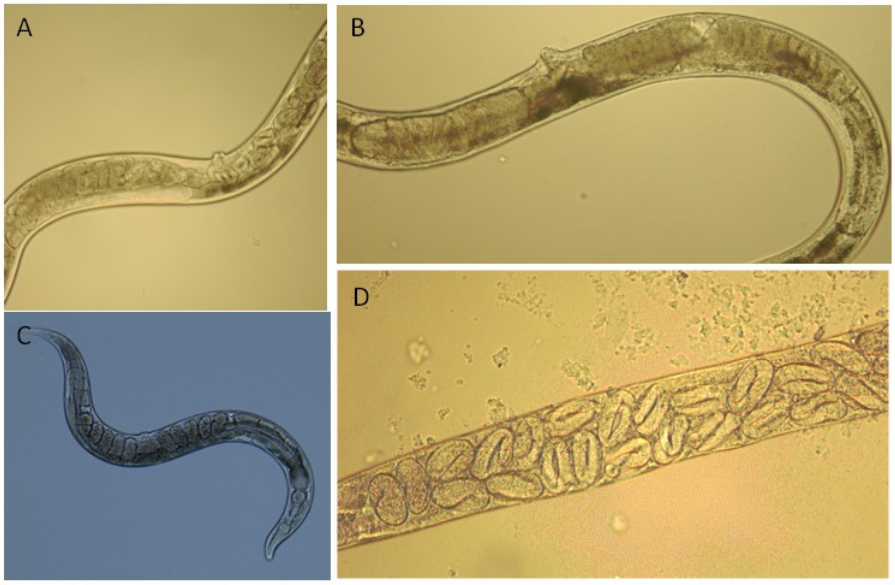

Figure 23: Embryos in four strains of gravid adult *C. elegans* exposed to citrate-coated Ag NPs (CIT-Ag NPs).

A) N2 wild type; B) *cup-5*; C) *cup-4*; D) *glo-1*. CIT-Ag NP concentration was 0.75 mg-Ag L^{-1}.

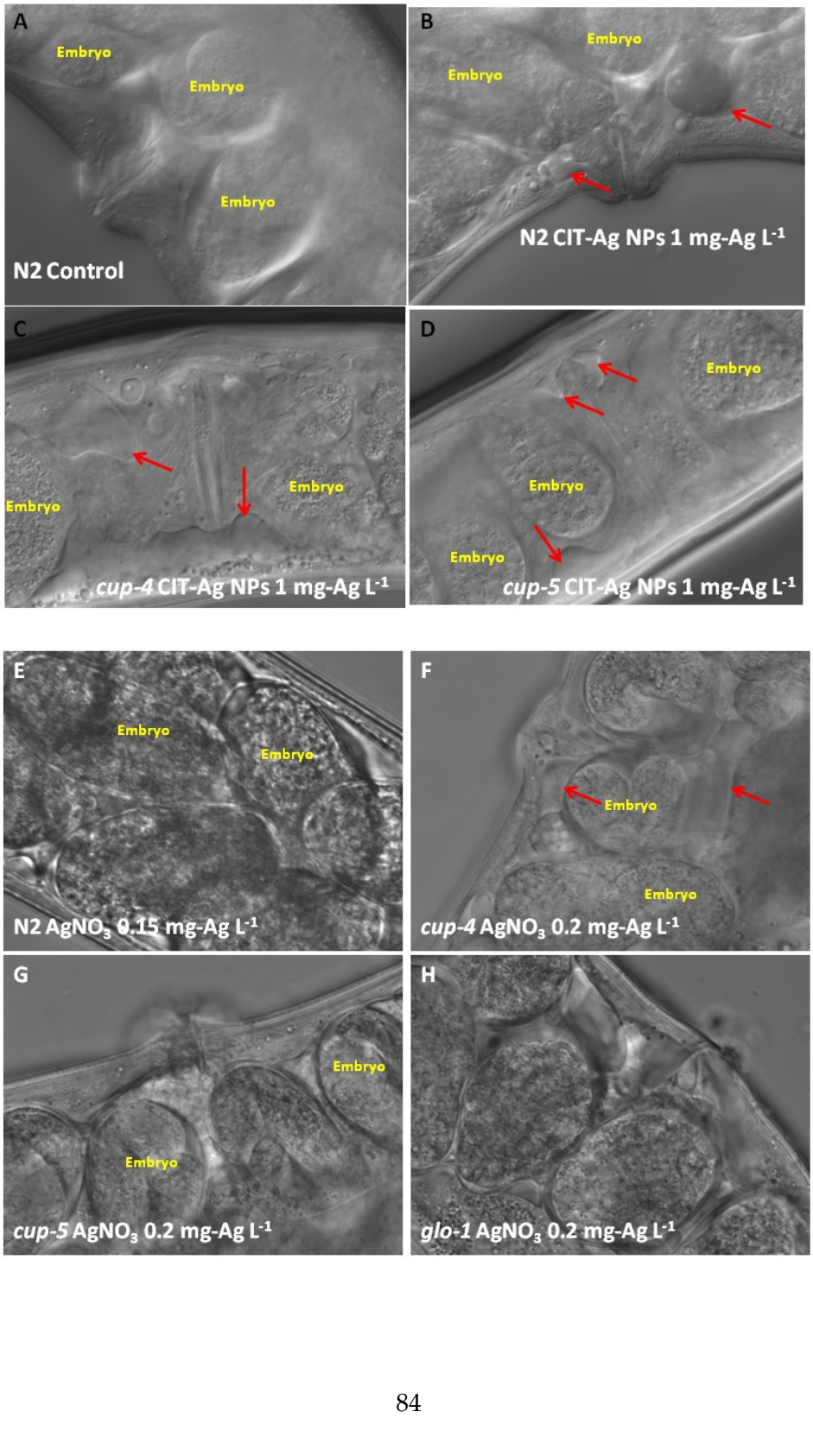
A
Embryo
Embryo
Embryo
N2 Control
B
Embryo
Embryo
N2 CIT-Ag NPs 1 mg-Ag L-1
C
Embryo
Embryo
cup-4 CIT-Ag NPs 1 mg-Ag L-1
D
Embryo
Embryo
Embryo
cup-5 CIT-Ag NPs 1 mg-Ag L-1
E
Embryo
Embryo
N2 AgNO3 0.15 mg-Ag L-1
F
Embryo
Embryo
cup-4 AgNO3 0.2 mg-Ag L-1
G
Embryo
Embryo
cup-5 AgNO3 0.2 mg-Ag L-1
H
glo-1 AgNO3 0.2 mg-Ag L-1

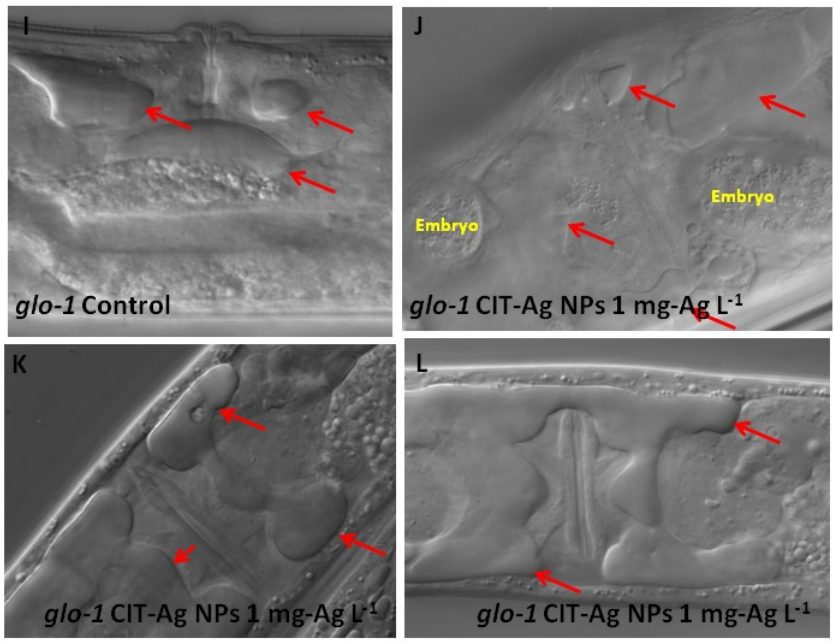

Figure 24: Examination of four nematode strains exposed to both $AgNO_3$ and citrate-coated Ag NPs (CIT-Ag NPs) using Nomarski microscopy.

A) N2 control; B) N2 CIT-Ag NPs 1 mg-Ag L^{-1}; C) *cup-4* CIT-Ag NPs 1 mg-Ag L^{-1}; D) *cup-5* CIT-Ag NPs 1 mg-Ag L^{-1}; E) N2 $AgNO_3$ 0.15 mg-Ag L^{-1}; F) *cup-4* $AgNO_3$ 0.15 mg-Ag L^{-1}; G) *cup-5* $AgNO_3$ 0.15 mg-Ag L^{-1}; H) *glo-1* $AgNO_3$ 0.15 mg-Ag L^{-1}; I) *glo-1* control; J, K, L) *glo-1* CIT-Ag NPs 1 mg-Ag L^{-1}. Red arrows indicate yolk deposits.

Table 4: Mutant analysis (endocytosis deficient strains) for all types of Ag NP exposure.

+ indicates baseline sensitivity; -- indicates increased resistance.

NP	N2	*rme-1*	*rme-6*	*rme-8*
$AgNO_3$	+	+	+	+
PVP_8-Ag NPs	+	+	+	+
PVP_{38}-Ag NPs	+	+	+	+
CIT-Ag NPs	+	+	--	+
GA_5-Ag NPs	+	+	+	+
GA_{22}-Ag NPs	+	+	+	+

4. Silver nanoparticle behavior, uptake, and toxicity in *Caenorhabditis elegans*: Effects of natural organic matter, temperature, sulfidation and mesocosm conditions

4.1 Introduction

Under various environmental conditions, Ag NPs can have different physical-chemical characteristics, leading to varied toxicities [68, 246, 247]. Complex environmental conditions can alter the subsequent fate, transport and toxicity of Ag NPs.

Ecological behavior of silver nanoparticles (Ag NPs) includes: agglomeration, altered ion-release kinetics, and surface modifications, all of which are attracting increased research [117, 248, 249]. Ecological implications of NMs, in terms of its fate and transport in the environment, are widely investigated [63, 165, 249, 250]. Meanwhile, there are increasing investigations on the impact of various environmental factors on Ag NP toxicity; however, the in-depth mechanistic study on those NP-environment interactions are lacking. Therefore, the aim of the work described in this chapter was to understand in-depth how ecological factors affect the biological response to Ag NPs in *C. elegans*.

4.1.1 Effect of natural organic matter on silver nanoparticles

Effect of NOM has become an important factor mitigating the impact of NPs in ecosystems [251]. NOM reduced the dissolution rate of Ag NPs [118] and increased aggregation [252, 253] of both fullerenes and iron oxide NPs due to the formation of bounds among NOM, Ca^{2+} and NPs. Significant reduction of toxicity was shown for

nanoscale zerovalent iron in the presence of NOM [254]. In addition, metal complexation by NOM has been considered and incorporated into environmental prediction models such as the biotic ligand model (BLM) [251].

In aquatic ecosystems, natural organic matter (NOM) plays an important role in the environmental fate and transport of NPs by influencing their physicochemical properties [251, 255-257] and therefore altering their agglomeration [258], bioavailability and toxicity [50, 125, 126, 259, 260]. For example, adsorption of NOM on NP surfaces results in a more stable aqueous suspension due to steric stabilization or electrostatic repulsion between particles [246, 261-266]. The NOM-NP interaction is strengthened in high salinity media [267]. Different types of NPs have variable binding sites in NOM structures, and NOM properties (carboxylate and thiol content, aromaticity and molecular weight) also affect NOM-NP interactions [255, 268, 269]. However, studies related to NOM-NP interactions *in vivo* have been limited.

Previous work indicates that in complex environmental media, Ag NPs can have different physicochemical characteristics, bioavailability, and toxicity [68, 246, 247, 270]. NOM has been found to mitigate the toxicity of various types of nanoparticles, e.g., Ag NPs [271], quantum dots (QDs) [272], functionalized cerium nanoparticles [273], CuO nanoparticles [274], etc. Humic acid reduces Ag NP toxicity to biofilms, due to binding to silver ions [271]. In addition, a *Daphnia* study showed a linear decrease in Ag NP toxicity with increasing concentrations of Suwannee River humic acid [275]. The

purpose of our study was to investigate how NOM affects Ag NP behavior in our test medium, and how it affects toxicity *in vivo* in the model organism, *Caenorhabditis elegans* (*C. elegans*). However, there is a lack of information on the understanding of how NOM-NP interactions affect the biological response. In addition, if NOM does rescue Ag NP toxicity, this can further strengthen the evidence for the mechanism of Ag NP toxicity.

4.1.2 Effect of temperature on Ag NPs

Temperature frequently alters chemical toxicity, due to changes in metabolic rate, chemical behavior and combined stress resulting from deviations from optimal temperatures. Temperature is also a major factor determining the dissolution rate of Ag NPs, with increasing storage temperature causing higher silver ion release, which leads to more toxicity [276]. Ionic silver binds to biotic ligands including algae, fungi, and other dead biomass in aquatic systems. This adsorption capacity can be decreased by increasing temperature [277]. On the organismal level, increasing temperature can result in a rise in metabolism below its upper critical limit, leading to increases in oxygen consumption and hemoglobin concentration [278, 279]. In addition, temperature also affects biochemical reaction rates, leading to alterations in the level of intermediate metabolites in the organism [280, 281].

4.1.3 Effect of sulfidation on silver Ag NPs

Sulfidation of NPs has been widely used to create hollow nano-structures in the fields of electronics, optics, catalysis, etc. [282, 283]. Also in nature, sulfidation is one of

the most likely transformations for silver nanoparticles [284], due to the relatively high affinity of S to Ag [165] and ubiquitous nature of reduced S species especially in anaerobic environment. The ratio of Ag to S varies depending on availability of S in the environment, and in some S-rich environment such as wastewater stream, this ratio can be close to 1 [285]. The formation of Ag_2S, either in micro or nano-scales [285], can lead to alterations in surface properties, aggregation status and oxidative dissolution of Ag NPs [284].

Other environmental variables, e.g., ultraviolet radiation, can also cause alterations in the physicochemical properties of Ag NPs, including a decrease in particle size and the formation of a core-shell structure [286].

4.2 Materials and Methods

4.2.1 Nanoparticle and NOM Characterization

The NPs used in this study were of different sizes (8~50 nm in monomer size) and surface functionalizations (citrate, polyvinyl pyrrolidone (PVP), or no functionalization). We used two types of functionalization. The first was previously characterized PVP-functionalized NPs (herein referred to as PVP_8- Ag NPs and PVP_{38}-Ag NPs, where the subscript indicates monomer diameter in nanometers) [187]. The second, citrate-functionalized Ag NPs (herein referred to as CIT-Ag NPs), were prepared using the same method as previously described [31]. However, the size distribution was larger (25 nm ± 9 nm) in the batch used in this study. The non-functionalized Ag NPs were

prepared by the Choi lab (University of Seoul), as described [287]. Pony Lake and Suwannee River fulvic acid (PLFA and SRFA) isolates (1R109F and 2S101F, International Humic Substances Society) were selected as two representative aquatic humic substances derived from autochthonous and terrestrial carbon sources. The NOM stock solutions were made by dissolving NOM powder in ultrapure water (> 17.8 MΩ·cm, Barnstead Nanopure, Thermo Scientific, US) and adjusting the pH to 6.0 with NaOH. The resultant NOM stock solutions were subsequently filtered to <0.2 μm, and the NOM concentration was determined using a Total Organic Carbon (TOC) Analyzer (TOC-L CPN, Shimadzu, Japan). Characterization of NOM is summarized in the Table S1 of the Supporting Information of Deonarine et al., 2011 [255].

4.2.2 Transmission Electron Microscopy (TEM) and Energy-Dispersive X-ray Spectroscopy (EDX) sample preparation and analysis

TEM sample preparation was as described in the method section of Chapter 3. For EDX samples, both osmium treatment and post-staining were omitted to avoid interference with silver peaks. EDX analysis was performed using an Oxford Instruments (San Jose, California, USA) LN2 Energy Dispersive X-Ray Spectroscopy Detector.

4.2.3 CytoViva hyperspectral image analysis

Samples were examined using darkfield-based hyperspectral imaging microscopy as described [288]. A few representative darkfield images were also collected to show uptake of NP or NP-PLFA complex in *C. elegans*. The optical

microscope (Olympus BX41) equipped with hyperspectral imaging spectrometer (CytoViva Hyperspectral Imaging System (HSI), Auburn, AL) and a novel illumination system with both Koehler and Critical illumination allowed direct visualization as well as spectral analysis of Ag NP and PLFA in the samples. All images were acquired under wet-sample conditions at identical gain (set at 5) and exposure time (set at 250 ms). In brief, the following steps were adapted to produce the final classification images: 1) hyperspectral images were treated to minimize the noise and decrease the dimensionality of the image data, 2) n-dimensional visualization was performed to identify the spectrally active endmembers, 3) the endmembers were matched with a spectral library of representative elements of the test sample using a spectral angle mapper (SAM) algorithm (threshold= 0.25 rads 0 radian corresponds to 100% match), and 4) SAM-matched endmembers were then applied to the hyperspectral image to produce the final classification image, which shows the location of the endmembers of interest (library spectra) and the corresponding spectra. The examination was done with the guidance from Appala Raju Badireddy.

4.2.4 Dissolved silver speciation calculation

This was calculated using MINEQL+ (Version 4.5); see Supporting Information for details. In brief, measured dissolved silver concentrations were used as the model input for total silver concentration. Concentrations of major inorganic ligands (e.g., Cl^-, $SO4^{2-}$) were based on EPA water recipe. Complexation of dissolved silver by PLFA was

modeled as interactions with two types of metal binding sites on the fulvic acid: "weak" binding sites that are likely to consist of carboxylate, phenol, or amine functional groups [289] and "strong" binding sites that comprise thiol functional groups [158, 290]. The molar concentration of each type of binding site was calculated by multiplying the PLFA concentration and the site density [289-291].

The speciation of dissolved silver was calculated using MINEQL+ (Version 4.5) for the experimental mixtures of silver nanoparticles with Pony Lake fulvic acid (PLFA). The calculations were performed for a solution of EPA water (Table 5 and 6), at pH 7.8 and 25ºC. The total carbonate concentration was set equal to 1.14×10^{-3} M.

Complexation of dissolved silver by PLFA was modeled as interactions with two types of metal binding sites on the fulvic acid: "weak" binding sites that are likely to consist of carboxylate, phenol, or amine functional groups and "strong" binding sites that comprise thiol functional groups. The molar concentration of each type of binding site was calculated by multiplying the PLFA concentration (in mg-C per L) and the site density (in mol per mg-C).

The density of weak silver-binding sites was estimated to be $(1.71\pm0.15)\times10^{-6}$ mol per mg-C, which was an average of three fulvic acids reported by Sikora and Stevenson [292]. These sites have an average silver binding affinity corresponding to:

$$Ag^{+} + NOM_{weak} <-> Ag\text{-}NOM_{weak} \qquad K_{weak} = 10^{3.76}$$

The concentration of thiol functional groups in PLFA is currently not available from the literature. Therefore, we performed the speciation calculations for a range of thiol site densities. This range of values was based on the reduced sulfur (reduced-S or S_{red}) content for PLFA and the concentration of strong binding sites quantified for Ag^+ and Hg^{2+} binding with other aquatic NOM isolates. For PLFA, the percentage of total sulfur as reduced-S is 68.2% [293], corresponding to a reduced-S content of 1.2×10^{-6} mol-S_{red} per mg-C of PLFA, which has a total sulfur content of 3.03% (mass fraction) (from the website of the International Humic Substances Society [294]).

A fraction of the reduced-S in NOM is expected to comprise strong binding sites (i.e. thiols) for soft sphere metals such as Hg^{2+} and Ag^+ [291]. In previous studies with other aquatic humic substances, the estimated proportion of the reduced-S as strong binding sites for Ag^+ and Hg^{2+} was between 0.6% and 1.6% [290, 291]. If these values apply to PLFA, then the density of strong binding sites would be approximately 7×10^{-9} to 2×10^{-8} mol per mg-C. In this paper, silver speciation calculation were performed under three scenarios, i.e. with the strong binding site density set equal to 4.0×10^{-9}, 1.0×10^{-8} and 2.0×10^{-8} mol per mg-C, respectively, as the lower range, a median value and the upper range (Table 7).

The Ag^+ affinity for the strong binding sites was estimated from the typical value corresponding to Ag^+ complexation with low molecular weight thiols [158]:

$$Ag^+ + RS^- \text{ <-> } RS\text{-}Ag \quad K_{strong} = 10^{12}$$

where the pK_a for the thiolate group was estimated to be 9 [295].

The total dissolved silver concentrations for the calculations corresponded to measured mean concentrations in the supernatant after ultracentrifugation of the mixtures (Table 8).

4.2.5 Ag NP dissolution experiment and nematode Ag content

Samples of CIT-Ag NPs and NOM mixture were prepared in EPA water [31] with 5 mg-Ag L^{-1} of CIT-Ag NPs and 0, 1, 5, or 10 mg-C $L^{-1}$of PLFA, sealed inside 4.5-mL Ultra-Clear centrifuge tubes (Beckman Coulter, US) with 3 layers of parafilm and a headspace of ~0.5 ml, and then held static in the dark for 24 h. Six replicate samples were prepared for each PLFA concentration. After 24 h, the samples were centrifuged at 370,000 g for 30 min, and the silver concentration in the supernatant was quantified by inductively coupled plasma – mass spectrometry (ICP-MS) (Agilent 7700x, Agilent Technologies, NC, US). The separation procedure was verified by use of control samples spiked with Ag NPs, and subsequent ultracentrifugation resulted in removal of no less than 98% of the silver from solution. In contrast, ultracentrifugation of samples containing 0.05 to 1 mg-Ag L^{-1} silver (added from dissolved $AgNO_3$ stocks) with 10 mg-C L^{-1} PLFA produced minimal sedimentation with a large percentage of silver (88%-95%) remaining in supernatant (Fig. 25).

For measurement of nematode silver content, exposed organisms (after 24 h exposure, $AgNO_3$ at 0.3 mg-Ag L^{-1}, CIT-Ag NPs at 10 mg-Ag L^{-1} with and without 10

mg-C L^{-1} of PLFA) were transferred to clean EPA water with food for 2 h to allow clearance of material from the gut (verification was done by microscopic analysis of nematode gut). Next, worms were centrifuged at 2,200 rpm for 2 min, rinsed with EPA water 3 times, and freeze-dried (Labconco, US) for 2 d. Resultant samples were digested with concentrated nitric acid (70%, Fisher Scientific, US) at ~ 90 °C for 4 h. The digest was diluted with ultrapure water, held overnight at room temperature (22 -23 ºC), and further diluted with mixed acid (2% HNO_3 and 0.5% HCl) prior to ICP-MS analysis.

4.2.6 Dynamic Light Scattering (DLS) size and zeta potential measurements

Average hydrodynamic diameters and zeta potential of the Ag NPs under typical exposure conditions (i.e. 5 mg-Ag L^{-1} of CIT-Ag NPs in the presence or absence of PLFA at 10 mg-C L^{-1}) were measured using a Zetasizer Nano-ZS instrument (ZEN3600, Malvern Instruments). Z-average hydrodynamic diameters were measured by analyzing the intensity fluctuations of light (wavelength = 663 nm) backscattered at 173°.

4.2.7 Mesocosm experiments

The effect of complex environmental on Ag NP toxicity was investigated using mesocosms modeled after North Carolina wetlands. 19 mesocosms were established in the Duke Forest, Durham, NC, USA. Mesocosms were built with wood and lined with polypropylene. Each mesocosm had three compartments, terrestrial, transitional, and aquatic environments. To establish a sustainable ecosystem, pristine groundwater, wetland riparian soil and a number of aquatic and terrestrial plants were incorporated

into the mesocosms. Details of mesocosm facility, experimental design, and treatment methods were described in Colman et al., 2013 [296].

Mesocosms were dosed with 2.5 mg-Ag L^{-1} as GA-Ag NPs, PVL-Ag NPs and $AgNO_3$. Mesocosm water was sampled at three different time points (right after spike, 1 week after spike and 2 weeks after spike) were included in the experiments. All of our experiments used L1 stage larvae ("L1s") obtained via bleaching and overnight hatch of embryos in the absence of food to obtain age-matched individuals [144, 145]. The volume of water samples added was balanced by addition of the same volume of 2X EPA water to ensure a final ionic strength equivalent to EPA water (1X). Four replicated dosing wells were assigned for each water sample, with 50 nematodes per well. UV-killed bacteria were used in the experiment to eliminate indirect effect on food quality upon exposures [94]. Detailed information of the growth assay has been described previously [51].

4.3 Results and Discussions

4.3.1 Characterization of nanoparticles

Experiments were performed with 4 different Ag NPs; characterizations of all have been previously published [51]. All Ag NPs were roughly spherical and polydisperse in purified water. Monomer diameters (mean particle size ± standard deviation) of PVP_8, PVP_{38}, non-coated and CIT-Ag NPs were 8±2 nm, 38±8 nm, 20 nm (SD not reported), 25±9 nm, respectively, as measured in TEM images. Hydrodynamic

diameter and zeta potential after one h in the exposure medium (EPA water) for the same particles were 129±6 nm and -21± 0.1 mV (PVP_8- Ag NPs), 72±1 nm and -12± 1.3 mV (PVP_{38}- Ag NPs), 41±3nm and -24± 0.7 mV (CIT-Ag NPs), and 122±4 nm and -24± 0.6 mV (non-functionalized).

4.3.2 Bacterial food decreased toxicity

Early in our investigations we found that food (UVC-inactivated bacteria) had a strong mitigating effect on Ag NP toxicity (Fig. 26). While this was consistent with a study on *Daphnia magna*, which showed a 40-fold decrease in lethality when food was added [297], by contrast, increased lethality was observed for amphipods exposed to quantum dots (QDs) via algal food source, although the uptake of QDs was lower than that observed for water-borne QDs [298]. No food was added in the studies within this chapter to avoid confounding effect.

4.3.3 Comparing rescue effect between PLFA and SRFA

PLFA rescued the toxicity of ionic Ag and Ag NPs more effectively than did SRFA (Fig. 27A-E) ($p<0.05$, using the Wilcoxon rank sum test with continuity correction). Observed differences between the two fulvic acids on Ag NP toxicity may be related to their compositional differences. Chelating ligands such as low molecular weight thiols reduce the toxicity of Ag NPs for *C. elegans*, either by binding to Ag+ ions in solution or sorbing to Ag NP surfaces [187]. While the Ag^+-binding capacities of the fulvic acids were not directly known, clues to their Ag-binding affinity could be gained by their

elemental composition. For example, the nitrogen content of the NOM isolates, a possible indicator of amine ligand groups, was greater with PLFA (6.5% N) relative to SRFA (0.72% N).[299] Likewise, PLFA contained greater sulfur content (3.0% S) relative to SRFA (0.44% S) in which about 53% to 72% of the sulfur comprises of reduced-S moieties (such as thiols) that were strong binding sites for Ag^{+} [293]. Therefore, the potential differences in Ag-binding capacities for the NOM isolates were consistent with the differences in toxicities for the Ag-PLFA and Ag-SRFA mixtures.

Other molecular characteristics of NOM could be predictors of surface association with the Ag NPs. For example, aromatic carbon content and specific UV absorbance at 280 nm (an indicator for aromaticity) for PLFA (12% aromatic C and 1.8 L mg-C-1 m-1) were less than the respective values for SRFA (24% and 2.7 L $mg\text{-}C^{-1}$ m^{-1}) [255]. Moreover, the average molecular weight (MW) of PLFA (1000-1300 Da) [255, 300] was slightly smaller than the average MW of SRFA (above 1360 Da) [301]. High aromaticity and high molecular weight of NOM tend to correlate with greater interaction with nanoparticles, and could explain observed decreases in aggregation rates [255] and other surface reactions such as dissolution [118]. However, this possibility would not explain our observation that PLFA is more effective than SRFA at decreasing Ag NP toxicity, suggesting that the content of N and S may be more important in this case than simply aromaticity or MW.

Comparisons of the four types of Ag nanoparticles indicated differences in the rescue effect by NOM. For example, the presence of NOM caused a greater decrease in mortality for PVP-coated Ag NPs (Figure 27C and 27D) than CIT-Ag NPs (Figure 27E). The surface coating on the nanoparticles was a possible factor in these differences. We note, however, that the total silver concentrations varied between the Ag NPs. (They were based on LC_{95} concentrations for each Ag NP without added NOM). Thus, the role of the surface coating was not a primary objective of this study. A more detailed study would require additional experiments under a range of silver and NOM concentrations for each Ag NP and in-depth analysis of dissolution, aggregation, and uptake.

To further investigate the mechanistic basis for protective effect of NOM, we conducted additional studies with CIT-Ag NPs and PLFA. We chose to focus on CIT-Ag NPs because it was the least toxic of the tested Ag NPs (comparative dose-responses are provided in Fig. 28) and therefore could be used at the highest concentrations facilitating microscopic imaging. We focused on PLFA because it showed a greater rescue effect than did SRFA.

4.3.4 PLFA-CIT-Ag NP Interactions

I first examined the effect of PLFA on CIT-Ag NP aggregation, but observed no significant alterations over 24 h after mixing (Fig. 29A).

The zeta potential of particles (ranging from -29.3±0.9 to -29.9±1.6 mV) also did not change appreciably after CIT-Ag NPs and PLFA were mixed. Hyperspectral

imaging-based detection of feature similarities between the CIT-Ag NP+PLFA mixture in medium (library) and CIT-Ag NP+PLFA exposed *C. elegans* imaging data (Figs 30A and D) confirmed the presence of CIT-Ag NP-PLFA complex inside nematodes (Spectral match ≥ 70%). Spectral profiles of only PLFA and only CIT-Ag NPs are shown in Figs 30 B and C, respectively.

Next an effect of PLFA on dissolution was tested, since NOM can either enhance or inhibit oxidative dissolution by ligand-promoting processes or steric protection, respectively [302]. The dissolved Ag concentration increased from 250 nM to 450 nM Ag as PLFA concentration increased from 1 mg-C L^{-1} to 10 mg-C L^{-1} (Fig. 29B). However, the extent of dissolution did not coincide with our toxicity results (lower toxicity with increasing PLFA concentration: Fig. 27E), and thus failed to explain PLFA's protective effect.

The amelioration by PLFA of Ag NP toxicity could also result from complexation of bioavailable forms of dissolved Ag (i.e. Ag^{+}). To test this hypothesis, equilibrium speciation calculations were performed to determine how PLFA might affect dissolved silver speciation. Although complexation of Ag by strong binding sites associated with NOM was dependent on the Ag-binding site densities used for calculation (Fig. 31), speciation calculations generally did not indicate a marked decrease of free Ag^{+} with increasing concentrations of PLFA.

Even if a high thiol content (20 nmol per mg-C) was assumed for PLFA, the free Ag^{+} at 1 mg-C L^{-1} was approximately equal to the calculated Ag+ concentration at 10 mg-C L-1, but mortality was drastically different at these two PLFA concentrations (100% and 0%, respectively) (Fig. 27E). Therefore, the effect of PLFA on dissolved Ag speciation was inconsistent with trends in toxicity; and, it is unlikely that PLFA complexation of Ag^{+} contributed to the rescue effect.

Interactions between NOM and NP might alter NP surfaces by functionalizing them and such properties could subsequently alter NP surface attachment (or agglomeration) mechanisms [303, 304]. However, this NOM-NP interaction was strongly dependent on NP functionalization, NOM concentration [257], and other environmental variables (pH and ionic strength) [264]. Interaction between PLFA and CIT-Ag NPs was examined using a dark-field hyperspectral imaging system, which revealed the formation of NP-PLFA structures (Fig. 32A-D). In addition, however, it was found that nematodes altered the CIT-Ag NP-PLFA interaction (Fig. 33). Unusual structures appeared outside nematodes where they formed "rings". Such structures were absent when nematodes were not present (Fig. 33A-C). Hyperspectral analysis of "ring structures" confirmed presence of Ag NP clusters. Mapping and spectral analysis revealed that PLFA sequestered and surrounded CIT-Ag NPs partially or completely, thereby inducing ring-like structures (Figs 34 and 35). We postulate that formation of

ring-like structures provides a protective response, altering the nanoparticle-organism interaction.

4.3.5 PLFA effect on total silver uptake

Since the rescue effect of PLFA could not be attributed to altered aggregation or dissolution, nematode uptake of Ag NPs was examined. We exposed nematodes to CIT-Ag NPs in the presence and absence of PLFA and allowed their gut contents to clear for 2 h by transferring the exposed nematodes to clean media with bacteria. Our initial studies confirmed that 30 min was sufficient for young adults to clear bacterial food. To separate nematodes from NPs in the medium (EPA water), nematodes were washed three times by centrifugation (2,200 rpm for 2 min) and followed this with removal of supernatant. The resultant pellet was freeze-dried for 2 d. The purpose of gut clearing and washing process was to remove most of the CIT-Ag NP aggregates loosely associated with nematode gut and cuticle surfaces (verification of removal was illustrated in Table 9). Total Ag uptake was measured by ICP-MS analysis of batches of whole nematodes. PLFA reduced silver concentrations *in vivo* after exposure to $AgNO_3$ (Wilcoxon rank sum test; $p = 0.008$; N=5) (Fig. 36). However, there was no effect of PLFA on nematode silver uptake after CIT-Ag NP exposure (Wilcoxon rank sum test; $p = 0.9372$; N=6). The silver content in the control samples (CTR and PLFA) and $AgNO_3$+PLFA samples are close to the limit of detection; silver contents in other samples were well above the limit of detection.

4.3.6 Persistence of CIT-Ag NPs in the gut of *C. elegans*

Differential toxicity after PLFA exposure in the absence of a difference in total organismal CIT-Ag NPs could be explained by uptake within certain individual organisms. To detect altered uptake/distribution in specific tissues, exposed nematodes were first examined using darkfield hyperspectral microscopy. Ag NP uptake was found in tissues both with and without PLFA (Fig. 37C-H). However, most CIT-Ag NPs remained in the gut (Fig. 4). The NPs persisted in the alimentary canal even after 24 h in fresh medium (Fig. 38), suggesting that the ICP-MS measurements described above were dominated by CIT-Ag NPs in the gut. Persistence of Ag NPs was also detected in the liver and spleen of exposed rats after a wash-out period up to 8 weeks [124]. Cellular uptake was further confirmed with EDX analysis in CIT-Ag NP-exposed nematodes with and without PLFA (Fig. 39A-B); unfortunately, quantitative comparisons were not possible due to the low signal for silver in the EDX spectrum. In the presence of PLFA in exposed nematodes, CIT-Ag NPs appeared to be tightly associated with the compound (Fig. 40A, B), and CIT-Ag NP size distribution in nematodes varied from largely dispersed to compact aggregates (at regions of accumulation) (Fig. 40D).

From the hyperspectral imaging, it was obvious that the gut was the principal site of uptake. The next question was whether this led to incorporation in specific cells of exposed nematodes. Therefore our emphasis in conducting transmission electron microscopy (TEM) analysis was to focus on intestinal lumen, luminal wall and epithelial

cells. In addition, I surveyed cells of the gonad and the muscle layer at the periphery and subjacent to the cuticle. A minimum of 10 nematodes per treatment were included in our ultrastructural analysis.

4.3.7 $AgNO_3$ and CIT-Ag NP produced cellular alterations

To explore tissue, cellular and subcellular distribution differences, and to determine alterations resulting from exposure, TEM was performed. In previous cell culture-based uptake studies with human macrophages, Ag NP deposits were mostly found in the cytosol, nucleus, and lysosomes [305]. An earlier whole-organism study indicated that Ag NP uptake occurred in gut epithelium, and the route of internalization was different for ionic and nanoparticulate Ag [212].

The ultrastructure of normal *C. elegans* is well established in the worm atlas (www.wormatlas.org) and worm book [306], and our observations of control nematodes were consistent with that previously described ultrastructure. The *C. elegans* intestine was composed of large, cuboidal epithelial cells. Outside the intestinal cells were the gonadal tissue, muscle tissue, and the cuticle at the worm surface. The intestinal cells had microvilli lining the lumenal surface. The gut epithelial cells contained nuclei with electron dense nucleoli. Organelles of the gut epithelial cells included numerous mitochondria, lysosomes, autophagosomes and peroxisomes. Gonadal cells were easily differentiated from gut epithelial cells by their more superficial location between between gut epithelial cells and overlying myocytes located immediately beneath the

cuticle. In addition, the gonadal cells exhibited higher electron density than seen in the gut epithelial cells and contained prominent nuclei and nucleoli. Gut epithelial cells were larger than gonadal cells.

Ultrastructural alterations resulting from exposure to $AgNO_3$ included severe swelling of intestinal epithelial cells with enlarged mitochondria showing altered shape and evidence of inner compartment swelling with rearrangement of cristae. Affected epithelial cells formed oval and expanded features at border of intestine (Fig. 41D-E). Plasma membranes of affected epithelial cells were apparently intact and thus these cells were clearly distinct from the surrounding gonadal cells. Figure 41D shows affected, apparent gonadal cells that were peripheral to the intestinal epithelial cells and between them and the outer layer of myocytes. Bizarre zones (arrow head) with low electron density were likely swollen and severely altered gonadal cells.

Intestinal epithelial cell damage was observed after exposure to CIT-Ag NPs; however, affected cells in CIT-Ag NP-treated nematodes revealed high amplitude swelling (Fig. 41G) when compared to $AgNO_3$ exposed cells (above). Figure 41H, an enlargement of a portion of Fig. 41G, shows peripheral relocation of organelles including mitochondria, lysosomes and/ peroxisomes [307] not seen in $AgNO_3$ treated nematodes. Note the three enlarged spaces (arrowheads) between intestinal epithelial cells and myocytes. These likely represent lysis of gonadal epithelial cells. CIT-Ag NPs definitely induced greater alteration than did $AgNO_3$. Whether this constitutes evidence for a

different mechanism of toxicity needs to be addressed in further studies. Since the doses used were similar in terms of organismal toxicity (~24 h LC_{75}), there may be different mechanisms.

4.3.8 PLFA protected against cellular damage from CIT-Ag NPs and $AgNO_3$

Importantly, $AgNO_3$-induced alterations were rescued in the presence of PLFA (Fig. 41F), as indicated by the intact intestinal, non-swollen epithelium with orthodox mitochondrial morphology and absence of alterations to gonadal epithelium in the $AgNO_3$+PLFA treated nematodes (Fig. 41F and Fig. 42A). Interestingly, PLFA also rescued CIT-induced damage, as demonstrated by intact and non-swollen intestinal epithelial cells, orthodox mitochondria and unaltered gonadal cells (Fig. 41I-J).

I attempted to use EDX to verify silver uptake at the cellular level, by using a modified fixation protocol that eliminated heavy metals, and while there was silver signal detected in both CIT-Ag NPs and CIT-Ag NP+PLFA treated nematodes, with signals close to the detection limit (0.5% of all elements down to carbon in atomic weight). However, due to the lack of osmium in the fixation process and post staining, the TEM images associated with EDX analysis had significantly reduced quality (i.e., resolution) obviating our attempts to localize silver signal to specific cells (Fig. 39).

Our review of relevant *C. elegans* literature showed that intestinal epithelium is comprised of 20 non-renewable cells which form a primary line of defense against pathogen invasion [308] and dietary toxins. Nuclei are often evaluated in studies of

necrosis and apoptosis [309, 310]. However, given the small number and therefore large volume of intestinal epithelial cells our planar analysis resulted in few nuclear profiles and these were only in sections of control organisms. I cannot definitively use nuclear alterations to state whether necrosis has occurred. However, our observations of swollen cells in exposed animals with mitochondrial alterations indicated these cells were susceptible to damage from $AgNO_3$ and CIT-Ag NPs. If intestinal epithelial cells are non-renewable, such changes could lead to irreversible damage in the host. Furthermore, the use of dietary administration argued that these epithelial cells were altered despite a normal appearing brush border with orthodox microvilli. The mechanism of uptake [311] therefore is one that involves microvesicular transport [312]. Cellular swelling of high amplitude was observed in the intestinal epithelium and in gonadal epithelial cells. This suggests migration of metal particles from altered intestinal epithelium to gonad. As indicated in the hyperspectral imaging studies, the major uptake site of NPs was the gut (Fig. 40-41), and this coincided with the finding that gut epithelium was the primary target for damage after both $AgNO_3$ and CIT-Ag NP exposure.

I considered the possibility that lysosomes were important in the uptake or effects of Ag NPs. Lysosomes are a common organelle responsible for sequestration of intracellular metal (both in ionic and nanoparticle form) [229]. Lysosomes have distinctive characteristics including an acidic interior (pH = 4.5~5), and the presence of

several acid hydrolases, esterases and other associated digestive enzymes [229, 313]. Acidic environments accelerate ion release from several metallic nanoparticles [314, 315] including Ag NPs [118]. Intracellular dissolution of ZnO NPs is an important mechanism of toxicity [316]. Since most previous TEM examinations of lysosomes in *C. elegans* have been carried out with nematodes raised on plates, I first explored whether any alterations in the abundance or morphology of lysosomes was associated with liquid exposure. I compared nematodes fixed directly after being washed from plates or fixed after growth in liquid media, and found similar populations of lysosomes (Fig. S12B). Interestingly, two types of lysosomes were observed in all treatments and controls, with one type having round profiles with no granules inside and the other type having more irregular borders and electron-dense granules located primarily at their periphery (Fig. 41C, J). I was unaware of previous reports of lysosomes in C. elegans with the irregular border morphology that was observed. However, there were no differences in morphology or roughly-estimated density of lysosomes between any treatment group and controls (Fig. 41). Future work on lysosome-deficient mutants would further test the hypothesis that lysosomes regulate Ag NP toxicity. For reasons explained in the Methods section, our TEM analyses were restricted to doses that resulted in lethality to 75% of the exposed nematodes. The mitochondrial alterations in intestinal epithelial cells may occur at lower doses. In this instance, the worm might survive but show reduction in energy related metabolic processes.

In summary, NOM, specifically PLFA, rescued $AgNO_3$ and CIT-Ag NP organismal toxicity and intestinal damage, reduced organismal uptake of $AgNO_3$ but not CIT-Ag NPs, and protected the nematodes from CIT-Ag NP-induced gut epithelium tissue injury. Thus, our results both demonstrate a powerful protective effect of NOM, and support evidence for a NP-specific type of damage in high amplitude swelling of intestinal epithelium and gonadal tissue.

4.3.9 Impact of sulfidation on Ag NP toxicity

C. elegans was tested for acute lethality and growth inhibitory effects of the pristine Ag NPs and sulfidized Ag NPs in high and low-ionic strength *C. elegans* liquid media (K^+ and EPA water, respectively). The extinction (EXT) values obtained from the Biosort (72 hrs postdosing) were fit to linear and exponential models, which are more appropriate for assays with a continuous endpoint. An exponential model (Model 4 in BMDS, with an assumed log-normal distribution of the response) was selected because the dose-response curves fit using this model achieved significantly lower AIC values than alternatives. We observed large variance in the *C. elegans* response (EXT values), which resulted in particularly poor model. However, our results in general indicated that increasing degree of sulfidation of the AgNPs resulted in lower toxicity (Fig. 43).

4.3.10 Effect of temperature on Ag NP toxicity

Higher temperatures resulted in more toxicity in Ag NPs (Fig. 44). Due to the fact that increased temperature didn't result in increased toxicity in the Ag ion positive

control, increased physiological susceptibility at higher temperature can be ruled out. Therefore, the increase in Ag NP toxicity is most likely explained mainly by the increased Ag NP dissolution at higher temperatures.

4.3.11 Toxicity of silver incubated in mesocosms to *C. elegans*

To test the effect of a more natural and complex environment on Ag NP toxicity, mesocosms were dosed with 2.5 mg-Ag L^{-1} as GA-Ag NPs, PVP-Ag NPs and $AgNO_3$. Mesocosm water was sampled at three different time points (right after spike, 1 week after spike and 2 weeks after spike) were included in the experiments. Right after spike, we found that all treated mesocosm water samples induced significant growth inhibition in *C. elegans* except for the PVP only treatment ($p=0.051$, compared to $p<0.001$ for all other treatments). GA only treatment resulted in approximately 20% growth inhibition (Fig. 45), while GA did not show any toxicity in *C. elegans* under laboratory spiked conditions. PVP Ag-NP, GA Ag-NP and $AgNO_3$ induced 21%, 45% and 25% growth inhibition, respectively (Fig. 45).

However, 1 week after the spike, water samples obtained from the mesocosm did not result in any growth inhibition in *C. elegans*, and no growth inhibition was found in the samples 2 weeks after spike as well. Nematodes showed very similar growth compared to controls. In parallel experiments, we also tested the *pcs-1* mutant, which was more sensitive to metal-induced toxicity [181, 317], showed no significant toxicity among all the treatment right after spike (Fig. 46). This might be due to the relatively

poorer growth in *pcs-1* controls (approximately 60% of wildtype control in size at the end of the 72 h experiment), which masked the exacerbation of mesocosm Ag NP exposure on growth.

Therefore, a complex environmental medium, e.g., mesocosm reduced Ag NP toxicity shortly after the spike. Water samples from the mesocosms were less toxic than laboratory water containing the same concentrations of spiked Ag NPs. After 1 week, the toxicity was eliminated in the mesocosm samples.

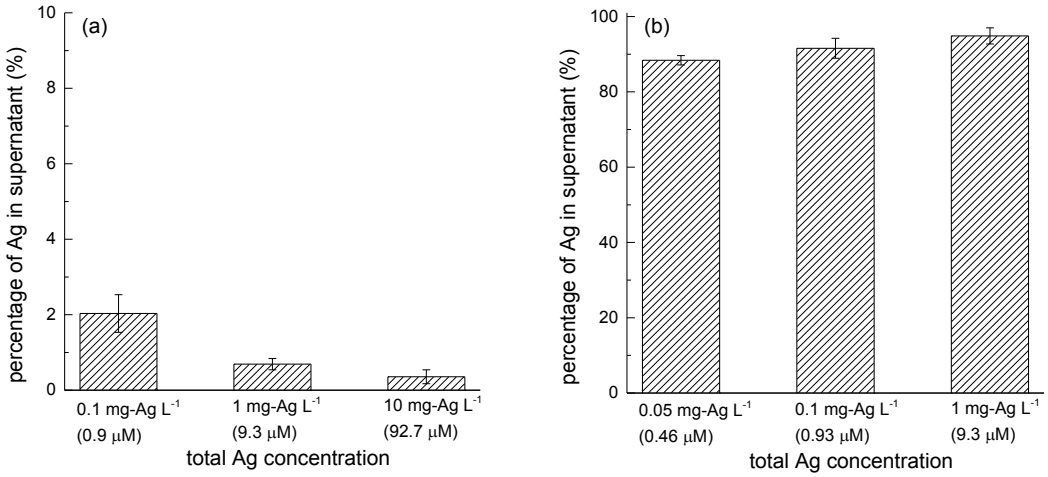

Figure 25: Percentage of silver remaining in the supernatant after ultracentrifugation of different concentrations of CIT-Ag NPs and $AgNO_3$.

(a) CIT-Ag NPs and (b) ionic silver ($AgNO_3$) in EPA water, in the presence of PLFA (10 mg-C L^{-1}). Ultracentrifugation was performed at 370,000 g for 30 min.

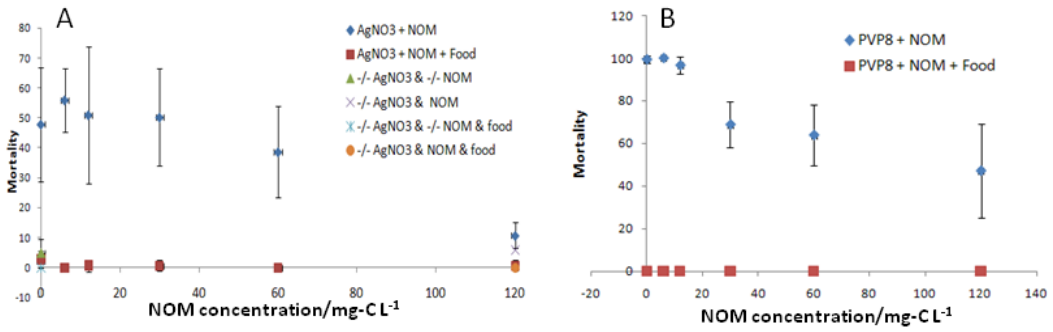

Figure 26: Impact of food and SRFA on ionic silver and PVP-coated Ag NP (8±2 nm) toxicity.

A) $AgNO_3$; B) PVP-coated AgNPs (8 nm). Data include 3 experimental replicates (total nematodes= 480 per treatment; $p<0.001$ for statistical significance for food and SRFA effect on silver toxicity by Wilcoxon rank sum test with continuity correction).

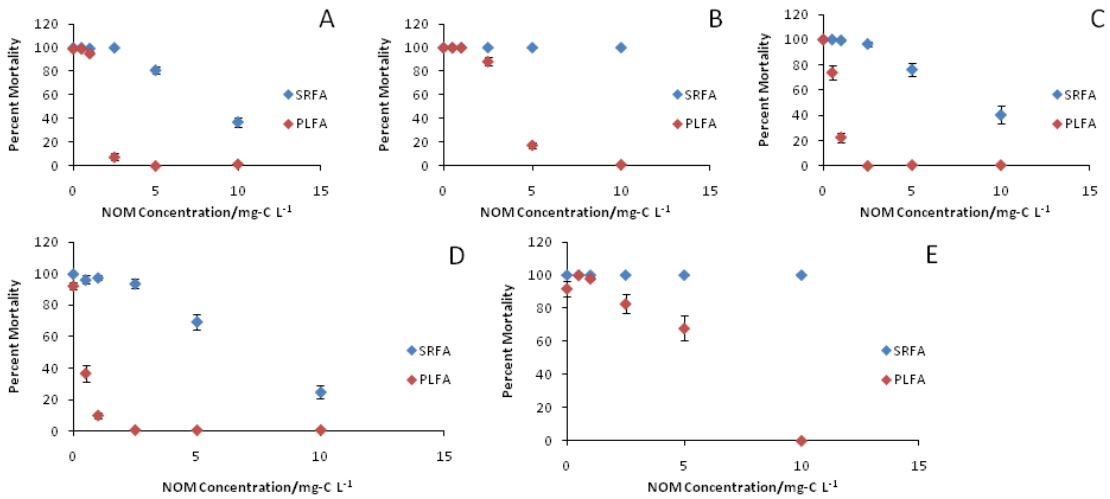

Figure 27. Percentage mortality of *C. elegans* exposed to ionic silver and Ag NPs with increasing concentrations of SRFA and PLFA (1-10 mg-C L^{-1}).

A) $AgNO_3$ at 0.15 mg-Ag L^{-1}; B) Non-functionalized Ag NPs at 0.15 mg-Ag L^{-1}; C) PVP-Ag NPs (8±2 nm) at 0.5 mg-Ag L^{-1}; D) PVP-Ag NPs (38±8 nm) at 0.5 mg-Ag L^{-1}; E) CIT-Ag NPs at 5 mg-Ag L^{-1}. Data includes 4 replicate experiments (640 nematodes per dose). The difference in rescue effect between PLFA and SRFA was statistically different in all cases ($p<0.05$ by Wilcoxon rank sum test with continuity correction)

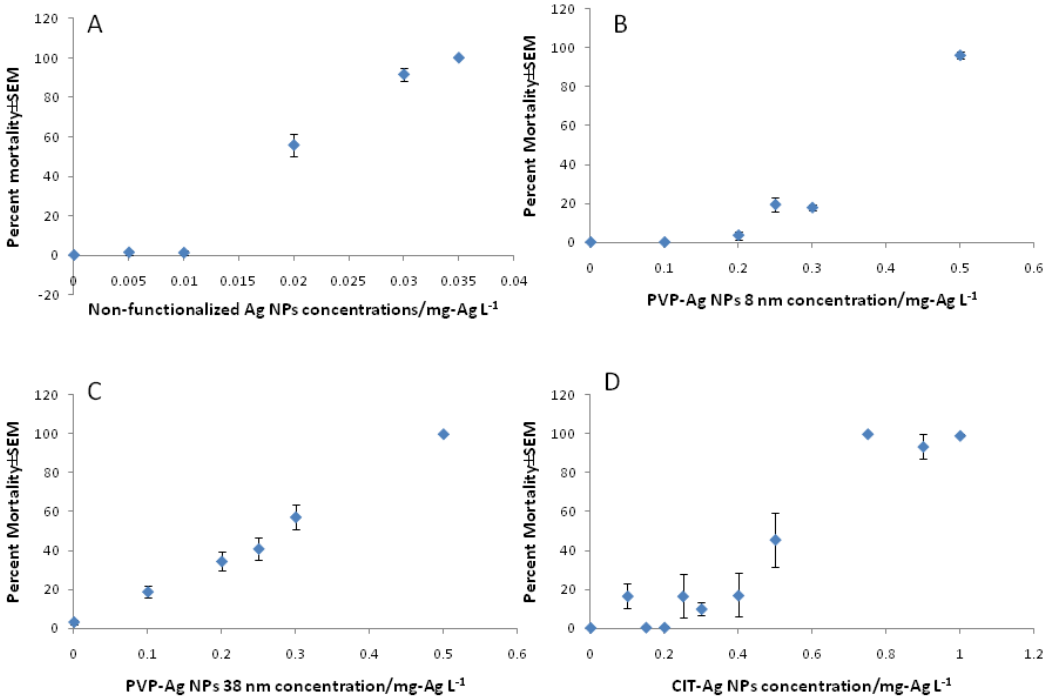

Figure 28: Range-finding dose-response curves for Ag NPs without food and without natural organic matter.

A) Non-functionalized Ag NPs; B) PVP-Ag NPs 8 nm; C) PVP-Ag NPs 38 nm; D) CIT-Ag NPs. Data from 4 experiments, each with 6 wells containing 20 nematodes/well (480 nematodes/data point).

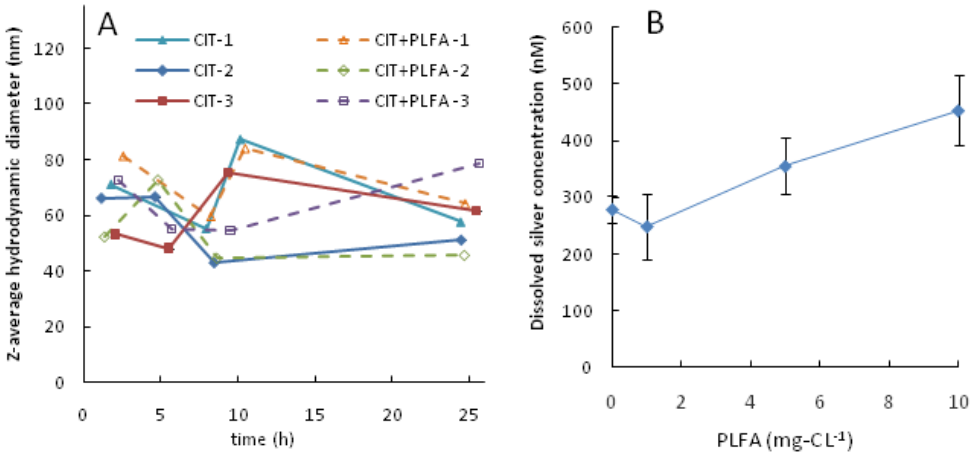

Figure 29. Hydrodynamic diameter and dissolved silver concentration of CIT-Ag NPs (5 mg-Ag L^{-1}) in the absence and presence of PLFA.

A) Hydrodynamic diameter of CIT-Ag NPs in the presence and absence of PLFA (10 mg-C L^{-1}), with replicate experiment; B) Dissolved silver concentration with increasing concentrations of PLFA (0-10 mg-C L^{-1}).

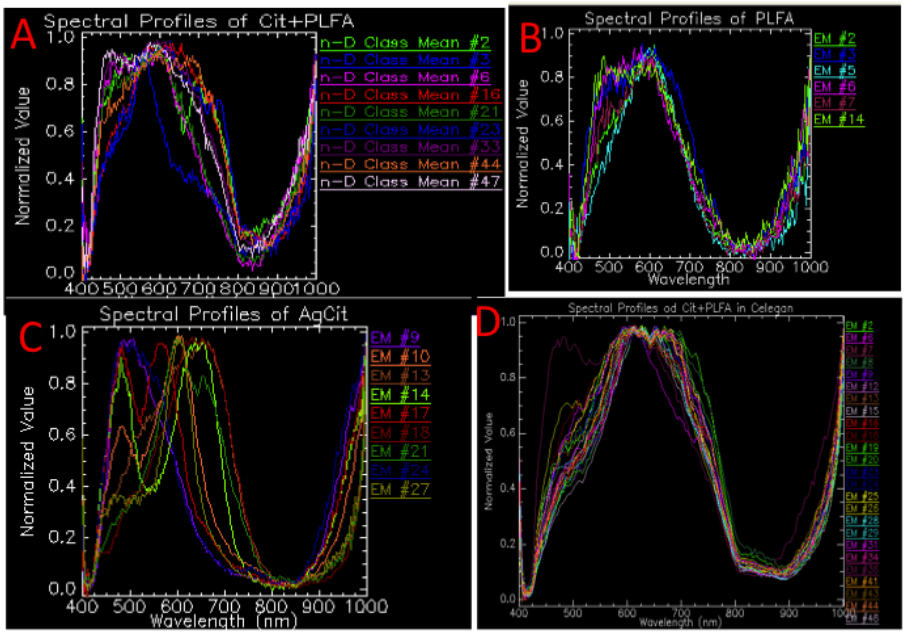

Figure 30: Hyperspectral endmembers illustrating the presence of complex formation from Citrate-coated Ag NPs (CIT-Ag NPs) and PLFA.

A) CIT-Ag NPs+PLFA library; B) PLFA library; C) CIT-Ag NPs library; D) CIT-Ag NPs+PLFA in *C. elegans*. CIT- Ag NPs (25±9 nm).

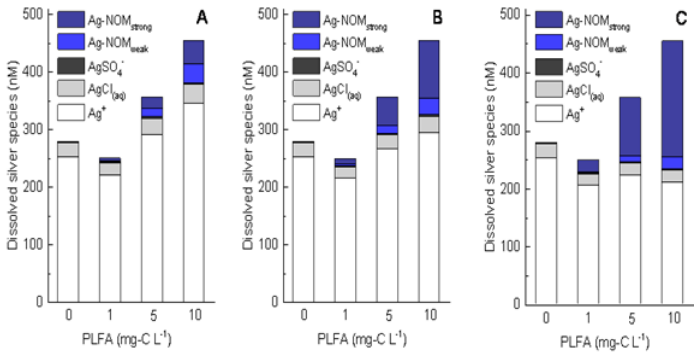

Figure 31: Equilibrium speciation of dissolved silver in mixtures comprising EPA water and dissolved Ag in the presence of varying concentrations of PLFA (0, 1, 5, 10 mg-C L^{-1}).

Total dissolved Ag concentrations at each PLFA concentration correspond to measured dissolved values in the CIT-Ag NP-PLFA mixtures. Complexation of Ag^+ by NOM was assumed to occur with 'weak' binding sites (1.7×10^{-6} mol per mg-C) and strong thiol binding sites with a concentration of (A) 4 nmol per mg-C; (B) 10 nmol per mg-C; and (C) 20 nmol per mg-C.

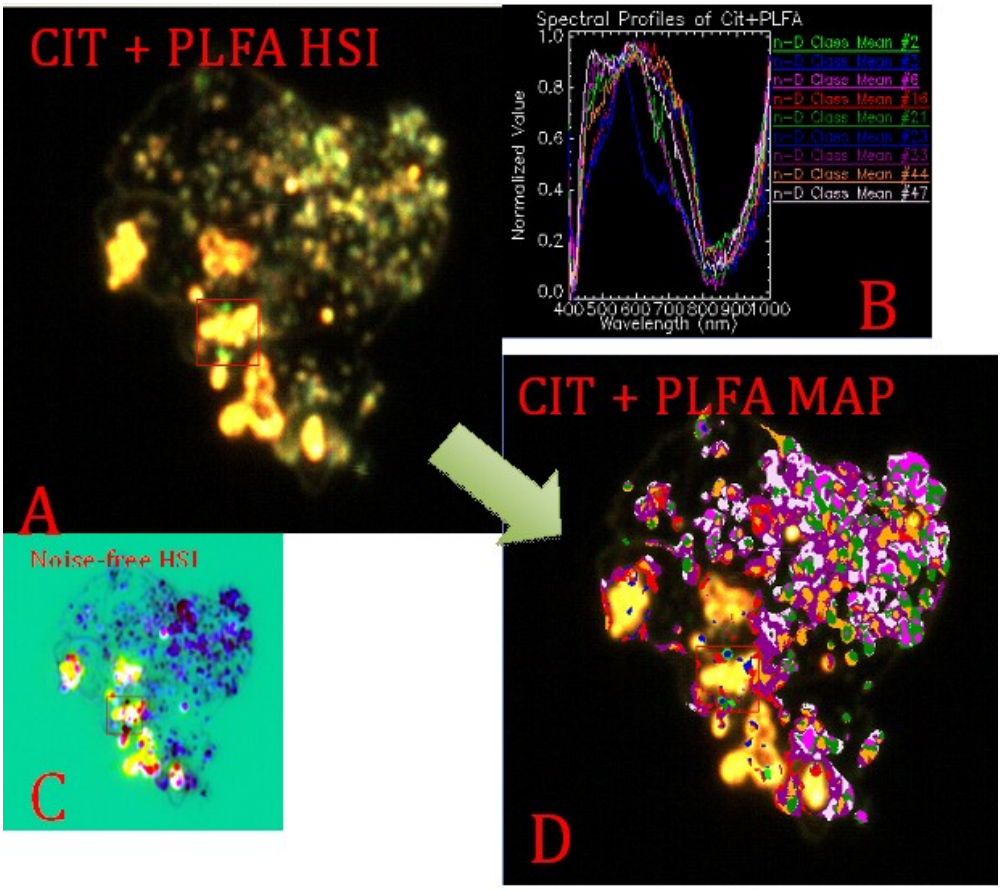

Figure 32: CIT-Ag NPs intercalate into "pockets" of PLFA in medium without nematodes, indicative of NP-NOM complex formation.

A) Hyperspectral image (HSI) of CIT-Ag NP-PLFA complex; B) Endmembers of PLFA and Ag NPs; C) Minimum noise fraction (MNF) image; D) Spectral angle mapper (SAM) classified image showing the location of the endmembers (Figure B) in the HIS image. Ag NP color in all HSI images is attributed to their surface plasmon resonance property.

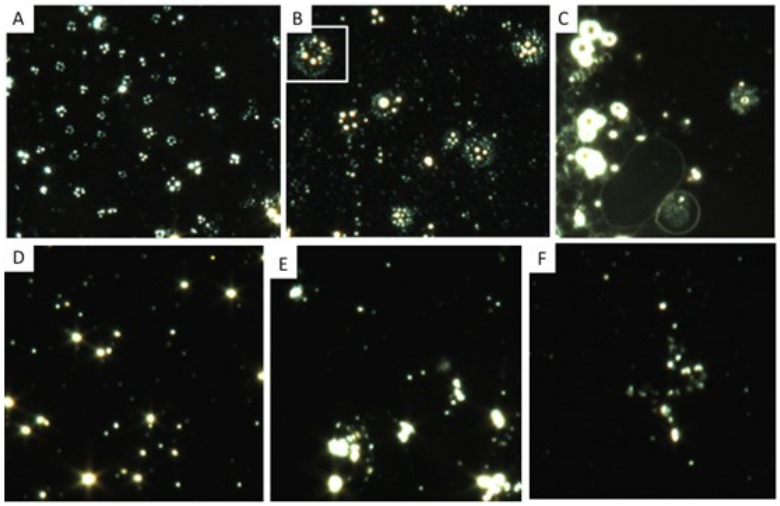

Figure 33: Darkfield images of association of CIT-Ag NPs (5 mg-Ag L^{-1}) and PLFA (10 mg- C L^{-1}) in the presence and absence of nematodes.

This is showing how the presence of nematodes affects CIT-Ag NP-NOM interaction. (A-C) "Ring"-like structures formed by CIT-Ag NPs+PLFA association are dominant in the presence of nematodes; (D-F) in the absence of nematodes, loose agglomerates of CIT-Ag NPs+PLFA are dominant.

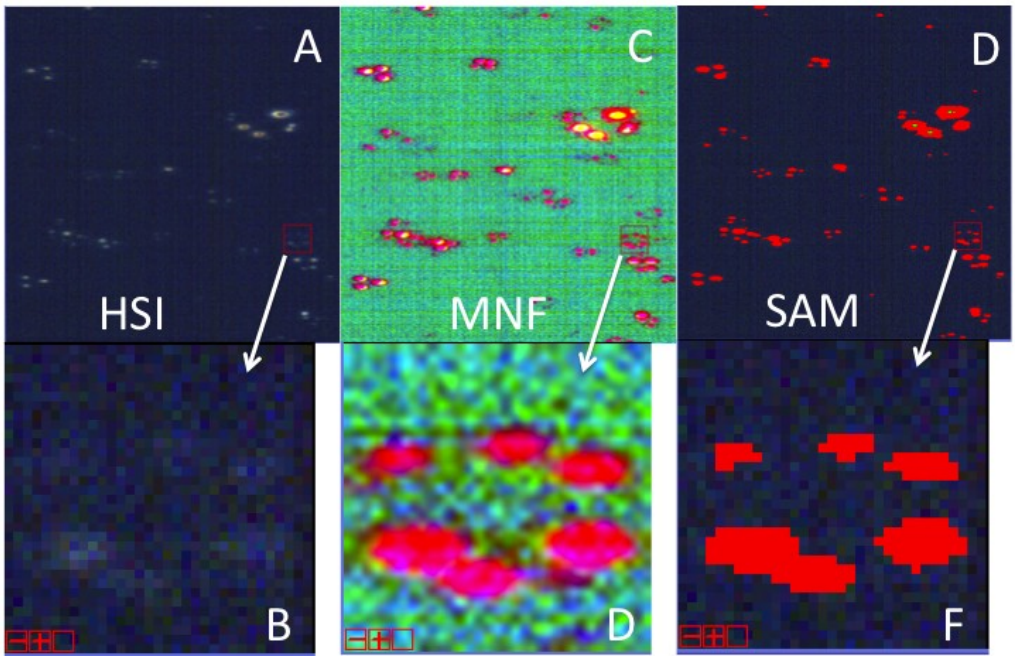

Figure 34: Analysis of CIT-Ag NPs+PLFA rings using spectral angle mapper (SAM technique).

A-B) Hyperspectral analysis with details; C-D) MNF technique and details; E-F) SAM technique and details.

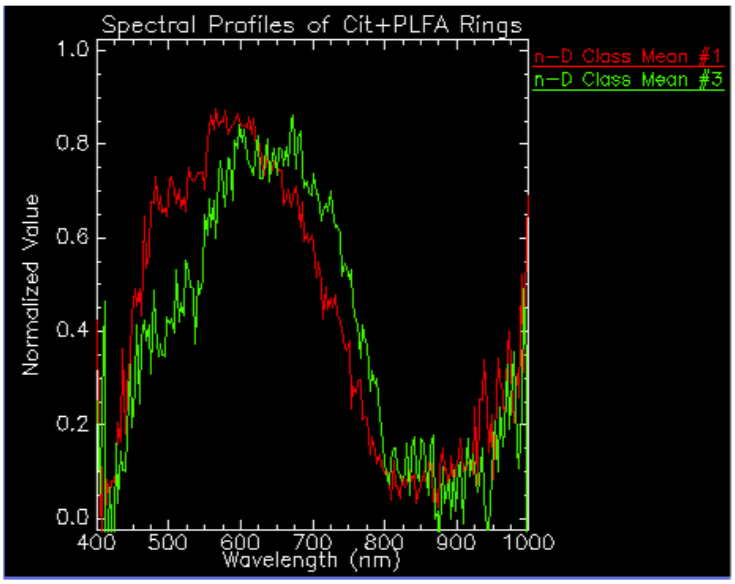

Figure 35: Spectral profiles for CIT-Ag NPs+PLFA rings.

This figure shows the presence of spectral profiles, mean #1 and #3, in close association with each other and these profiles were in agreement with the profiles shown in the hyperspectral imaging of CIT-Ag NPs+PLFA rings. The bright nodes in each ring are the regions where Ag NPs were localized.

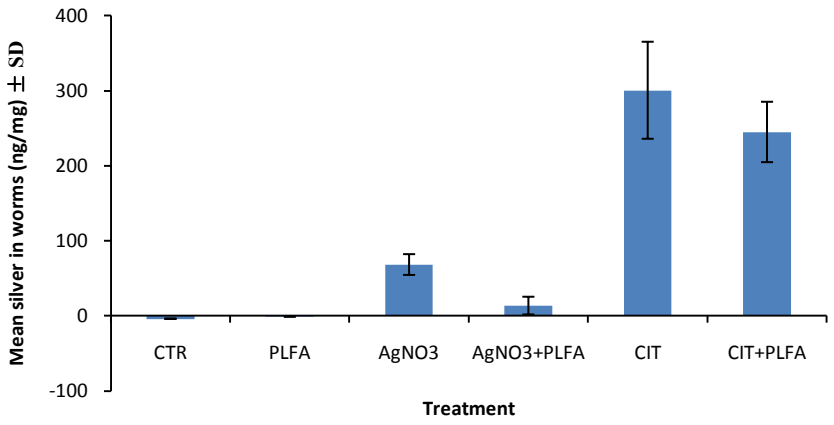

Figure 36. Total silver measurement in nematodes.

PLFA (10 mg-C L^{-1}) reduced whole-organism uptake of $AgNO_3$ (0.15 mg-Ag L^{-1}) but not CIT-Ag NPs (5 mg-Ag L^{-1}) by *C. elegans* ($p = 0.2752$; N=5 for $AgNO_3$ +/- PLFA and N=6 for CIT-Ag NPs +/- PLFA).

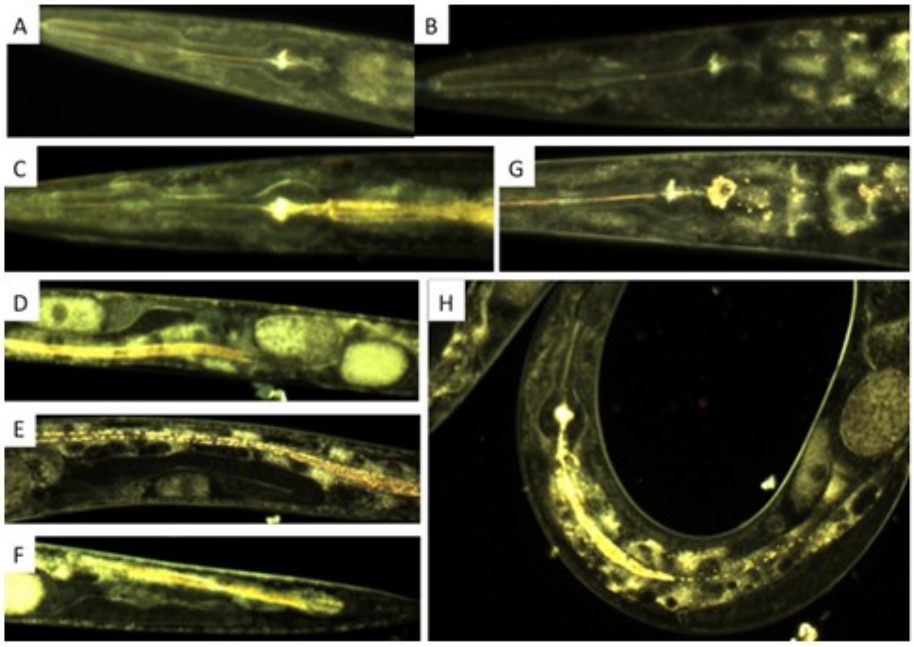

Figure 37: CIT-Ag NPs were detectable via darkfield microscopy in the gut and tissues of *C. elegans* with and without PLFA.

Nematodes were subjected to following treatments: (A) not exposed to Ag NPs (control); (B) exposed to PLFA only (10 mg-C L^{-1}); (C-F) exposed to CIT-Ag NPs only (5 mg-Ag L^{-1}); (G-H) exposed to CIT-Ag NPs (5 mg-Ag L^{-1}) + PLFA (10 mg-C L^{-1}).

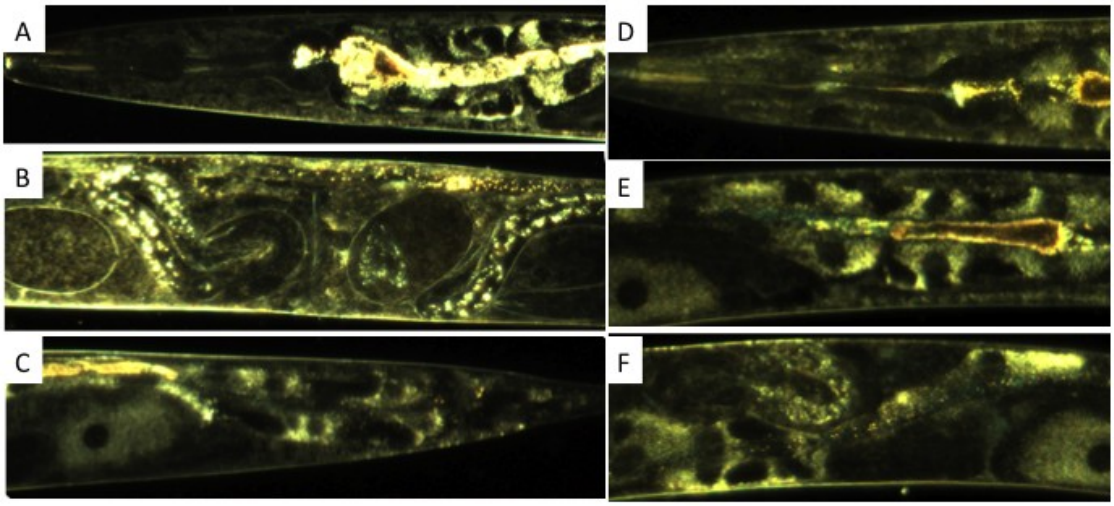

Figure 38: Shown here are the darkfield images of body residue of CIT-Ag NPs with and without PLFA in *C. elegans* after 24 h elimination in fresh medium followed by 24 hrs uptake period.

A-C) CIT-Ag NPs only (5 mg-Ag L^{-1}); D-F) CIT-Ag NPs (5 mg-Ag L^{-1})+PLFA (10 mg-C L^{-1}).

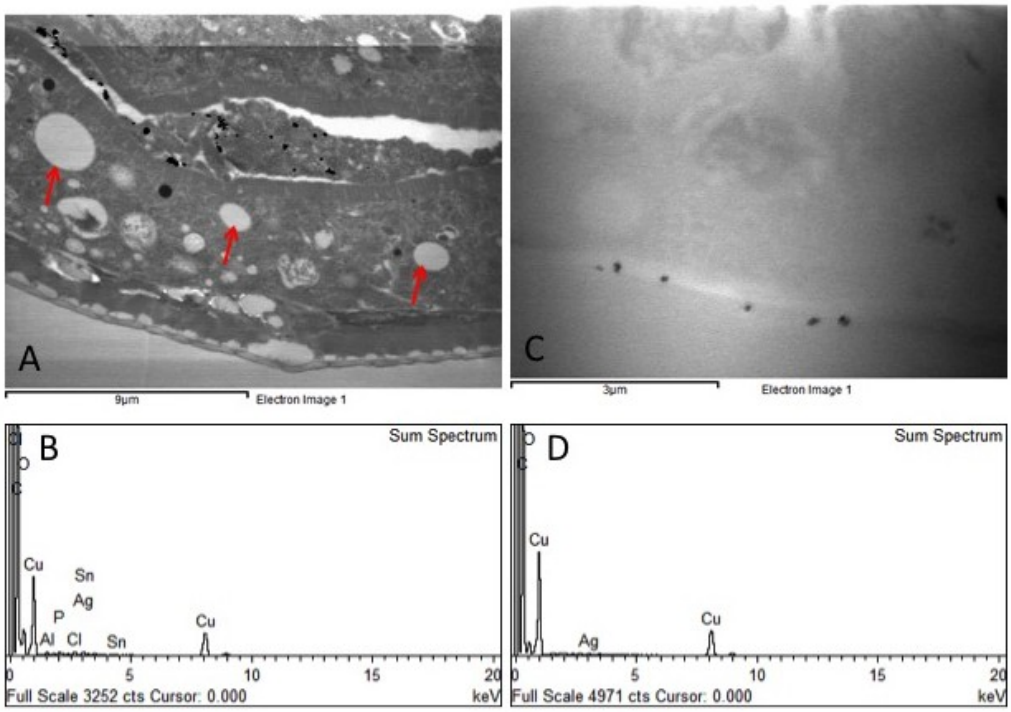

Figure 39: TEM image and metal peak detection using energy dispersive X-Ray Analysis.

A-B) CIT-Ag NP-treated nematodes; C-D) CIT-Ag NP + PLFA-treated nematodes.

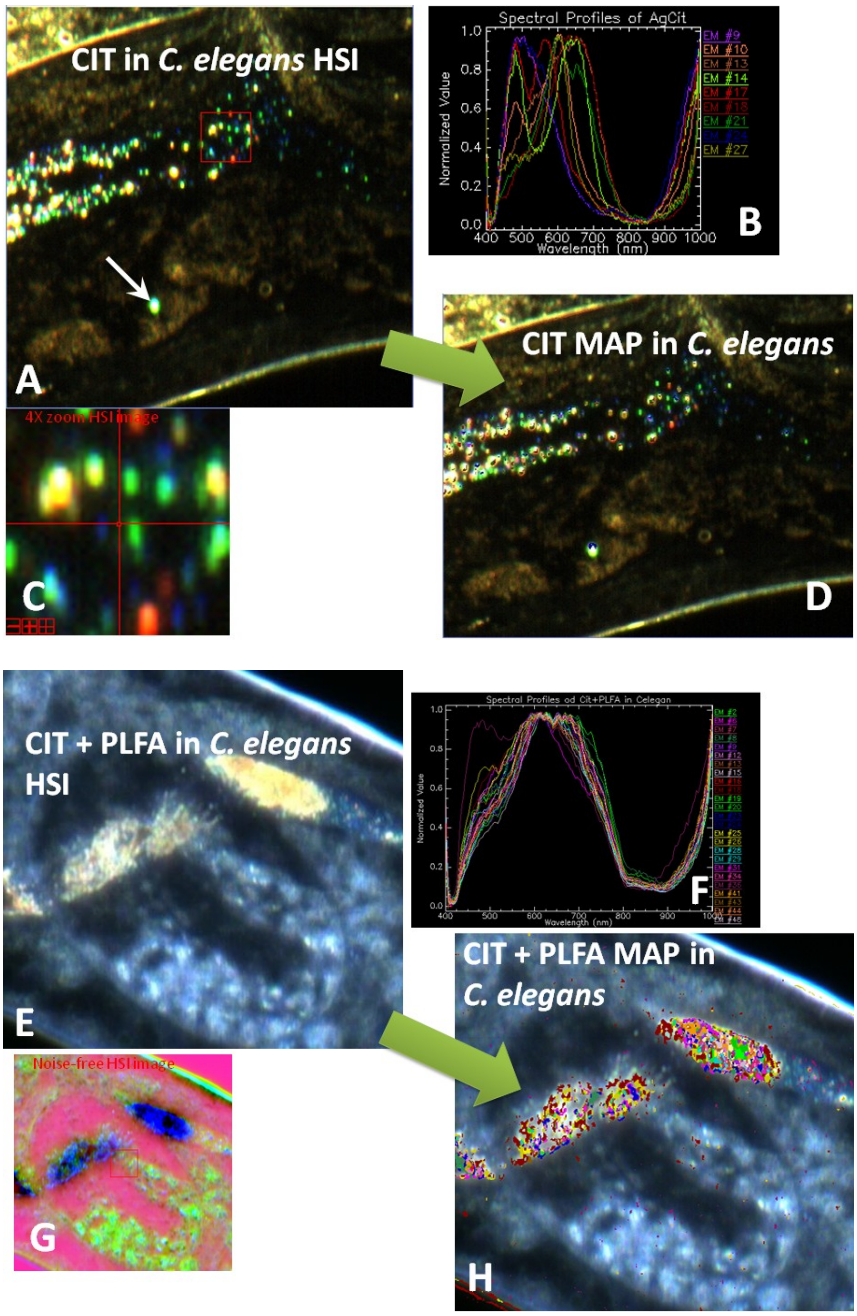

Figure 40: Hyperspectral image mapping confirmed gut uptake of CIT-Ag NP (5 mg-Ag L^{-1}) with and without PLFA in *C. elegans*.

A) CIT-Ag NP localized mostly in nematode gut; (arrow indicates an example of tissue uptake beyond the gut); B) CIT-Ag NP endmembers derived from HSI and matched with CIT-Ag NP spectral library; C) Minimum Noise Fraction (MNF) image; D) Spectral angle mapper (SAM) classified image showing the location of the endmembers (panel B) in the HSI image (A). Ag NPs color in all HSI images is attributed to their surface plasmon resonance property. (E-H) hyperspectral image mapping identified NP-NOM interaction and complex formation in *C. elegans* after exposure to CIT-Ag NP (5 mg-Ag L^{-1}) + PLFA (10 mg-C L^{-1}). E) CIT-Ag NPs+PLFA localization in nematode; F) endmembers derived from HSI and matched with CIT-Ag NP spectral library; G) MNF image; H) Spectral angle mapper (SAM) classified image showing the location of the endmembers (panel F) in the HSI image (E). Ag NPs color in all HSI images is attributed to their surface plasmon resonance property (collective oscillation of electrons in solid or liquid stimulated by light).

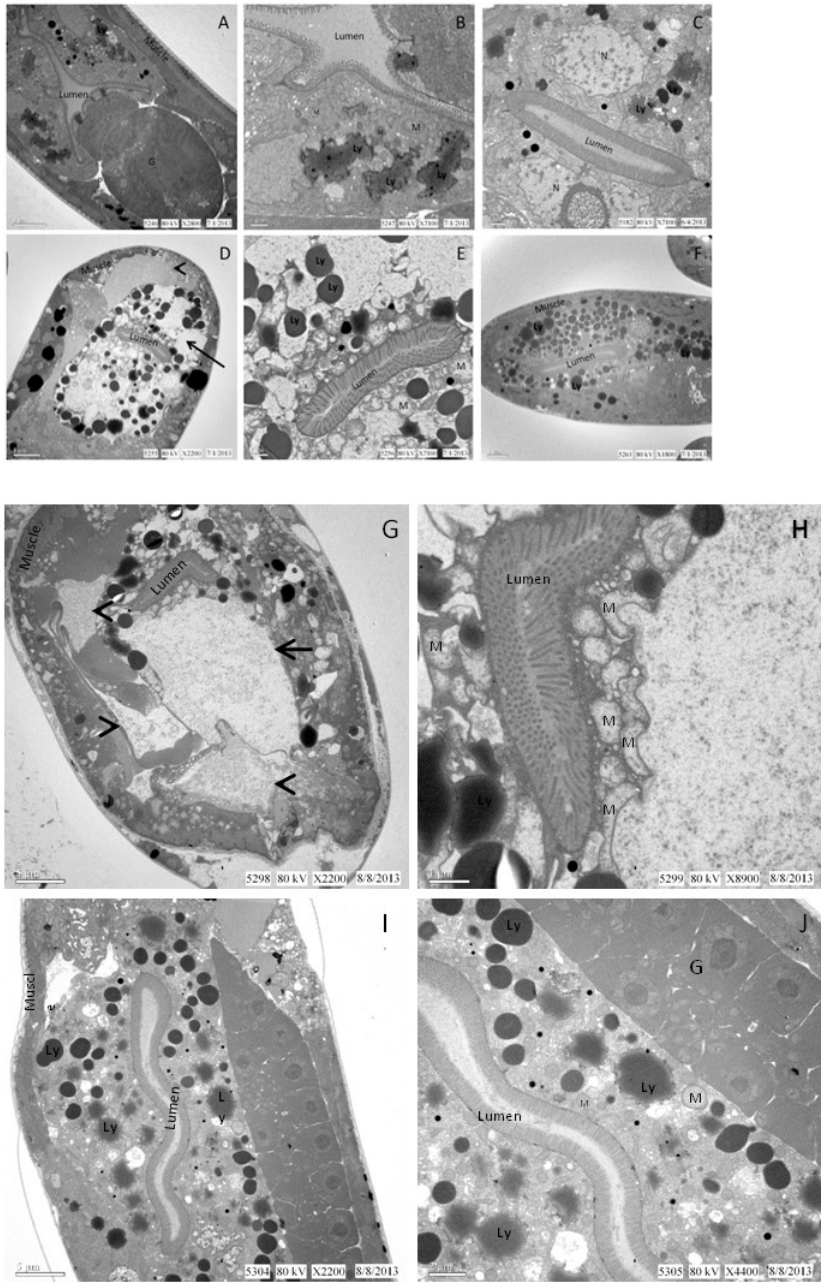

Figure 41. TEM micrographs of control and treated nematodes.

A-C) Control. TEM examinations included the gut lumen, epithelium, gonad (G) and muscle. M- mitochondria, N- nucleus and Ly- lysosome; D) $AgNO_3$ 10 mg-Ag L^{-1} (LC_{75} for the number of nematodes exposed). Arrow and arrowhead indicate necrotic

epithelial cells and likely fluid-filled space, respectively; E) $AgNO_3$ 10 mg-Ag L^{-1}; F) $AgNO_3$ 10 mg-Ag L^{-1} + PLFA 10 mg-C L^{-1}; G) Citrate-functionalized Ag NPs (CIT-Ag NPs) 24 mg-Ag L^{-1} (LC_{75} for the number of nematodes exposed). Arrowhead indicates likely fluid-filled space; H) CIT 24 mg-Ag L^{-1}; I) CIT-Ag NPs 24 mg-Ag L^{-1} + PLFA 10 mg-C L^{-1}; J) CIT-Ag NPs 24 mg-Ag L^{-1} + PLFA 10 mg-C L^{-1}. Magnification: A) 2000X; B) 7100X; C) 7100X; D) 2200X; E) 8900X; F) 1800X; G) 2200X; H) 8900X; I) 2200X; J) 4400X. Scale bars represent: A) 5 μm; B) 1 μm; C) 1 μm; D) 5 μm; E) 1 μm; F) 5 μm; G) 5 μm; H) 1 μm; I) 5 μm; J) 2 μm.

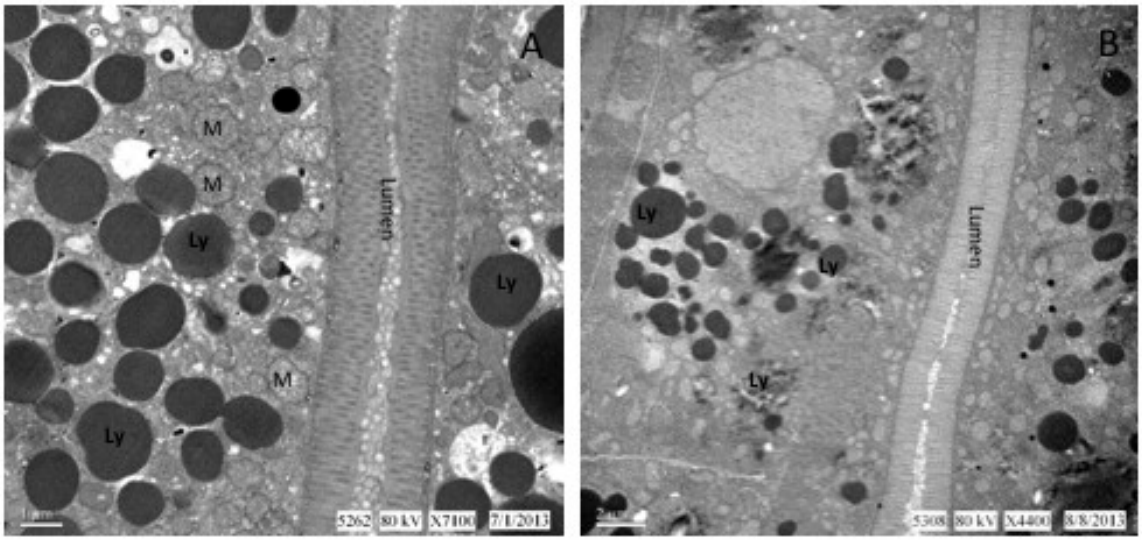

Figure 42: TEM micrograph showing nematode ultrastructures from $AgNO_3$+PLFA and controls.

A) $AgNO_3$ 1 mg-Ag L^{-1}+ PLFA 10 mg-C L^{-1} at higher magnification 7100X; M-mitochondria, Ly- lysosome; B) control nematodes on plate, without liquid exposure.

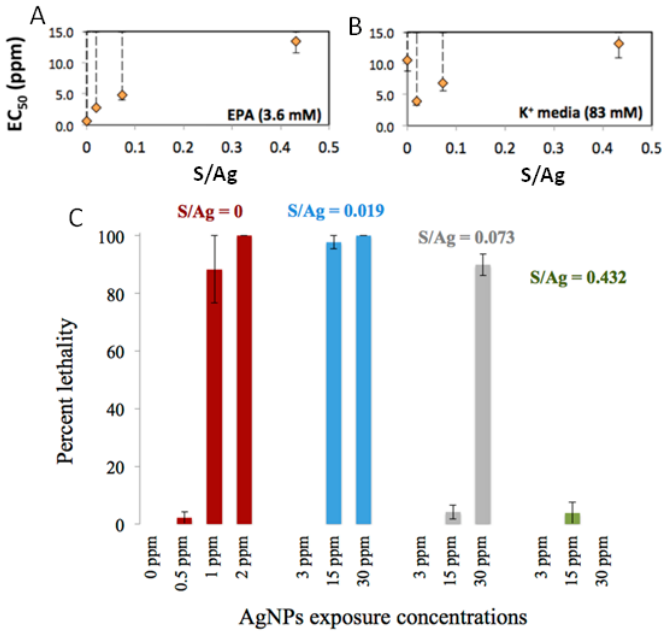

Figure 43. A-B) LC_{50} and EC_{50} responses (in ppm) of *C. elegans* to the presence of Ag NPs.

Error bars denote a one-sided 95% confidence interval. One-sided intervals calculated by BMDS reflect the fact that potential toxicity (lower bound) is generally of greater concern than potential nontoxicity (effective upper bound of infinity). Open diamonds indicate that the predicted EC_{50} or LC_{50} exceeded the tested range of AgNP concentrations (error bars not shown). As sulfidation of the silver particles increases along the x-axis (from 0 to 0.5, where 0.5 represents a 100% Ag_2S AgNP), nematodes are less sensitive to the particles. C) Influence of sulfidation on the mortality caused by AgNPs for *C. elegans* in EPA water (low ionic strength and low Cl^-). Mortality is defined as the number of unresponsive organisms over the total number of organisms. Error bars represent the standard error of the mean (four replicates). At high ionic strength, there was no mortality for pristine AgNPs or any of the sulfidized AgNPs (data not shown).

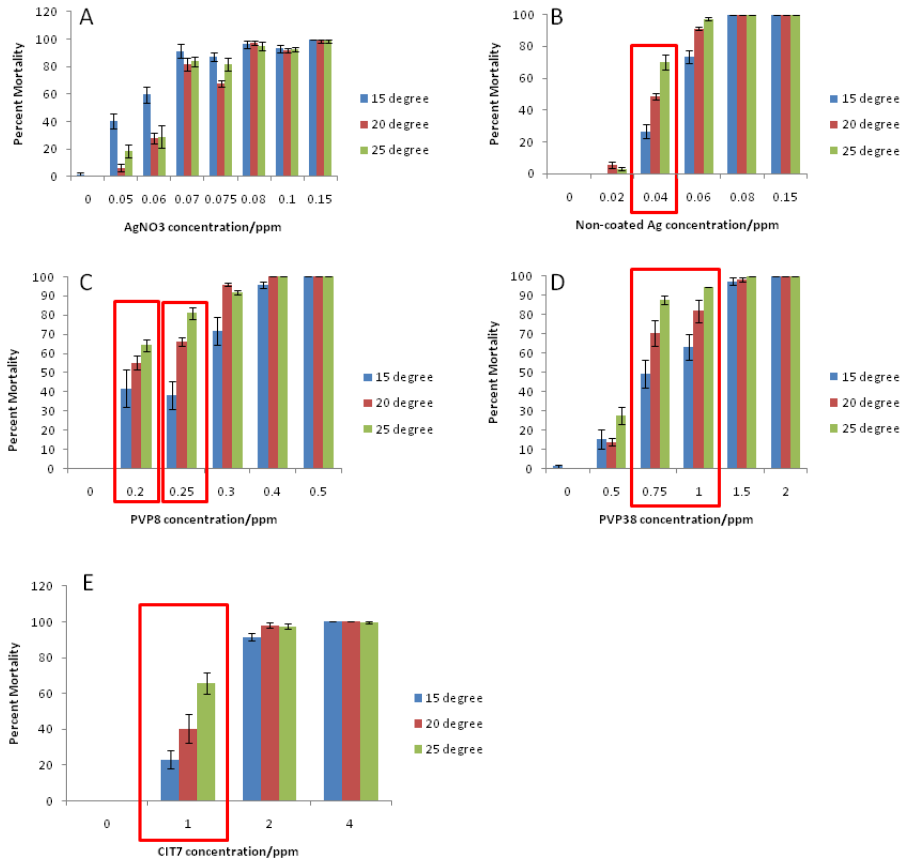

Figure 44. Impact of temperature on toxicity of $AgNO_3$ and Ag NPs.

A) $AgNO_3$; B) non-coated Ag NPs (50 nm); C) PVP-coated Ag NPs (8±2 nm); D) PVP-coated Ag NPs (38±8 nm); E) Citrate-coated Ag NPs (25±9 nm). Error bars represent standard error. Data were combined from 4 separate experiments.

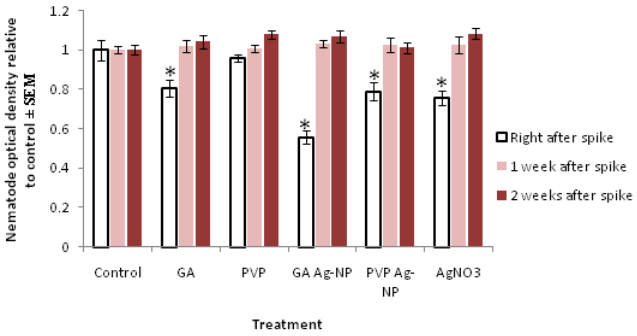

Figure 45. 72 h nematode optical density (relative to control) +/- SEM of wild type (N2) *C. elegans* exposed to GA Ag-NPs, PVP Ag-NPs, and $AgNO_3$.

Right after spike indicates water samples obtained right after mesocosm was spiked; N=4 experimental replicates, 50 larvae/sample. Results shown as mean ± SEM. * indicates statistical significance.

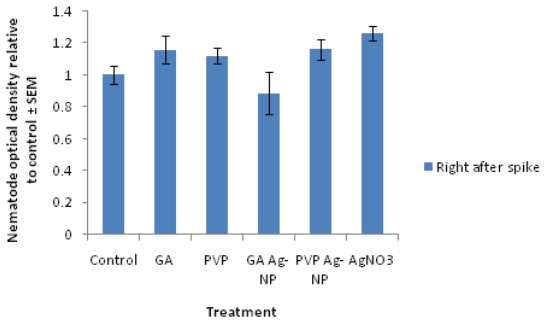

Figure 46. 72 h nematode optical density (relative to control) +/- SEM of *pcs-1 C. elegans* exposed to GA Ag-NPs, PVP Ag-NPs, and $AgNO_3$.

Right after spike indicates water samples obtained right after mesocosm was spiked; N=4 experimental replicates, 50 larvae/sample. Results shown as mean ± SEM.

Table 5. Recipe for EPA water

chemical	conc. (mg/L)	F.W. (g/mol)	conc. (M)
$NaHCO_3$	96	84.00	1.14×10^{-3}
$MgSO_4 7H_2O$	60	246.47	2.43×10^{-4}
$CaSO_4 2H_2O$	60	172.17	3.48×10^{-4}
KC1	4	74.55	5.37×10^{-5}

Table 6. Total concentration of major ions except carbonate for the EPA water matrix

ion	conc. (M)	ion	conc. (M)
Na^+	1.14×10^{-3}	Ca^{2+}	3.48×10^{-4}
K^+	5.37×10^{-5}	Cl^-	5.37×10^{-5}
Mg^{2+}	2.43×10^{-4}	SO_4^{2-}	5.92×10^{-4}

Table 7. Site density and concentrations of silver-binding sites for solutions with varying PLFA concentration (in mg-C L^{-1})

NOM silver binding site	site density	Ag-binding site concentration (M)			
	mol $(mg\text{-}C)^{-1}$	0 mg-C L^{-1}	1 mg-C L^{-1}	5 mg-C L^{-1}	10 mg-C L^{-1}
weak	1.7×10^{-6}	0	1.7×10^{-6}	8.5×10^{-6}	1.7×10^{-5}
strong -lower range	4.0×10^{-9}	0	4.0×10^{-9}	2.0×10^{-8}	4.0×10^{-8}
strong -median	1.0×10^{-8}	0	1.0×10^{-8}	5.0×10^{-8}	1.0×10^{-7}
strong -upper range	2.0×10^{-8}	0	2.0×10^{-8}	1.0×10^{-7}	2.0×10^{-7}

Table 8. Total dissolved silver concentration (M) (mean and standard deviation) measured in the samples

PLFA (mg-C L^{-1})	mean	SD
0	2.79×10^{-7}	2.46×10^{-8}
1	2.49×10^{-7}	5.74×10^{-8}
5	3.56×10^{-7}	4.92×10^{-8}
10	4.54×10^{-7}	6.25×10^{-8}

Table 9. Settling velocity (U), settling distance (L) and removal percentage (η) of silver NPs of different diameter (d) during centrifugation.

d (nm)	U (m/s)	L (m)	η (%)
5	3.9×10^{-7}	4.6×10^{-5}	0.1
10	1.5×10^{-6}	1.9×10^{-4}	0.5
20	6.2×10^{-6}	7.4×10^{-4}	1.9
25	9.7×10^{-6}	1.2×10^{-3}	2.9
50	3.9×10^{-5}	4.6×10^{-3}	11.6
70	7.6×10^{-5}	9.1×10^{-3}	22.7

Notes: The settling velocity was calculated by Stoke's Law. The removal percentage (η) was calculated as the ratio of distance travelled by the particle (L) during centrifugation to the depth of liquid in the centrifugation tubes (i.e. 4 cm). The Ag NPs were assumed to be spherical in shape and have a density of bulk solid silver.

5. Conclusions

5.1 Summary

The overall goal of this dissertation was to study in depth the uptake, mechanism(s) of toxicity, and environmental interactions of Ag NPs. Despite extensive toxicity data for Ag NPs in multiple organisms [122, 318-320], there existed very limited in-depth mechanistic studies regarding the toxicity drivers of Ag NPs [54, 321]. Further there was little understanding of the uptake mechanism of Ag NPs *in vivo* [322]. Finally, Ag NP toxicity within a more complex environment needed to be investigated to better inform ecological risk assessment. Therefore, the first hypothesis addressed in this work was to test whether Ag NP toxicity was driven by release of dissolved silver, or had unique toxicity resulting from their nanoparticulate form. In chapter 2, data showed that a lower ionic strength medium resulted in greater toxicity (measured as growth inhibition) of all tested Ag NPs to *Caenorhabditis elegans*, and that both the dissolved silver and coating influenced Ag NP toxicity. There was a linear correlation between Ag NP toxicity and dissolved silver, but no correlation existed between size and toxicity. Furthermore, in Chapter 2 I showed that some Ag NPs (typically less soluble due to size or coating) also acted via oxidative stress [323], an effect unique to nanoparticulate silver. These data demonstrate that Ag NP toxicity is mainly driven by dissolution and that for those less dissolvable (or larger) Ag NPs, toxicity also results from oxidative stress [324].

Secondly, I hypothesized that if endocytosis were also the pathway for cellular uptake of Ag NPs *in vivo* (based on *in vitro* data), then I could manipulate this pathway and the downstream lysosomal pathway in order to understand the role of intracellular trafficking in Ag NP toxicity. In chapter 3, data showed that the clathrin-mediated endocytosis inhibitor chlorpromazine reduced the toxicity of CIT-Ag NPs but not $AgNO_3$. I also tested the sensitivity of three endocytosis-deficient mutants (*rme-1*, *rme-6*, and *rme-8*), two lysosomal function deficient mutants (*cup-5* and *glo-1*), and one coelomocyte fluid endocytosis mutant (*cup-4*), as compared to wild-type (N2 strain) *C. elegans*. One of the endocytosis-deficient mutants (*rme-6*) took up less silver and was resistant to the acute toxicity of CIT-Ag NPs as compared to N2, and none of those mutants showed altered sensitivity to $AgNO_3$. Interestingly, the lysosomal mutants were more sensitive to the growth-inhibiting effects of CIT-Ag NPs, and were in fact more sensitive to CIT-Ag NP-mediated inhibition of reproduction. Most intriguingly, the *glo-1* mutants were much more sensitive than wild type to inhibition of reproduction after exposure to CIT-Ag NPs but not $AgNO_3$, constituting a clear nanoparticle-specific toxic effect. Furthermore, microscopic examination of the reproduction-impaired *glo-1* mutants revealed a phenotype of egg retention in the adult, possibly resulting from both insufficient yolk in the embryo and blockage of embryo transport to the vulval opening by excess yolk accumulation.

Thirdly, I hypothesized that environmental factors could mitigate Ag NP toxicity. The overall conclusion from Chapter 4 was that environmental conditions (salinity, NOM, sulfidation, mesocosm conditions) tended to reduce Ag NP toxicity. Effect of salinity on Ag NP toxicity was included in chapter 2, suggesting that a higher chloride medium (K+ medium) resulted in reduced toxicity compared to lower chloride EPA water (Table 2). PLFA rescued toxicity more effectively than SRFA. In our experiments, the effect of NOM on Ag NP dissolution was minor, however, other researchers showed a decreased dissolution rate with increasing NOM content [325]. Measurement of total tissue silver content indicated that PLFA reduced total organismal (including digestive tract) uptake of ionic silver but not that of citrate-coated Ag NPs (CIT-Ag NPs). The majority of the CIT-Ag NP uptake was in the digestive tract. Limited tissue uptake was detected by hyperspectral microscopy but not by transmission electron microscopy. Co-exposure to PLFA resulted in the formation of NOM-Ag NP composites (both in medium and nematodes) and rescued $AgNO_3$ and CIT-Ag NP-induced cellular damage, potentially by decreasing intracellular uptake of CIT-Ag NPs. Not only did NP-NOM interactions alter the impact of the Ag NPs on exposed nematodes, but the presence of nematodes also affected NP-NOM interactions. We observed "ring"-like structures formed by Ag NPs and NOM only in the presence of nematodes. A recent study found that the extracellular dissolved organic carbon produced by algal cells mitigated silver

nanoparticle toxicity and behavior [326]; therefore, it was possible that the gut or body fluid generated from the nematodes was altering the NP-PLFA interaction.

5.2 Broad Implications and Future Directions

Understanding the correlation between silver nanoparticle toxicity and its physicochemical characteristics will facilitate Ag NP optimization for lower toxicity and its green synthesis. Meanwhile, the mechanism of uptake will provide valuable information for the modeling of fate and toxicokinetics both in cells and organisms. The linkage between Ag NPs and complex environmental variables can also improve the nanosilver safety assessment process. All of the research findings will provide valuable information for the prediction and modeling of nanosilver effects on human health and better facilitate the implementation of regulations on nanosilver products.

This dissertation work has contributed to our understanding of the mechanism by which Ag NPs exert adverse effects in both cells and whole organisms, although uncertainties exist in several perspectives.

NP-specific effect (or ROS generation) has been well studied in cell culture; however, the accuracy of ROS detection in live organisms still needs improvement and optimization. Furthermore, it is still uncertain and controversies remain whether the NP-induced ROS increases that others have reported are caused by direct generation of ROS, or are due to indirect ROS generation that is secondary to cellular dysfunction. Further research needs to focus more on real-time *in vivo* detection (Mitotracker deep

red with fluorescent confocal microscopy), LC-MS, bioluminescence whole animal imaging, etc. [327]. As bench scientists, we are struggling to fill the gap between *in vitro* and *in vivo* data. The study in Chapter 3 aimed to address that gap, applying endocytosis theory to *in vivo* uptake in *C. elegans*. Intracellular trafficking of NPs has been extensively studied [328-330]; however, there is a lack of related studies *in vivo*. Much more work needs to be done in testing the essential cellular pathways which have been demonstrated in cell culture and applying those ideas to whole organism studies [331].

Ag NP behavior, transformation and speciation (especially in aquatic systems) have been intensively investigated [332-334]; however, there are very limited studies focusing on better characterization of Ag NPs *in vivo* [335, 336]. Future research should explore the cellular uptake and speciation of Ag NPs *in vivo* with the aid of X-ray absorption near edge structure (XANES) spectroscopy, EDX, and synchrotron speciation analysis. After the uncertainties of the cellular behavior of Ag NPs are further elucidated, much progress can be made in understanding the Ag NP-bio-organelle interactions and facilitating systematic probing of Ag NP toxicity based on their properties.

There are a large number of molecular pathways that are likely to be involved in regulating Ag NP toxicity other than the limited pathways in this dissertation. Those alternative pathways include receptor activation, lysosomal dysfunction, mitochondrial signaling, protein damage, altered transcription and signaling, etc. More research needs

to focus on the cellular and tissue level, especially the above-mentioned Ag NP-organelle or Ag NP-protein interactions, etc.

At the ecosystem level, further research needs to focus more on the interactive effects between Ag NPs and other ubiquitous contaminants. More ecologically relevant studies are needed to better predict their fate and toxicity in the environment.

C. elegans is a great model for nanotoxicological and mechanistic studies, and so far the general magnitude of toxicity and molecular mechanisms of NP toxicity extrapolate quite well with other model organisms. This model organism will continue to serve an important role in filling the gap between *in vitro* and *in vivo* studies. However, even if *C. elegans* is a great model, the molecular mechanism and toxicity data cannot be directly extrapolated to human health implications. Science is a process of continuously filling the gaps and providing inputs for a much broader context, and nanotoxicological studies will continue to elucidate uncertainties and contribute to the overall public health.

Appendix A- Do Ag NPs cause oxidative stress?

One of the original goals of this dissertation work was to examine ROS generation after Ag NP exposures to determine if direct measurement of ROS production would confirm the results from pharmacological rescue and genetic mutant analysis. In order to test this Mitosox dye was used to examine Ag NP-exposed nematodes with fluorescent confocal microscopy. This work was done collaboratively with Laura Macaulay.

A.1 Nematode dosing and Mitosox incubation

Approximately 25-50 age-matched young adult nematodes were exposed to paraquat and Ag NPs in liquid suspensions mixed with mitochondrial dyes and food. Expsure was done for 24 hrs on an orbit shaker. Triplicate exposures were performed for each treatment. Dosing concentrations for paraquat, PVP_{38}-Ag NPs and GA_{22}-Ag NPs were 18 μM, 0.75 mg-Ag L^{-1} and 0.2 mg-Ag L^{-1}. Mitosox stock was made by dissolving 50 μg Mitosox in 13 μL of Dimethylsulfoxide (DMSO), resulting in a 5 mM Mitosox reagent stock solution. For each 750 μL of dosing suspension (K-Medium mixture), in addition to dosing chemical and food (60 μL of concentrated bacteria suspension with bacteria cells concentrated to approximately $1* 10^{10}$ cells/mL), there were 10 μM Mitosox and 12 μM Mitotracker Green. TMRE was used to normalize mitochondria mass. For TMRE incubation, 12 μM Mitotracker Green and 0.1 μM TMRE were used.

Prior to imaging, nematodes were transferred to no food plates for 2 hrs to clear their guts. Light exposure was minimized to avoid photo-degradation of the dye. Incubating plates were covered in aluminum foil at every point in the process. Worms were imaged by using a 2% agarose pad and immobilized using 5 μL of 10 mg/mL Levamisole. Image J software was used to compare fluorescence of a set area (the pharyngeal bulb) on each emission channel. Background noise was substracted, and then ratios of these emission channels were used to normalize the data. Bright field images were used to minimize bias.

A.2 No significant superoxide detected upon Ag NP exposures

Mitosox, a dye exclusively specific to superoxide, was shown to work in live organisms [337, 338]. This experiment showed that PVP_{38} exposure resulted in less superoxide anion generation than in control nematodes, in a wildtype (N2) background (Fig. 47). However, even paraquat, a very potent ROS inducer and a positive control in this experiment, failed to increase superoxide anion generation (Fig. 47), suggesting that the assay requires further optimization before it can be employed reliably in *C. elegans*.

Mitosox worked well in well controlled systems, e.g., cell cultures [339, 340], once cells were completely in focus, the dyes could be applied completely in dark. However, in our exposure systems, the dyes were highly likely to be auto-exposed especially during the handling of nematodes, which potentially complicated imaging results [341]. Besides, there was quite high fluorescent variability among individual

nematodes, perhaps due to different levels of dye uptake for each nematode. Furthermore, focusing the microscope on nematodes was much more difficult than in cell cultures, but it was critical to maintain microscopic settings (e.g., detection gain) to ensure reliability of the imaging data. In order to achieve much higher accuracy of detection, LC-MS in parallel with fluorescent confocal imaging could be perfomed.

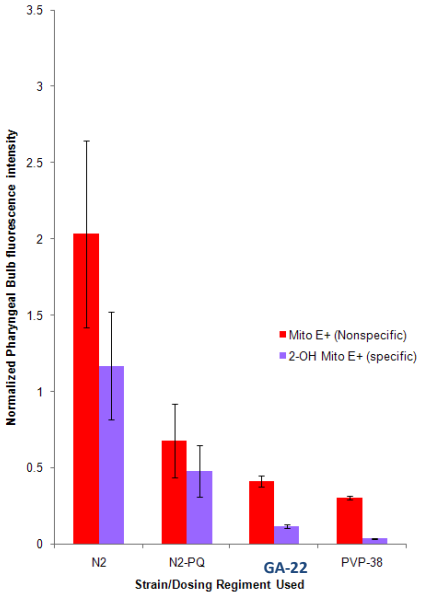

Figure 47. Normalized fluorescent intensity using specific and nonspecific oxidation products.

Appendix B- Do Ag NPs cause DNA damage?

This was a collaborative study with Jinhee Choi from University of Seoul, examining the effects of PVP surface coating and size on the organismal and genetic toxicity of Ag NPs in *C. elegans*. My role in this project was to explore the toxicity (both acute and DNA damage) of $AgNO_3$ and 3 types of Ag NPs in *C. elegans* (wildtype and a DNA damage and oxidative stress response mutant, *cep-1*)

Polymerase-blocking DNA damage was detected using a quantitative long amplicon PCR (QPCR) assay [342, 343]. QPCR detected any alterations to the genomic DNA template that resulted in altered PCR amplification of a large (~10kb) region of the mitochondrial and nuclear genomes, such that damage of any sort results in reduced PCR product. The amplification of these large targets is normalized to genome copy number via measurement of mitochondrial and nuclear genomes using the amplification by real-time PCR of small mitochondrial and nuclear targets [344], in conjunction with standard curves [343]. Any reduction in PCR product, compared to control samples, is converted mathematically to a number of lesions per 10 kb [343].

B.1 QPCR-based DNA damage assay

QPCR was used to measure DNA polymerase-inhibiting DNA lesions [342] upon exposures to Ag NPs. Young adult nematodes were generated by placing synchronized L1's on OP50 plate for 46 hrs at 20 °C, and then exposed to silver nanoparticles in EPA moderately hard water supplemented with cholesterol as described [51]. Exposures

were in 96-well plates, with 50 worms/well dispensed by COPAS Biosort. The treatments were $AgNO_3$ (0.05 ppm), PVP_8 (0.25 ppm), PVP_{38} (0.75 ppm), and noncoated NPs (0.04 ppm) in 100 μL total volume. The dosing concentrations corresponded to approximately the 24 h LC_{10} for each silver type under these conditions (based pilot exposures, which gave similar results for the N2 and *cep-1* strains). The exposure duration was 24 hrs without food. 50 J/m^2 Ultraviolet C radiation (UVC) was used as a positive control for nuclear and mitochondria DNA damage. After 24 hrs of exposure, worms were transferred to no peptone plates to dry and half of the control nematodes were exposed to UVC (UV dosing protocol previously described [344]). For each exposure condition, 6 nematodes were picked into 90 μL of the lysis buffer in triplicate, lysed, and analyzed for DNA damage as previously described [342]. Only living nematodes were picked. For this experiment, we used 26 and 24 cycles for long nuclear and long mitochondrial PCR reactions; mitochondrial and nuclear copy number were measured by real-time PCR as described [344]. The exposures were carried out twice and all samples were analyzed by duplicate QPCR runs.

B.2 No significant DNA damage was indicated (either nuclear or mitochondrial)

Our results suggested very limited DNA damage both in mitochondria and nuclear genome. The level of nuclear DNA (nDNA) damage observed after exposing the nematodes to UVC (positive control) was significantly higher than the controls

($p<0.0001$), but neither $AgNO_3$ nor any of the Ag NPs tested resulted in increased damage compared to the controls ($p>0.05$ in all cases) (Fig. 48A). Mitochondrial DNA (mtDNA) damage was also observed after exposure to UVC. The UCV-exposed nematodes had significantly more mtDNA damage than the controls ($p<0.0001$), but no other treatments resulted in increased damage compared to the controls ($p>0.05$ in all cases) (Fig. 48B). The mtDNA:nDNA ratio was also investigated but no significant trend was observed in any of the sample tested (Fig. 7C). Because negative results were obtained with wildtype *C. elegans*, I additionally conducted the same experiments using a DNA damage sensitive strains, *cep-1*(gk138), which lacks the *C. elegans* homolog of p53. However, none of the types of silver tested led to an increase in DNA lesions either in nDNA or mtDNA of the *cep-1* (gk138) strain (published in Chemosphere) [345].

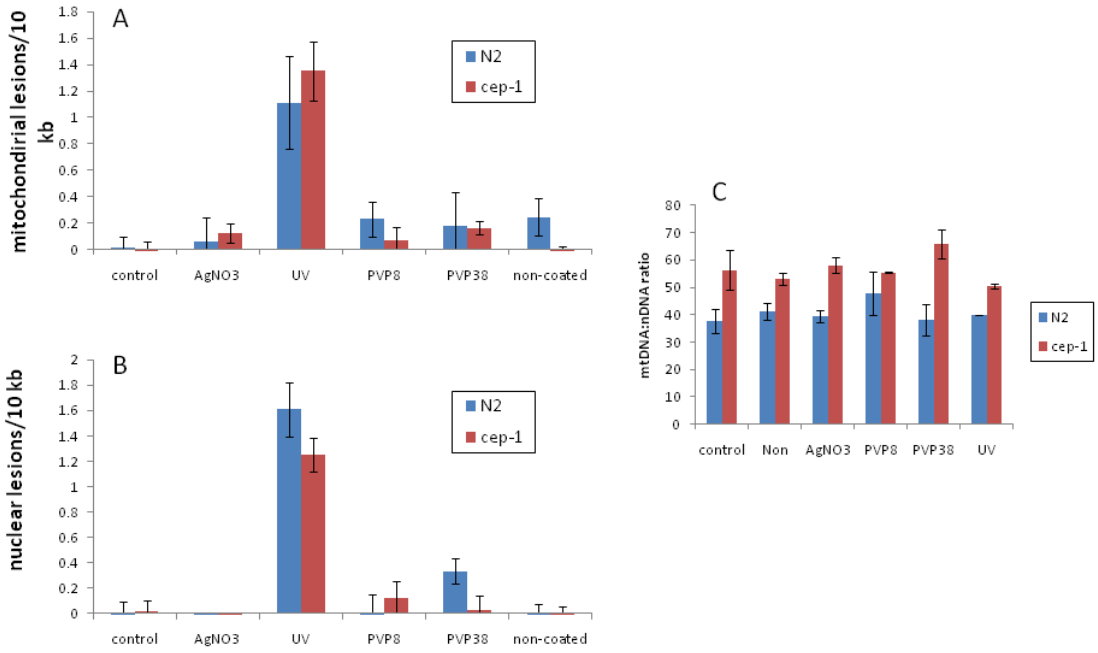

Figure 48. Polymerase-inhibiting DNA lesions were not detected in wildtype or *cep-1* (gk138) *C. elegans* exposed to $AgNO_3$ and Ag NPs.

A) QPCR in the nuclear genome; B) QPCR in the mitochondrial genome; C) The mitochondrial:nuclear DNA ratio measured in the same nematodes. UVC was used as a positive control for the assay. n= 3 experiments were preformed and 2-3 replicates were designed for each treatment. Two QPCR runs were done for each experimental samples.

Appendix C- Do Ag NPs cause unfolded protein response?

C.1 Introduction: the unfolded protein response (UPR) and endoplasmic reticulum (ER) stress

A variety of stresses (endogenous and exogenous) can lead to protein misfolding and aggregation, which further result in cell proteotoxicity [346]. In order to protect against this proteotoxicity, cells employ series of compartment-specific stress responses, including targeted induction of chaperone and degradation organelles within certain subcellular sites [347]. The ER UPR, induced by ER stress, is mediated through three pathways involving the genes XBP-1, ATF-6 and PEK-1 [348, 349]. XBP-1 is protective against the ER stress induced by immune response or inflammation [350]. Expression of a constitutively active form of XBP-1 and XBP-1s can rescue the age-related loss of ER proteostasis [347]. The *xbp-1* loss-of-function mutant of *Caenorhabditis elegans* exhibits constitutively higher ER stress, and higher expression of compensatory genes, e.g., ATF-6 and PEK-1 [349]. XBP-1 plays important roles in the activation of the innate immune response in *C. elegans*, which is involved in defending against the infection with *Pseudomonas aeruginosa* [350]. Therefore, the *xbp-1* mutant was more susceptible to pathogenic infections, leading to severely altered ER morphology, arrested development and larval mortality[350]. This suggested that the IRE-1-xbp-1 pathway of the UPR is

important in the resistance to pathogens such as *Pseudomonas aeruginosa* and pore-forming toxins (PFT) [351].

The major aim of this work was to understand whether Ag NP toxicity is dependent on the immune response-induced ER stress. If so, knocking out the UPR-regulating genes (e.g., XBP-1, ATF-6 and PEK-1) can cause more unfolded protein accumulation (especially in the intestine), which further lead to higher mortality.

Very limited information has been published about how those UPR mutants respond to environmental chemicals (other than pathogens) differently from the wildtype. Therefore, this study was intended to test a potential new pathway of nanotoxicity.

C.2 Methods

Mutant sensitivity analysis between the *xbp-1* strain and wildtype was based on the 72-h growth assay using L1 stage larvael (L1's) of both strains. Both the *xbp-1* and hsp-4::gfp strains were generous provided from Jingru Sun in Aballay lab at Duke University. Details of the growth assay were described in the supporting information of our previous paper [51]. Dosing concentrations of $AgNO_3$ and CIT-Ag NPs were 0-0.2 mg-Ag L^{-1} and 0-2 mg-Ag L^{-1}, respectively. Young adults of the hsp-4::gfp strain were exposed to CIT-Ag NPs (0-2 mg-Ag L^{-1}) for 24 hrs before analysis of GFP in whole organismal level using COPAS Biosort.

C.3 The ER stress-deficient mutant xbp-1 was more sensitive to Ag NPs but not to $AgNO_3$

Our result suggested that the *xbp-1* mutant was more sensitive to citrate-coated Ag NPs but not to Ag^+. However, our hsp-4::gfp strain, which was an indicator of the expression of ER stress response genes, did not show any fluorescence upon Ag NP exposure. These contradictory results need to be further investigated to provide better interpretations.

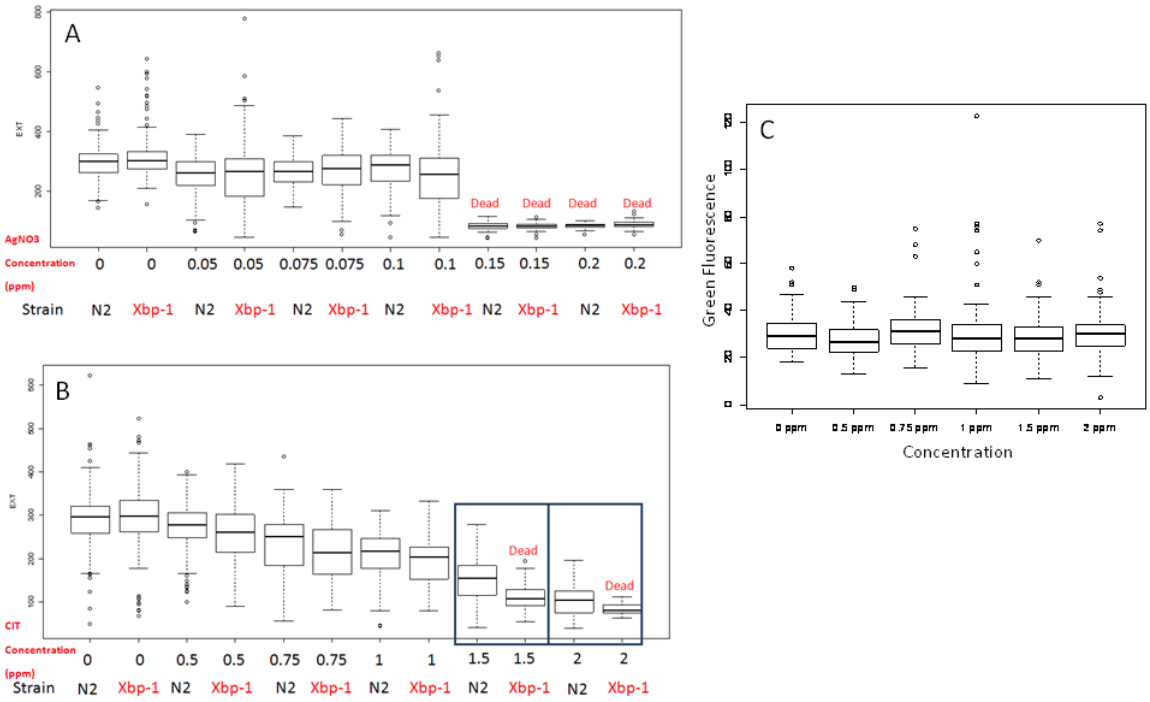

Figure 49. Comparative sensitivity between *xbp-1* and wildtype and fluorescence of hsp-4::gfp strain upon Ag NP exposure.

A) Two strain comparison upon exposure to $AgNO_3$; B) exposure to citrate-coated Ag NPs (CIT-Ag NPs); Boxplots show the 10%, 25%, median, 75% and 90% quantiles of EXT (extinction; a proxy for nematode size) values 72 h post exposure; C) Green fluorescence of hsp-4::gfp strain upon exposure to CIT-Ag NPs. The data points are combined from 3 to 4 replicate experiments.

References

1. Ahamed, M., et al., *DNA damage response to different surface chemistry of silver nanoparticles in mammalian cells.* Toxicology and Applied Pharmacology, 2008. **233**(3): p. 404-410.

2. de Lima, R., A.B. Seabra, and N. Duran, *Silver nanoparticles: a brief review of cytotoxicity and genotoxicity of chemically and biogenically synthesized nanoparticles.* Journal of Applied Toxicology, 2012. **32**(11): p. 867-879.

3. Panyala, N.R., E.M. Pena-Mendez, and J. Havel, *Silver or silver nanoparticles: a hazardous threat to the environment and human health?* Journal of Applied Biomedicine, 2008. **6**(3): p. 117-129.

4. Wijnhoven, S.W.P., et al., *Nano-silver - a review of available data and knowledge gaps in human and environmental risk assessment.* Nanotoxicology, 2009. **3**(2): p. 109-U78.

5. Chen, X. and H.J. Schluesener, *Nanosilver: A nanoproduct in medical application.* Toxicology Letters, 2008. **176**(1): p. 1-12.

6. Lansdown, A.B., *A pharmacological and toxicological profile of silver as an antimicrobial agent in medical devices.* Adv Pharmacol Sci, 2010. **2010**: p. 910686.

7. Silver, S., *Bacterial silver resistance: molecular biology and uses and misuses of silver compounds.* Fems Microbiology Reviews, 2003. **27**(2-3): p. 341-353.

8. Drake, P.L. and K.J. Hazelwood, *Exposure-related health effects of silver and silver compounds: A review.* Annals of Occupational Hygiene, 2005. **49**(7): p. 575-585.

9. Lansdown, A.B., et al., *Silver absorption and antibacterial efficacy of silver dressings.* J Wound Care, 2005. **14**(4): p. 155-60.

10. Lansdown, A.B.G., et al., *Silver aids healing in the sterile skin wound: experimental studies in the laboratory rat.* British Journal of Dermatology, 1997. **137**(5): p. 728-735.

11. Schierholz, J.M., et al., *Silver-containing polymers.* Antimicrobial Agents and Chemotherapy, 1999. **43**(11): p. 2819-2820.

12. Venugopal B, L.T., ed. *Chemical toxicology of metals and metalloids*. 1978, Academic Press: New York. 32-36.

13. Luoma, S.N., Y.B. Ho, and G.W. Bryan, *Fate, Bioavailability and Toxicity of Silver in Estuarine Environments.* Marine Pollution Bulletin, 1995. **31**(1-3): p. 44-54.

14. (BSI), B.S.I., *PAS136 Terminology for nanomaterias.* 2007.

15. (SCENIHR), S.C.o.E.a.N.I.H.R., *Opinion on: The appropriateness of existing methodologies to assess the potential risk associated with engineered and adventitious products of nanotechnologies.* 2006.

16. Wong, K.K.Y. and X.L. Liu, *Silver nanoparticles-the real "silver bullet" in clinical medicine?* Medchemcomm, 2010. **1**(2): p. 125-131.

17. Gubin, S.P., et al., *Magnetic nanoparticles: Preparation methods, structure and properties.* Uspekhi Khimii, 2005. **74**(6): p. 539-574.

18. Jiang, S., et al., *Surface-functionalized nanoparticles for biosensing and imaging-guided therapeutics.* Nanoscale, 2013. **5**(8): p. 3127-3148.

19. Dallas, P., V.K. Sharma, and R. Zboril, *Silver polymeric nanocomposites as advanced antimicrobial agents: Classification, synthetic paths, applications, and perspectives.* Advances in Colloid and Interface Science, 2011. **166**(1-2): p. 119-135.

20. De Jong, W.H. and P.J.A. Borm, *Drug delivery and nanoparticles: Applications and hazards.* International Journal of Nanomedicine, 2008. **3**(2): p. 133-149.

21. Souto, E.B. and R.H. Muller, *Cosmetic features and applications of lipid nanoparticles (SLN, NLC).* Int J Cosmet Sci, 2008. **30**(3): p. 157-65.

22. Wissing, S.A. and R.H. Muller, *Cosmetic applications for solid lipid nanoparticles (SLN).* International Journal of Pharmaceutics, 2003. **254**(1): p. 65-68.

23. Shipway, A.N., E. Katz, and I. Willner, *Nanoparticle arrays on surfaces for electronic, optical, and sensor applications.* Chemphyschem, 2000. **1**(1): p. 18-52.

24. Yan, W.L., et al., *Iron nanoparticles for environmental clean-up: recent developments and future outlook.* Environmental Science-Processes & Impacts, 2013. **15**(1): p. 63-77.

25. Lohse, S.E. and C.J. Murphy, *Applications of Colloidal Inorganic Nanoparticles: From Medicine to Energy.* Journal of the American Chemical Society, 2012. **134**(38): p. 15607-15620.

26. Das, M., et al., *Need for Safety of Nanoparticles Used in Food Industry.* Journal of Biomedical Nanotechnology, 2011. **7**(1): p. 13-14.

27. Salata, O., *Applications of nanoparticles in biology and medicine.* J Nanobiotechnology, 2004. **2**(1): p. 3.

28. De Jong, W.H. and P.J. Borm, *Drug delivery and nanoparticles:applications and hazards.* Int J Nanomedicine, 2008. **3**(2): p. 133-49.

29. Zhao, J.S. and V. Castranova, *Toxicology of Nanomaterials Used in Nanomedicine.* Journal of Toxicology and Environmental Health-Part B-Critical Reviews, 2011. **14**(8): p. 593-632.

30. Maurer-Jones, M.A., et al., *Toxicity of therapeutic nanoparticles.* Nanomedicine, 2009. **4**(2): p. 219-241.

31. Linkov, I., F.K. Satterstrom, and L.M. Corey, *Nanotoxicology and nanomedicine: making hard decisions.* Nanomedicine-Nanotechnology Biology and Medicine, 2008. **4**(2): p. 167-171.

32. Potera, C., *Understanding the Germicidal Effects of Silver Nanoparticles.* Environmental Health Perspectives, 2012. **120**(10): p. A386-A386.

33. Morones, J.R., et al., *The bactericidal effect of silver nanoparticles.* Nanotechnology, 2005. **16**(10): p. 2346-2353.

34. Ji, J.H., et al., *Twenty-eight-day inhalation toxicity study of silver nanoparticles in Sprague-Dawley rats.* Inhalation Toxicology, 2007. **19**(10): p. 857-871.

35. Galdiero, S., et al., *Silver Nanoparticles as Potential Antiviral Agents.* Molecules, 2011. **16**(10): p. 8894-8918.

36. Brandt, O., et al., *Nanoscalic silver possesses broad-spectrum antimicrobial activities and exhibits fewer toxicological side effects than silver sulfadiazine.* Nanomedicine-Nanotechnology Biology and Medicine, 2012. **8**(4): p. 478-488.

37. Choi, H., et al., *Multipositional Silica-Coated Silver Nanoparticles for High-Performance Polymer Solar Cells.* Nano Letters, 2013. **13**(5): p. 2204-2208.

38. Kokura, S., et al., *Silver nanoparticles as a safe preservative for use in cosmetics.* Nanomedicine-Nanotechnology Biology and Medicine, 2010. **6**(4): p. 570-574.

39. Abou El-Nour, K.M.M., et al., *Synthesis and applications of silver nanoparticles.* Arabian Journal of Chemistry, 2010. **3**(3): p. 135-140.

40. Gracia-Pinilla, M.A., et al., *On the structure and properties of silver nanoparticles.* Journal of Physical Chemistry C, 2008. **112**(35): p. 13492-13498.

41. George, S., et al., *Surface Defects on Plate-Shaped Silver Nanoparticles Contribute to Its Hazard Potential in a Fish Gill Cell Line and Zebrafish Embryos.* ACS Nano, 2012. **6**(5): p. 3745-3759.

42. Stoehr, L.C., et al., *Shape matters: effects of silver nanospheres and wires on human alveolar epithelial cells.* Particle and Fibre Toxicology, 2011. **8**.

43. Sperling, R.A. and W.J. Parak, *Surface modification, functionalization and bioconjugation of colloidal inorganic nanoparticles.* Philosophical Transactions of the Royal Society a-Mathematical Physical and Engineering Sciences, 2010. **368**(1915): p. 1333-1383.

44. Chatterjee, U., S.K. Jewrajka, and S. Guha, *Dispersion of Functionalized Silver Nanoparticles in Polymer Matrices: Stability, Characterization, and Physical Properties.* Polymer Composites, 2009. **30**(6): p. 827-834.

45. Balachandran, Y.L., et al., *Differently Environment Stable Bio-Silver Nanoparticles: Study on Their Optical Enhancing and Antibacterial Properties.* Plos One, 2013. **8**(10).

46. Meyer, M.W. and E.A. Smith, *Optimization of silver nanoparticles for surface enhanced Raman spectroscopy of structurally diverse analytes using visible and near-infrared excitation.* Analyst, 2011. **136**(17): p. 3542-3549.

47. Zhang, W.X., *Nanoscale iron particles for environmental remediation: An overview.* Journal of Nanoparticle Research, 2003. **5**(3-4): p. 323-332.

48. Ma, R., et al., *Size-Controlled Dissolution of Organic-Coated Silver Nanoparticles.* Environmental Science & Technology, 2012. **46**(2): p. 752-759.

49. Levard, C., et al., *Effect of Chloride on the Dissolution Rate of Silver Nanoparticles and Toxicity to E. coli.* Environmental Science & Technology, 2013. **47**(11): p. 5738-5745.

50. El Badawy, A.M., et al., *Surface Charge-Dependent Toxicity of Silver Nanoparticles.* Environmental Science & Technology, 2011. **45**(1): p. 283-287.

51. Yang, X.Y., et al., *Mechanism of Silver Nanoparticle Toxicity Is Dependent on Dissolved Silver and Surface Coating in Caenorhabditis elegans.* Environmental Science & Technology, 2012. **46**(2): p. 1119-1127.

52. Suresh, A.K., et al., *Cytotoxicity Induced by Engineered Silver Nanocrystallites Is Dependent on Surface Coatings and Cell Types.* Langmuir, 2012. **28**(5): p. 2727-2735.

53. Sharma, V.K., et al., *Organic-coated silver nanoparticles in biological and environmental conditions: Fate, stability and toxicity.* Adv Colloid Interface Sci, 2013.

54. Reidy, B., et al., *Mechanisms of Silver Nanoparticle Release, Transformation and Toxicity: A Critical Review of Current Knowledge and Recommendations for Future Studies and Applications.* Materials, 2013. **6**(6): p. 2295-2350.

55. Li, X. and J.J. Lenhart, *Aggregation and Dissolution of Silver Nanoparticles in Natural Surface Water.* Environmental Science & Technology, 2012. **46**(10): p. 5378-5386.

56. Whiteley, C.M., et al., *Challenges in assessing release, exposure and fate of silver nanoparticles within the UK environment.* Environmental Science-Processes & Impacts, 2013. **15**(11): p. 2050-2058.

57. Ma, R., et al., *Fate of zinc oxide and silver nanoparticles in a pilot wastewater treatment plant and in processed biosolids.* Environmental Science & Technology, 2014. **48**(1): p. 104-12.

58. Levard, C., et al., *Sulfidation of Silver Nanoparticles: Natural Antidote to Their Toxicity.* Environmental Science & Technology, 2013. **47**(23): p. 13440-13448.

59. Huynh, K.A. and K.L. Chen, *Aggregation kinetics of silver nanoparticles in monovalent and divalent electrolyte solutions: Implications for environmental fate and transport.* Abstracts of Papers of the American Chemical Society, 2010. **240**.

60. Kanel, S.R., et al., *Fate and transport of silver nanoparticles and silver ions in saturated porous media: Laboratory experiments and modeling.* Abstracts of Papers of the American Chemical Society, 2012. **244**.

61. Kanel, S.R., et al., *Fate and transport of silver nanoparticles and related products in saturated porous media.* Abstracts of Papers of the American Chemical Society, 2012. **243**.

62. Yu, S.J., Y.G. Yin, and J.F. Liu, *Silver nanoparticles in the environment.* Environmental Science-Processes & Impacts, 2013. **15**(1): p. 78-92.

63. Wiesner, M.R., et al., *Decreasing Uncertainties in Assessing Environmental Exposure, Risk, and Ecological Implications of Nanomaterials.* Environmental Science & Technology, 2009. **43**(17): p. 6458-6462.

64. Seltenrich, N., *Nanosilver Weighing the Risks and Benefits.* Environmental Health Perspectives, 2013. **121**(7): p. A220-A225.

65. Benn, T.M. and P. Westerhoff, *Nanoparticle silver released into water from commercially available sock fabrics (vol 42, pg 4133, 2008).* Environmental Science & Technology, 2008. **42**(18): p. 7025-7026.

66. Sathyavathi, R., et al., *Biosynthesis of Silver Nanoparticles Using Coriandrum Sativum Leaf Extract and Their Application in Nonlinear Optics.* Advanced Science Letters, 2010. **3**(2): p. 138-143.

67. Zhang, Z., et al., *Detection of Engineered Silver Nanoparticle Contamination in Pears.* Journal of Agricultural and Food Chemistry, 2012. **60**(43): p. 10762-10767.

68. Fabrega, J., et al., *Silver nanoparticles: Behaviour and effects in the aquatic environment.* Environment International, 2011. **37**(2): p. 517-531.

69. Blinova, I., et al., *Toxicity of two types of silver nanoparticles to aquatic crustaceans Daphnia magna and Thamnocephalus platyurus (vol 20, pg 3456, 2013).* Environmental Science and Pollution Research, 2013. **20**(6): p. 4293-4293.

70. Oukarroum, A., et al., *Silver nanoparticle toxicity effect on growth and cellular viability of the aquatic plant Lemna gibba.* Environmental Toxicology and Chemistry, 2013. **32**(4): p. 902-907.

71. Asghari, S., et al., *Toxicity of various silver nanoparticles compared to silver ions in Daphnia magna.* Journal of Nanobiotechnology, 2012. **10**.

72. Quadros, M.E. and L.C. Marr, *Environmental and Human Health Risks of Aerosolized Silver Nanoparticles.* Journal of the Air & Waste Management Association, 2010. **60**(7): p. 770-781.

73. Sung, J.H., et al., *Subchronic Inhalation Toxicity of Silver Nanoparticles.* Toxicological Sciences, 2009. **108**(2): p. 452-461.

74. Levard, C., et al., *Environmental Transformations of Silver Nanoparticles: Impact on Stability and Toxicity.* Environmental Science & Technology, 2012. **46**(13): p. 6900-6914.

75. van Aerle, R., et al., *Molecular Mechanisms of Toxicity of Silver Nanoparticles in Zebrafish Embryos.* Environmental Science & Technology, 2013. **47**(14): p. 8005-8014.

76. Miao, A.J., et al., *Intracellular Uptake: A Possible Mechanism for Silver Engineered Nanoparticle Toxicity to a Freshwater Alga Ochromonas danica.* Plos One, 2010. **5**(12).

77. Kiontke, K. and W. Sudhaus, *Ecology of Caenorhabditis species.* WormBook, 2006: p. 1-14.

78. Tax, F.E., J.J. Yeargers, and J.H. Thomas, *Sequence of C-Elegans Lag-2 Reveals a Cell-Signaling Domain Shared with Delta and Serrate of Drosophila.* Nature, 1994. **368**(6467): p. 150-154.

79. Rothman, J.H. and A. Singson, *Caenorhabditis elegans: molecular genetics and development.* Methods Cell Biol, 2011. **106**: p. xv-xviii.

80. Nehme, R. and B. Conradt, *egl-1: a key activator of apoptotic cell death in C-elegans.* Oncogene, 2008. **27**: p. S30-S40.

81. Goodman, M.B., et al., *Electrophysiological Methods for Caenorhabditis elegans Neurobiology.* Caenorhabditis Elegans: Cell Biology and Physiology, Second Edition, 2012. **107**: p. 409-436.

82. Brooks, K.K., B. Liang, and J.L. Watts, *The Influence of Bacterial Diet on Fat Storage in C. elegans.* Plos One, 2009. **4**(10).

83. Shtonda, B.B. and L. Avery, *Dietary choice behavior in Caenorhabditis elegans.* Journal of Experimental Biology, 2006. **209**(1): p. 89-102.

84. Barriere, A. and M.A. Felix, *Natural variation and population genetics of Caenorhabditis elegans.* WormBook, 2005: p. 1-19.

85. *Genome sequence of the nematode C. elegans: A platform for investigating biology (vol 282, pg 2012, 1998).* Science, 1999. **285**(5433): p. 1493-1493.

86. Lai, C.H., et al., *Identification of novel human genes evolutionarily conserved in Caenorhabditis elegans by comparative proteomics.* Genome Research, 2000. **10**(5): p. 703-713.

87. Baumeister, R. and L.M. Ge, *The worm in us - Caenorhabditis elegans as a model of human disease.* Trends in Biotechnology, 2002. **20**(4): p. 147-148.

88. Shaye, D.D. and I. Greenwald, *OrthoList: a compendium of C. elegans genes with human orthologs.* Plos One, 2011. **6**(5): p. e20085.

89. Vranic, S., et al., *Deciphering the mechanisms of cellular uptake of engineered nanoparticles by accurate evaluation of internalization using imaging flow cytometry.* Particle and Fibre Toxicology, 2013. **10**: p. 2.

90. Zhang, L.W. and N.A. Monteiro-Riviere, *Mechanisms of Quantum Dot Nanoparticle Cellular Uptake.* Toxicological Sciences, 2009. **110**(1): p. 138-155.

91. Lenaerts, V., et al., *In vivo uptake of polyisobutyl cyanoacrylate nanoparticles by rat liver Kupffer, endothelial, and parenchymal cells.* J Pharm Sci, 1984. **73**(7): p. 980-2.

92. Wang, T.T., et al., *Cellular Uptake of Nanoparticles by Membrane Penetration: A Study Combining Confocal Microscopy with FTIR Spectroelectrochemistry.* ACS Nano, 2012. **6**(2): p. 1251-1259.

93. Liu, X.S., et al., *Enhanced Retention and Cellular Uptake of Nanoparticles in Tumors by Controlling Their Aggregation Behavior.* ACS Nano, 2013. **7**(7): p. 6244-6257.

94. Meyer, J.N., et al., *Intracellular uptake and associated toxicity of silver nanoparticles in Caenorhabditis elegans.* Aquatic Toxicology, 2010. **100**(2): p. 140-150.

95. Cha, Y.J., J. Lee, and S.S. Choi, *Apoptosis-mediated in vivo toxicity of hydroxylated fullerene nanoparticles in soil nematode Caenorhabditis elegans.* Chemosphere, 2012. **87**(1): p. 49-54.

96. Zhang, Y.Q., et al., *Selection of Reliable Reference Genes in Caenorhabditis elegans for Analysis of Nanotoxicity.* Plos One, 2012. **7**(3).

97. Tyne, W., et al., *A new medium for Caenorhabditis elegans toxicology and nanotoxicology studies designed to better reflect natural soil solution conditions.* Environ Toxicol Chem, 2013. **32**(8): p. 1711-7.

98. Qu, Y., et al., *Full Assessment of Fate and Physiological Behavior of Quantum Dots Utilizing Caenorhabditis elegans as a Model Organism.* Nano Letters, 2011. **11**(8): p. 3174-3183.

99. Daewlaetsina, G.I., R.T. Minullina, and R.F. Fakhrullin, *Microworms swallow the nanobait: the use of nanocoated microbial cells for the direct delivery of nanoparticles into Caenorhabditis elegans.* Nanoscale, 2013. **5**(23): p. 11761-11769.

100. Kim, E., et al., *Long-Term Imaging of Caenorhabditis elegans Using Nanoparticle-Mediated Immobilization.* Plos One, 2013. **8**(1).

101. Ahamed, M., M.S. Alsalhi, and M.K. Siddiqui, *Silver nanoparticle applications and human health.* Clin Chim Acta, 2010.

102. Benn, T.M. and P. Westerhoff, *Nanoparticle silver released into water from commercially available sock fabrics.* Environmental Science & Technology, 2008. **42**(11): p. 4133-4139.

103. Bryaskova, R., et al., *Antibacterial activity of poly(vinyl alcohol)-b-poly(acrylonitrile) based micelles loaded with silver nanoparticles.* Journal of Colloid and Interface Science, 2010. **344**(2): p. 424-428.

104. Lara, H.H., et al., *Bactericidal effect of silver nanoparticles against multidrug-resistant bacteria.* World Journal of Microbiology & Biotechnology, 2010. **26**(4): p. 615-621.

105. Lee, S.M., K.C. Song, and B.S. Lee, *Antibacterial activity of silver nanoparticles prepared by a chemical reduction method.* Korean Journal of Chemical Engineering, 2010. **27**(2): p. 688-692.

106. Li, W.R., et al., *Antibacterial activity and mechanism of silver nanoparticles on Escherichia coli.* Applied Microbiology and Biotechnology, 2010. **85**(4): p. 1115-1122.

107. Bar-Ilan, O., et al., *Toxicity Assessments of Multisized Gold and Silver Nanoparticles in Zebrafish Embryos.* Small, 2009. **5**(16): p. 1897-1910.

108. Asharani, P.V., et al., *Toxicity of silver nanoparticles in zebrafish models.* Nanotechnology, 2008. **19**(25): p. -.

109. Lee, K.J., et al., *In vivo imaging of transport and biocompatibility of single silver nanoparticles in early development of zebrafish embryos.* Acs Nano, 2007. **1**(2): p. 133-143.

110. Chae, Y.J., et al., *Evaluation of the toxic impact of silver nanoparticles on Japanese medaka (Oryzias latipes).* Aquatic Toxicology, 2009. **94**(4): p. 320-327.

111. Bilberg, K., et al., *Silver nanoparticles and silver nitrate cause respiratory stress in Eurasian perch (Perca fluviatilis).* Aquatic Toxicology, 2010. **96**(2): p. 159-165.

112. AshaRani, P.V., M.P. Hande, and S. Valiyaveettil, *Anti-proliferative activity of silver nanoparticles.* Bmc Cell Biology, 2009. **10**: p. -.

113. Chen, D.F., T.F. Xi, and J. Bai, *Biological effects induced by nanosilver particles: in vivo study.* Biomedical Materials, 2007. **2**(3): p. S126-S128.

114. Rahman, M.F., et al., *Expression of genes related to oxidative stress in the mouse brain after exposure to silver-25 nanoparticles.* Toxicology Letters, 2009. **187**(1): p. 15-21.

115. Roh, J.Y., et al., *Ecotoxicity of Silver Nanoparticles on the Soil Nematode Caenorhabditis elegans Using Functional Ecotoxicogenomics.* Environmental Science & Technology, 2009. **43**(10): p. 3933-3940.

116. Meyer, J.N., et al., *Intracellular uptake and associated toxicity of silver nanoparticles in Caenorhabditis elegans.* Aquatic Toxicology, 2010. **100**(2): p. 140-50.

117. Auffan, M., et al., *Inorganic manufactured nanoparticles: how their physicochemical properties influence their biological effects in aqueous environments.* Nanomedicine, 2010. **5**(6): p. 999-1007.

118. Liu, J. and R.H. Hurt, *Ion Release Kinetics and Particle Persistence in Aqueous Nano-Silver Colloids.* Environmental Science & Technology, 2010. **44**(6): p. 2169-2175.

119. Kvitek, L., et al., *Initial Study on the Toxicity of Silver Nanoparticles (NPs) against Paramecium caudatum.* Journal of Physical Chemistry C, 2009. **113**(11): p. 4296-4300.

120. Kittler, S., et al., *Synthesis of PVP-coated silver nanoparticles and their biological activity towards human mesenchymal stem cells.* Mat.-wiss.u.Werkstofftech, 2009. **40**(4): p. 258-264.

121. Miao, A.J., et al., *The algal toxicity of silver engineered nanoparticles and detoxification by exopolymeric substances.* Environmental Pollution, 2009. **157**(11): p. 3034-3041.

122. Navarro, E., et al., *Toxicity of Silver Nanoparticles to Chlamydomonas reinhardtii.* Environmental Science & Technology, 2008. **42**(23): p. 8959-8964.

123. Xiu, Z.M., J. Ma, and P.J. Alvarez, *Differential Effect of Common Ligands and Molecular Oxygen on Antimicrobial Activity of Silver Nanoparticles versus Silver Ions.* Environ Sci Technol, 2011.

124. van der Zande, M., et al., *Distribution, Elimination, and Toxicity of Silver Nanoparticles and Silver Ions in Rats after 28-Day Oral Exposure.* ACS Nano, 2012. **6**(8): p. 7427-7442.

125. Carlson, C., et al., *Unique Cellular Interaction of Silver Nanoparticles: Size-Dependent Generation of Reactive Oxygen Species.* Journal of Physical Chemistry B, 2008. **112**(43): p. 13608-13619.

126. Choi, O. and Z.Q. Hu, *Size dependent and reactive oxygen species related nanosilver toxicity to nitrifying bacteria.* Environmental Science & Technology, 2008. **42**(12): p. 4583-4588.

127. Kim, S., et al., *Oxidative stress-dependent toxicity of silver nanoparticles in human hepatoma cells.* Toxicology in Vitro, 2009. **23**(6): p. 1076-1084.

128. Foldbjerg, R., et al., *PVP-coated silver nanoparticles and silver ions induce reactive oxygen species, apoptosis and necrosis in THP-1 monocytes.* Toxicology Letters, 2009. **190**(2): p. 156-162.

129. AshaRani, P.V., et al., *Cytotoxicity and Genotoxicity of Silver Nanoparticles in Human Cells.* ACS Nano, 2009. **3**(2): p. 279-290.

130. Kawata, K., M. Osawa, and S. Okabe, *In Vitro Toxicity of Silver Nanoparticles at Noncytotoxic Doses to HepG2 Human Hepatoma Cells.* Environmental Science & Technology, 2009. **43**(15): p. 6046-6051.

131. Eom, H.-J. and J. Choi, *p38 MAPK Activation, DNA Damage, Cell Cycle Arrest and Apoptosis As Mechanisms of Toxicity of Silver Nanoparticles in Jurkat T Cells.* Environmental Science & Technology, 2010. **44**(21): p. 8337-8342.

132. Kittler, S., et al., *Synthesis of PVP-coated silver nanoparticles and their biological activity towards human mesenchymal stem cells.* Materialwissenschaft Und Werkstofftechnik, 2009. **40**(4): p. 258-264.

133. Liu, F., et al., *Ultrathin Diamond-like Carbon Film Coated Silver Nanoparticles-Based Substrates for Surface-Enhanced Raman Spectroscopy.* Acs Nano, 2010. **4**(5): p. 2643-2648.

134. Lu, W.T., et al., *Effect of surface coating on the toxicity of silver nanomaterials on human skin keratinocytes.* Chemical Physics Letters, 2010. **487**(1-3): p. 92-96.

135. Suresh, A.K., et al., *Silver Nanocrystallites: Biofabrication using Shewanella oneidensis, and an Evaluation of Their Comparative Toxicity on Gram-negative and Gram-positive Bacteria.* Environmental Science & Technology, 2010. **44**(13): p. 5210-5215.

136. Jin, X., et al., *High-Throughput Screening of Silver Nanoparticle Stability and Bacterial Inactivation in Aquatic Media: Influence of Specific Ions.* Environmental Science & Technology, 2010. **44**(19): p. 7321-7328.

137. Muhling, M., et al., *Impact of Silver Nanoparticle Contamination on the Genetic Diversity of Natural Bacterial Assemblages in Estuarine Sediments.* Environmental Science & Technology, 2009. **43**(12): p. 4530-4536.

138. Kennedy, A.J., et al., *Fractionating Nanosilver: Importance for Determining Toxicity to Aquatic Test Organisms.* Environmental Science & Technology, 2010. **44**(24): p. 9571-9577.

139. Damm, C. and H. Munstedt, *Kinetic aspects of the silver ion release from antimicrobial polyamide/silver nanocomposites.* Applied Physics a-Materials Science & Processing, 2008. **91**(3): p. 479-486.

140. Williams, P.L. and D.B. Dusenbery, *Using the Nematode Caenorhabditis-Elegans to Predict Mammalian Acute Lethality to Metallic Salts.* Toxicology and Industrial Health, 1988. **4**(4): p. 469-478.

141. Yin, L., et al., *More than the Ions: The Effects of Silver Nanoparticles on Lolium multiflorum.* Environmental Science & Technology, 2011. **45**(6): p. 2360-2367.

142. Silvert, P.-Y., et al., *Preparation of colloidal silver dispersions by the polyol process. Part 1-Synthesis and characterization.* Journal of Materials Chemistry, 1996. **6**(4): p. 573-577.

143. Silvert, P.-Y., R. Herrera-Urbina, and K. Tekaia-Elhsissen, *Preparation of colloidal silver dispersions by the polyol process.* Journal of Materials Chemistry, 1997. **7**(2): p. 293-299.

144. Meyer, J.N., et al., *Decline of nucleotide excision repair capacity in aging Caenorhabditis elegans.* Genome Biology, 2007. **8**(5): p. -.

145. Khanna, N., et al., *Tolerance of the nematode Caenorhabditis elegans to pH, salinity, and hardness in aquatic media.* Archives of Environmental Contamination and Toxicology, 1997. **32**(1): p. 110-114.

146. Smith, M.V., et al., *A Discrete Time Model for the Analysis of Medium-Throughput C. elegans Growth Data.* Plos One, 2009. **4**(9): p. -e7018.

147. Leung, M.C., et al., *Caenorhabditis elegans Generates Biologically Relevant Levels of Genotoxic Metabolites from Aflatoxin B1 but Not Benzo[a]pyrene In Vivo.* Toxicological Sciences, 2010. **118**(2): p. 444-453.

148. EPA, *Methods for measuring the acute toxicity of elluents and receiving waters to freshwater and marine organisms.* 2002.

149. Aballay, A., L.E. Fuhrman, and K.V. Shianna, *High-Throughput Isolation and Mapping of C. elegans Mutants Susceptible to Pathogen Infection.* Plos One, 2008. **3**(8).

150. M. Elimelech, J.G., Xiadong Jia, Richard Williams, ed. *Particle deposition and aggregation: measurement, modelling and simulation*. 1998. 27-29.

151. Vairavamurthy, A. and K. Mopper, *Field methods for determination of traces of thiols in natural waters.* Analytica Chimica Acta, 1990. **236**: p. 363-370.

152. Hsu-Kim, H., *Stability of metal - glutathione complexes during oxidation by hydrogen peroxide and Cu(II) catalysis.* Environmental Science & Technology, 2007. **41**: p. 2338-2342.

153. Schecher, W.D., *MINEQL+: A Chemical Equilibrium Program for Personal Computers*. 4.5 ed. 2001, Hallowell, ME: Environmental Research Software.

154. National Institute of Standards and Technology, *Critical Stability Constants of Metal Complexes Database*. v. 2.0 ed, ed. N.S.R. Database. 1993.

155. Adams, N.W.H. and J.R. Kramer, *Potentiometric determination of silver thiolate formation constants using a Ag_2S electrode.* Aquatic Geochemistry, 1999. **5**: p. 1-11.

156. Schecher, W.D., *MINEQL+: A Chemical Equilibrium Program for Personal Computers.* Hallowell, ME: Environmental Research Software, 2001.

157. *Critical Stability Constants of Metal Complexes Database.* v. 2.0 ed, ed. N.S.R. Database, 1993.

158. Adams, N.W.H. and J.R. Kramer, *Potentiometric determination of silver thiolate formation constants using a Ag2S electrode.* Aquatic Geochemistry, 1999. **5**(1): p. 1-11.

159. Technology, N.I.o.S.a., *Critical Stability Constants of Metal Complexes Database.* v. 2.0 ed, ed. N.S.R. Database, 1993.

160. Proux, O. and et al., *FAME: a new beamline for x-ray absorption investigations of very-diluted systems of environmental, material and biological interests.* Physica Scripta, 2005. **2005**(T115): p. 970.

161. Proux, O., et al., *Feedback system of a liquid-nitrogen-cooled double-crystal monochromator: design and performances.* Journal of synchrotron radiation, 2006. **13**(Pt 1): p. 59-68.

162. Ravel, B. and M. Newville, *ATHENA, ARTEMIS, HEPHAESTUS: data analysis for X-ray absorption spectroscopy using IFEFFIT.* Journal of Synchrotron Radiation, 2005. **12**: p. 537-541.

163. Pulak, R., *Techniques for analysis, sorting, and dispensing of C. elegans on the COPAS flow-sorting system.* Methods Mol Biol, 2006. **351**: p. 275-86.

164. Li, X.A., J.J. Lenhart, and H.W. Walker, *Dissolution-Accompanied Aggregation Kinetics of Silver Nanoparticles.* Langmuir, 2010. **26**(22): p. 16690-16698.

165. Lead, J.R., et al., *Silver nanoparticles: Behaviour and effects in the aquatic environment.* Environment International, 2011. **37**(2): p. 517-531.

166. Elzey, S. and V.H. Grassian, *Agglomeration, isolation and dissolution of commercially manufactured silver nanoparticles in aqueous environments.* Journal of Nanoparticle Research, 2010. **12**(5): p. 1945-1958.

167. Liu, J., et al., *Controlled Release of Biologically Active Silver from Nanosilver Surfaces.* Acs Nano, 2010: p. 6903-6913.

168. Nurmi, J.T., et al., *Characterization and properties of metallic iron nanoparticles: Spectroscopy, electrochemistry, and kinetics.* Environmental Science & Technology, 2005. **39**(5): p. 1221-1230.

169. Stoeger, T., et al., *Inflammatory response to TiO2 and Carbonaceous particles scales best with BET surface area.* Environmental Health Perspectives, 2007. **115**(6): p. A290-A291.

170. Wittmaack, K., *In Search of the Most Relevant Parameter for Quantifying Lung Inflammatory Response to Nanoparticle Exposure: Particle Number, Surface Area, or What?* Environ Health Perspect, 2006. **115**(2).

171. Kristiansen, S., P. Ifversen, and G. Danscher, *Ultrastructural localization and chemical binding of silver ions in human organotypic skin cultures.* Histochemistry and Cell Biology, 2008. **130**(1): p. 177-184.

172. Boyd, W.A., et al., *Nucleotide excision repair genes are expressed at low levels and are not detectably inducible in Caenorhabditis elegans somatic tissues, but their function is required for normal adult life after UVC exposure.* Mutation Research/Fundamental and Molecular Mechanisms of Mutagenesis, 2010. **683**(1-2): p. 57-67.

173. Vazquez-Manrique, R.P., et al., *Reduction of Caenorhabditis elegans frataxin increases sensitivity to oxidative stress, reduces lifespan, and causes lethality in a mitochondrial complex II mutant.* Faseb Journal, 2005. **19**(12): p. 172-+.

174. Ishii, N., et al., *A Methyl Viologen-Sensitive Mutant of the Nematode Caenorhabditis-Elegans.* Mutation Research, 1990. **237**(3-4): p. 165-171.

175. Dingley, S., et al., *Mitochondrial respiratory chain dysfunction variably increases oxidant stress in Caenorhabditis elegans.* Mitochondrion, 2010. **10**(2): p. 125-136.

176. Swain, S.C., et al., *C-elegans metallothioneins: New insights into the phenotypic effects of cadmium toxicosis.* Journal of Molecular Biology, 2004. **341**(4): p. 951-959.

177. Jiang, G.C.T., et al., *Caenorhabditis elegans Metallothioneins Protect against Toxicity Induced by Depleted Uranium.* Toxicological Sciences, 2009. **111**(2): p. 345-354.

178. Cui, Y.X., et al., *Toxicogenomic analysis of Caenorhabditis elegans reveals novel genes and pathways involved in the resistance to cadmium toxicity.* Genome Biology, 2007. **8**(6): p. -.

179. Hughes, S.L., et al., *The Metabolomic Responses of Caenorhabditis elegans to Cadmium Are Largely Independent of Metallothionein Status, but Dominated by Changes in Cystathionine and Phytochelatins.* Journal of Proteome Research, 2009. **8**(7): p. 3512-3519.

180. Di Giulio RT, M.J., *Reactive oxygen species and oxidative stress*. The Toxicology of Fishes ed. D.G.R.a.H. DE. 2008, Taylor and Francis, Washington, DC. 273-324.

181. Hughes, S.L., et al., *The Metabolomic Responses of Caenorhabditis elegans to Cadmium Are Largely Independent of Metallothionein Status, but Dominated by Changes in Cystathionine and Phytochelatins.* Journal of Proteome Research, 2009. **8**(7): p. 3512-3519.

182. Powers, C.M., et al., *Silver Impairs Neurodevelopment: Studies in PC12 Cells.* Environmental Health Perspectives, 2010. **118**(1): p. 73-79.

183. Powers, C.M., et al., *Silver Nanoparticles Compromise Neurodevelopment in PC12 Cells: Critical Contributions of Silver Ion, Particle Size, Coating, and Composition.* Environmental Health Perspectives, 2011. **119**(1): p. 37-44.

184. Häfeli, U.O., et al., *Cell Uptake and in Vitro Toxicity of Magnetic Nanoparticles Suitable for Drug Delivery.* Molecular Pharmaceutics, 2009. **6**(5): p. 1417-1428.

185. Hauck, T.S., A.A. Ghazani, and W.C.W. Chan, *Assessing the effect of surface chemistry on gold nanorod uptake, toxicity, and gene expression in mammalian cells.* Small, 2008. **4**(1): p. 153-159.

186. Lenaerts, V., et al., *In Vivo uptake of polyisobutyl cyanoacrylate nanoparticles by rat liver Kupffer, endothelial, and parenchymal cells.* Journal of Pharmaceutical Sciences, 1984. **73**(7): p. 980-982.

187. Yang, X., et al., *Mechanism of Silver Nanoparticle Toxicity Is Dependent on Dissolved Silver and Surface Coating in Caenorhabditis elegans.* Environmental Science & Technology, 2011. **46**(2): p. 1119-1127.

188. Shoults-Wilson, W.A., et al., *Effect of silver nanoparticle surface coating on bioaccumulation and reproductive toxicity in earthworms (Eisenia fetida).* Nanotoxicology, 2011. **5**(3): p. 432-444.

189. Gorth, D.J., D.M. Rand, and T.J. Webster, *Silver nanoparticle toxicity in Drosophila: size does matter.* International Journal of Nanomedicine, 2011. **6**: p. 343-350.

190. Skebo, J.E., et al., *Assessment of Metal Nanoparticle Agglomeration, Uptake, and Interaction Using High-Illuminating System.* International Journal of Toxicology, 2007. **26**(2): p. 135-141.

191. Davda, J. and V. Labhasetwar, *Characterization of nanoparticle uptake by endothelial cells.* International Journal of Pharmaceutics, 2002. **233**(1-2): p. 51-59.

192. Lunov, O., et al., *Differential Uptake of Functionalized Polystyrene Nanoparticles by Human Macrophages and a Monocytic Cell Line.* ACS Nano, 2011. **5**(3): p. 1657-1669.

193. Baltazar, G.C., et al., *Acidic Nanoparticles Are Trafficked to Lysosomes and Restore an Acidic Lysosomal pH and Degradative Function to Compromised ARPE-19 Cells.* Plos One, 2012. **7**(12).

194. Kenzaoui, B.H., et al., *Induction of oxidative stress, lysosome activation and autophagy by nanoparticles in human brain-derived endothelial cells.* Biochemical Journal, 2012. **441**: p. 813-821.

195. Meng, W., et al., *Evaluation of Poly (Glycerol-Adipate) Nanoparticle Uptake in an In Vitro 3-D Brain Tumor Co-Culture Model.* Experimental Biology and Medicine, 2007. **232**(8): p. 1100-1108.

196. Lee, J.H., et al., *Biopersistence of silver nanoparticles in tissues from Sprague-Dawley rats.* Particle and Fibre Toxicology, 2013. **10**.

197. Clift, M.J.D., et al., *The impact of different nanoparticle surface chemistry and size on uptake and toxicity in a murine macrophage cell line.* Toxicology and Applied Pharmacology, 2008. **232**(3): p. 418-427.

198. Zhu, Z.J., et al., *Surface Properties Dictate Uptake, Distribution, Excretion, and Toxicity of Nanoparticles in Fish.* Small, 2010. **6**(20): p. 2261-2265.

199. Vacha, R., F.J. Martinez-Veracoechea, and D. Frenkel, *Receptor-Mediated Endocytosis of Nanoparticles of Various Shapes.* Nano Letters, 2011. **11**(12): p. 5391-5395.

200. Iversen, T.-G., T. Skotland, and K. Sandvig, *Endocytosis and intracellular transport of nanoparticles: Present knowledge and need for future studies.* Nano Today, 2011. **6**(2): p. 176-185.

201. Zhang, S.L., et al., *Size-Dependent Endocytosis of Nanoparticles.* Advanced Materials, 2009. **21**(4): p. 419-+.

202. Kim, S. and I.H. Choi, *Phagocytosis and Endocytosis of Silver Nanoparticles Induce Interleukin-8 Production in Human Macrophages.* Yonsei Medical Journal, 2012. **53**(3): p. 654-657.

203. Motley, A., et al., *Clathrin-mediated endocytosis in AP-2-depleted cells.* Journal of Cell Biology, 2003. **162**(5): p. 909-918.

204. Nabi, I.R. and P.U. Le, *Caveolae/raft-dependent endocytosis.* Journal of Cell Biology, 2003. **161**(4): p. 673-677.

205. Commisso, C., et al., *Macropinocytosis of protein is an amino acid supply route in Ras-transformed cells.* Nature, 2013. **497**(7451): p. 633-+.

206. Flannagan, R.S., V. Jaumouille, and S. Grinstein, *The Cell Biology of Phagocytosis.* Annual Review of Pathology: Mechanisms of Disease, Vol 7, 2012. **7**: p. 61-98.

207. Hurley, J.H. and B. Wendland, *Endocytosis: Driving membranes around the bend.* Cell, 2002. **111**(2): p. 143-146.

208. Wang, H.Y., L.X. Wu, and B.M. Reinhard, *Scavenger Receptor Mediated Endocytosis of Silver Nanoparticles into J774A.1 Macrophages Is Heterogeneous.* ACS Nano, 2012. **6**(8): p. 7122-7132.

209. Gao, H.L., et al., *Ligand modified nanoparticles increases cell uptake, alters endocytosis and elevates glioma distribution and internalization.* Scientific Reports, 2013. **3**.

210. Caballero-Diaz, E., et al., *The Toxicity of Silver Nanoparticles Depends on Their Uptake by Cells and Thus on Their Surface Chemistry.* Particle & Particle Systems Characterization, 2013. **30**(12): p. 1079-1085.

211. Dragoni, S., et al., *Gold Nanoparticles Uptake and Cytotoxicity Assessed on Rat Liver Precision-Cut Slices.* Toxicological Sciences, 2012. **128**(1): p. 186-197.

212. Garcia-Aonso, J., et al., *Cellular Internalization of Silver Nanoparticles in Gut Epithelia of the Estuarine Polychaete Nereis diversicolor.* Environmental Science & Technology, 2011. **45**(10): p. 4630-4636.

213. Ma, X.W., et al., *Gold Nanoparticles Induce Autophagosome Accumulation through Size-Dependent Nanoparticle Uptake and Lysosome Impairment.* ACS Nano, 2011. **5**(11): p. 8629-8639.

214. AshaRani, P., M.P. Hande, and S. Valiyaveettil, *Anti-proliferative activity of silver nanoparticles.* BMC Cell Biology, 2009. **10**(1): p. 65.

215. Dziendzikowska, K., et al., *Time-dependent biodistribution and excretion of silver nanoparticles in male Wistar rats.* Journal of Applied Toxicology, 2012. **32**(11): p. 920-928.

216. Panariti, A., G. Miserocchi, and I. Rivolta, *The effect of nanoparticle uptake on cellular behavior: disrupting or enabling functions?* Nanotechnol Sci Appl, 2012. **5**: p. 87-100.

217. Frohlich, E., et al., *Action of polystyrene nanoparticles of different sizes on lysosomal function and integrity.* Particle and Fibre Toxicology, 2012. **9**.

218. Leung, M.C.K., et al., *Caenorhabditis elegans: An emerging model in biomedical and environmental toxicology.* Toxicological Sciences, 2008. **106**(1): p. 5-28.

219. Yang, X., et al., *Silver nanoparticle behavior, uptake, and toxicity in Caenorhabditis elegans: Effects of natural organic matter.* Environmental Science & Technology, 2014.

220. Boyd, W.A., et al., *A high-throughput method for assessing chemical toxicity using a Caenorhabditis elegans reproduction assay.* Toxicology and Applied Pharmacology, 2010. **245**(2): p. 153-+.

221. Dykstra, M.J., et al., *Suggested Standard Operating Procedures (SOPs) for the Preparation of Electron Microscopy Samples for Toxicology/Pathology Studies in a GLP Environment.* Toxicologic Pathology, 2002. **30**(6): p. 735-743.

222. Dykstra, M.J. and L.E. Reuss, *Biological electron microscopy: theory, techniques, and troubleshooting*. 2003: Springer.

223. Bar-Ilan, O., et al., *Toxicity assessments of multisized gold and silver nanoparticles in zebrafish embryos.* Small, 2009. **5**(16): p. 1897-910.

224. Lee, K.J., et al., *In vivo imaging of transport and biocompatibility of single silver nanoparticles in early development of zebrafish embryos.* ACS Nano, 2007. **1**(2): p. 133-43.

225. Scown, T.M., et al., *Effects of Aqueous Exposure to Silver Nanoparticles of Different Sizes in Rainbow Trout.* Toxicological Sciences, 2010. **115**(2): p. 521-534.

226. Pluskota, A., et al., *In Caenorhabditis elegans nanoparticle-bio-interactions become transparent: silica-nanoparticles induce reproductive senescence.* PLoS One, 2009. **4**(8): p. e6622.

227. Klaus, T., et al., *Silver-based crystalline nanoparticles, microbially fabricated.* Proc Natl Acad Sci U S A, 1999. **96**(24): p. 13611-4.

228. Rejman, J., A. Bragonzi, and M. Conese, *Role of clathrin- and caveolae-mediated endocytosis in gene transfer mediated by lipo- and polyplexes.* Molecular Therapy, 2005. **12**(3): p. 468-474.

229. Stern, S.T., P.P. Adiseshaiah, and R.M. Crist, *Autophagy and lysosomal dysfunction as emerging mechanisms of nanomaterial toxicity.* Particle and Fibre Toxicology, 2012. **9**.

230. Tsyusko, O.V., et al., *Toxicogenomic Responses of the Model Organism Caenorhabditis elegans to Gold Nanoparticles.* Environmental Science & Technology, 2012. **46**(7): p. 4115-4124.

231. Hersh, B.M., E. Hartwieg, and H.R. Horvitz, *The Caenorhabditis elegans mucolipin-like gene cup-5 is essential for viability and regulates lysosomes in multiple cell types.* Proceedings of the National Academy of Sciences of the United States of America, 2002. **99**(7): p. 4355-4360.

232. Sun, T., et al., *CUP-5, the C. elegans ortholog of the mammalian lysosomal channel protein MLN1/TRPML1, is required for proteolytic degradation in autolysosomes.* Autophagy, 2011. **7**(11): p. 1308-1315.

233. Campbell, E.M. and H. Fares, *Roles of CUP-5, the Caenorhabditis elegans orthologue of human TRPML1, in lysosome and gut granule biogenesis.* BMC Cell Biology, 2010. **11**.

234. McGhee, J.D., *The C. elegans intestine.* 2007.

235. Artal-Sanz, M., et al., *Lysosomal biogenesis and function is critical for necrotic cell death in Caenorhabditis elegans.* Journal of Cell Biology, 2006. **173**(2): p. 231-239.

236. Rabbitts, B.M., et al., *glo-3, a Novel Caenorhabditis elegans Gene, Is Required for Lysosome-Related Organelle Biogenesis.* Genetics, 2008. **180**(2): p. 857-871.

237. Hermann, G., C. Hieb, and J. Priess. *glo-1 is necessary for lysosome-related organelle biogenesis in C. elegans*. 2002.

238. Patton, A., et al., *Endocytosis function of a ligand-gated ion channel homolog in Caenorhabditis elegans.* Current Biology, 2005. **15**(11): p. 1045-1050.

239. Song, H.-O., et al., *Calcineurin regulates coelomocyte endocytosis via DYN-1 and CUP-4 in Caenorhabditis elegans.* Molecules and Cells, 2010. **30**(3): p. 255-262.

240. Settembre, C., et al., *Signals from the lysosome: a control centre for cellular clearance and energy metabolism.* Nature Reviews Molecular Cell Biology, 2013. **14**(5): p. 283-296.

241. Boya, P., *Lysosomal Function and Dysfunction: Mechanism and Disease.* Antioxidants & Redox Signaling, 2012. **17**(5): p. 766-774.

242. Kim, S.W., S.-H. Nam, and Y.-J. An, *Interaction of Silver Nanoparticles with Biological Surfaces of Caenorhabditis elegans.* Ecotoxicology and Environmental Safety, 2012. **77**(0): p. 64-70.

243. Tahseen, Q., *Coelomocytes: Biology and Possible Immune Functions in Invertebrates with Special Remarks on Nematodes.* International Journal of Zoology, 2009. **2009**.

244. Fares, H. and I. Greenwald, *Genetic analysis of endocytosis in Caenorhabditis elegans: Coelomocyte uptake defective mutants.* Genetics, 2001. **159**(1): p. 133-145.

245. Poteryaev, D., et al., *Caenorhabditis elegans SAND-1 is essential for RAB-7 function in endosomal traffic.* Embo Journal, 2007. **26**(2): p. 301-312.

246. Cumberland, S.A. and J.R. Lead, *Particle size distributions of silver nanoparticles at environmentally relevant conditions.* Journal of Chromatography A, 2009. **1216**(52): p. 9099-9105.

247. Kashiwada, S., *Distribution of nanoparticles in the see-through medaka (Oryzias latipes).* Environmental Health Perspectives, 2006. **114**(11): p. 1697-1702.

248. Lowry, G.V., et al., *Environmental Occurrences, Behavior, Fate, and Ecological Effects of Nanomaterials: An Introduction to the Special Series.* Journal of Environmental Quality, 2010. **39**(6): p. 1867-1874.

249. Lin, D.H., et al., *Fate and Transport of Engineered Nanomaterials in the Environment.* Journal of Environmental Quality, 2010. **39**(6): p. 1896-1908.

250. Lowry, G.V., et al., *Environmental Occurrences, Behavior, Fate, and Ecological Effects of Nanomaterials: An Introduction to the Special Series.* J. Environ. Qual., 2010. **39**(6): p. 1867-1874.

251. Aiken, G.R., H. Hsu-Kim, and J.N. Ryan, *Influence of Dissolved Organic Matter on the Environmental Fate of Metals, Nanoparticles, and Colloids.* Environmental Science & Technology, 2011. **45**(8): p. 3196-3201.

252. Chen, K.L. and M. Elimelech, *Influence of humic acid on the aggregation kinetics of fullerene (C-60) nanoparticles in monovalent and divalent electrolyte solutions.* Journal of Colloid and Interface Science, 2007. **309**(1): p. 126-134.

253. Chen, K.L., S.E. Mylon, and M. Elimelech, *Enhanced aggregation of alginate-coated iron oxide (hematite) nanoparticles in the presence of calcium, strontium, and barium cations.* Langmuir, 2007. **23**(11): p. 5920-5928.

254. Lowry, G.V., et al., *Adsorbed Polymer and NOM Limits Adhesion and Toxicity of Nano Scale Zerovalent Iron to E. coli.* Environmental Science & Technology, 2010. **44**(9): p. 3462-3467.

255. Deonarine, A., et al., *Effects of Humic Substances on Precipitation and Aggregation of Zinc Sulfide Nanoparticles.* Environmental Science & Technology, 2011. **45**(8): p. 3217-3223.

256. King, S.M. and H.P. Jarvie, *Exploring How Organic Matter Controls Structural Transformations in Natural Aquatic Nanocolloidal Dispersions.* Environmental Science & Technology, 2012. **46**(13): p. 6959-6967.

257. Nason, J.A., S.A. McDowell, and T.W. Callahan, *Effects of natural organic matter type and concentration on the aggregation of citrate-stabilized gold nanoparticles.* Journal of Environmental Monitoring, 2012. **14**(7): p. 1885-1892.

258. Bae, S., et al., *Effects of water chemistry on aggregation and soil adsorption of silver nanoparticles.* Environ Health Toxicol, 2013. **28**: p. e2013006.

259. Lankveld, D.P., et al., *The kinetics of the tissue distribution of silver nanoparticles of different sizes.* Biomaterials, 2010. **31**(32): p. 8350-61.

260. Zhang, S., et al., *Size-Dependent Endocytosis of Nanoparticles.* Advanced Materials, 2009. **21**(4): p. 419-424.

261. Phenrat, T., et al., *Estimating Attachment of Nano- and Submicrometer-particles Coated with Organic Macromolecules in Porous Media: Development of an Empirical Model.* Environmental Science & Technology, 2010. **44**(12): p. 4531-4538.

262. Delay, M., et al., *Interactions and stability of silver nanoparticles in the aqueous phase: Influence of natural organic matter (NOM) and ionic strength.* Journal of Chromatography A, 2011. **1218**(27): p. 4206-4212.

263. Illes, E. and E. Tombacz, *The effect of humic acid adsorption on pH-dependent surface charging and aggregation of magnetite nanoparticles.* Journal of Colloid and Interface Science, 2006. **295**(1): p. 115-123.

264. Stankus, D.P., et al., *Interactions between Natural Organic Matter and Gold Nanoparticles Stabilized with Different Organic Capping Agents.* Environmental Science & Technology, 2010. **45**(8): p. 3238-3244.

265. Baalousha, M., *Aggregation and disaggregation of iron oxide nanoparticles: Influence of particle concentration, pH and natural organic matter.* Science of The Total Environment, 2009. **407**(6): p. 2093-2101.

266. Quik, J.T.K., et al., *Effect of natural organic matter on cerium dioxide nanoparticles settling in model fresh water.* Chemosphere, 2010. **81**(6): p. 711-715.

267. Millour, M., E. Pelletier, and J.P. Gagné, *Interactions Between Silver Nanoparticles and Dissolved Natural Organic Matter Under Estuarine Conditions*, in *Functions of Natural Organic Matter in Changing Environment*, J. Xu, J. Wu, and Y. He, Editors. 2013, Springer Netherlands. p. 805-809.

268. Cabaniss, S.E., *Forward Modeling of Metal Complexation by NOM: II. Prediction of Binding Site Properties.* Environmental Science & Technology, 2010. **45**(8): p. 3202-3209.

269. Quigg, A., et al., *Direct and Indirect Toxic Effects of Engineered Nanoparticles on Algae: Role of Natural Organic Matter.* Acs Sustainable Chemistry & Engineering, 2013. **1**(7): p. 686-702.

270. Jiang, J.K., G. Oberdorster, and P. Biswas, *Characterization of size, surface charge, and agglomeration state of nanoparticle dispersions for toxicological studies.* Journal of Nanoparticle Research, 2009. **11**(1): p. 77-89.

271. Wirth, S.M., G.V. Lowry, and R.D. Tilton, *Natural Organic Matter Alters Biofilm Tolerance to Silver Nanoparticles and Dissolved Silver.* Environmental Science & Technology, 2012. **46**(22): p. 12687-12696.

272. Lee, S., et al., *Biotoxicity of nanoparticles: effect of natural organic matter.* Journal of Nanoparticle Research, 2011. **13**(7): p. 3051-3061.

273. Collin, B., et al., *Influence of natural organic matter and surface charge on the toxicity and bioaccumulation of functionalized ceria nanoparticles in Caenorhabditis elegans.* Environmental Science & Technology, 2013.

274. Mashayekhi, H., et al., *Effect of natural organic matter on aggregation behavior of C60 fullerene in water.* J Colloid Interface Sci, 2012. **374**(1): p. 111-7.

275. Gao, J., et al., *Influence of Suwannee River humic acid on particle properties and toxicity of silver nanoparticles.* Chemosphere, 2012. **89**(1): p. 96-101.

276. Kittler, S., et al., *Toxicity of Silver Nanoparticles Increases during Storage Because of Slow Dissolution under Release of Silver Ions.* Chemistry of Materials, 2010. **22**(16): p. 4548-4554.

277. I. Herrera, J.L.G.-T., K.J. Tiemann, J.R. Peralta-Videa, V. Armendariz, and J.G. and Parsons, *Binding Of Silver(i) Ions Byalfalfabiomass (medicago Sativa): Batch Ph, Time, Temperature, And Ionic Strength Studies* Journal of Hazardous Substance Research, 2003. **4**: p. 1-16.

278. Khan, M.A.Q., et al., *Effect of temperature on heavy metal toxicity to earthworm Lumbricus terrestris (Annelida: Oligochaeta).* Environmental Toxicology, 2007. **22**(5): p. 487-494.

279. Khan, M.A.Q., et al., *Effect of temperature on heavy metal toxicity to juvenile crayfish, Orconectes immunis (Hagen).* Environmental Toxicology, 2006. **21**(5): p. 513-520.

280. Vedamanikam, V. and N. Shazilli, *Comparative Toxicity of Nine Metals to Two Malaysian Aquatic Dipterian Larvae with Reference to Temperature Variation.* Bulletin of Environmental Contamination and Toxicology, 2008. **80**(6): p. 516-520.

281. Chapman, P.M., et al., *Global geographic differences in marine metals toxicity.* Marine Pollution Bulletin, 2006. **52**(9): p. 1081-1084.

282. Chen, C.-J. and R.-K. Chiang, *Sulfidation of rock-salt-type transition metal oxide nanoparticles as an example of a solid state reaction in colloidal nanoparticles.* Dalton Transactions, 2011. **40**(4): p. 880-885.

283. Cheng, G. and A. Hight Walker, *Transmission electron microscopy characterization of colloidal copper nanoparticles and their chemical reactivity.* Analytical and Bioanalytical Chemistry, 2010. **396**(3): p. 1057-1069.

284. Levard, C.m., et al., *Sulfidation Processes of PVP-Coated Silver Nanoparticles in Aqueous Solution: Impact on Dissolution Rate.* Environmental Science & Technology, 2011. **45**(12): p. 5260-5266.

285. Kim, B., et al., *Discovery and Characterization of Silver Sulfide Nanoparticles in Final Sewage Sludge Products.* Environmental Science & Technology, 2010. **44**(19): p. 7509-7514.

286. Gorham, J.M., et al., *UV-induced photochemical transformations of citrate-capped silver nanoparticle suspensions.* Journal of Nanoparticle Research, 2012. **14**(10).

287. Eom, H.-J., et al., *Hypoxia inducible factor-1 (HIF-1)–flavin containing monooxygenase-2 (FMO-2) signaling acts in silver nanoparticles and silver ion toxicity in the nematode, Caenorhabditis elegans.* Toxicology and Applied Pharmacology, 2013. **270**(2): p. 106-113.

288. Badireddy, A.R., M.R. Wiesner, and J. Liu, *Detection, Characterization, and Abundance of Engineered Nanoparticles in Complex Waters by Hyperspectral Imagery with Enhanced Darkfield Microscopy.* Environmental Science & Technology, 2012. **46**(18): p. 10081-10088.

289. Sikora, F.J. and F.J. Stevenson, *Silver Complexation by Humic Substances - Conditional Stability-Constants and Nature of Reactive Sites.* Geoderma, 1988. **42**(3-4): p. 353-363.

290. Chen, Z.Z., P.G.C. Campbell, and C. Fortin, *Silver Binding by Humic Acid as Determined by Equilibrium Ion-Exchange and Dialysis.* Journal of Physical Chemistry A, 2012. **116**(25): p. 6532-6539.

291. Haitzer, M., G.R. Aiken, and J.N. Ryan, *Binding of mercury(II) to dissolved organic matter: The role of the mercury-to-DOM concentration ratio.* Environmental Science & Technology, 2002. **36**(16): p. 3564-3570.

292. Sikora, F.J. and F.J. Stevenson, *Silver complexation by humic substances - Conditional stability constants and nature of reactive sites.* Geoderma, 1988. **42**(3-4): p. 353-363.

293. Manceau, A. and K.L. Nagy, *Quantitative analysis of sulfur functional groups in natural organic matter by XANES spectroscopy.* Geochimica et Cosmochimica Acta, 2012. **99**: p. 206-223.

294. *http://www.humicsubstances.org/elements.html*.

295. Stumm, W. and J.J. Morgan, *Aquatic chemistry: chemical equilibria and rates in natural waters*. 3 ed. 1996, New York: John Wiley & Sons, Inc.

296. Colman, B.P., et al., *Low Concentrations of Silver Nanoparticles in Biosolids Cause Adverse Ecosystem Responses under Realistic Field Scenario.* Plos One, 2013. **8**(2).

297. Allen, H.J., et al., *Effects from filtration, capping agents, and presence/absence of food on the toxicity of silver nanoparticles to Daphnia magna.* Environmental Toxicology and Chemistry, 2010. **29**(12): p. 2742-2750.

298. Jackson, B.P., et al., *Bioavailability, Toxicity, and Bioaccumulation of Quantum Dot Nanoparticles to the Amphipod Leptocheirus plumulosus.* Environmental Science & Technology, 2012. **46**(10): p. 5550-5556.

299. *International Humic Substances Society Website*. Available from: http://www.ihss.gatech.edu/.

300. Brown, A., et al., *Chemical characterization of dissolved organic material in Pony Lake, a saline coastal pond in Antarctica.* Marine Chemistry, 2004. **89**(1–4): p. 327-337.

301. Chin, Y.P., G. Aiken, and E. Oloughlin, *Molecular-Weight, Polydispersity, and Spectroscopic Properties of Aquatic Humic Substances.* Environmental Science & Technology, 1994. **28**(11): p. 1853-1858.

302. Yoon, T.H., S.B. Johnson, and G.E. Brown, *Adsorption of Organic Matter at Mineral/Water Interfaces. IV. Adsorption of Humic Substances at Boehmite/Water Interfaces and Impact on Boehmite Dissolution.* Langmuir, 2005. **21**(11): p. 5002-5012.

303. Lowry, G.V., et al., *Transformations of Nanomaterials in the Environment.* Environmental Science & Technology, 2012. **46**(13): p. 6893-6899.

304. Baalousha, M., et al., *Aggregation and surface properties of iron oxide nanoparticles: Influence of ph and natural organic matter.* Environmental Toxicology and Chemistry, 2008. **27**(9): p. 1875-1882.

305. Haase, A., et al., *Toxicity of silver nanoparticles in human macrophages: uptake, intracellular distribution and cellular responses.* Journal of Physics: Conference Series, 2011. **304**(1): p. 012030.

306. Kramer, J.M., *Basement membranes.* Worm Book, 2005.

307. Yokota, S., et al., *Peroxisomes of the nematode Caenorhabditis elegans: distribution and morphological characteristics.* Histochemistry and Cell Biology, 2002. **118**(4): p. 329-336.

308. Irazoqui, J.E., et al., *Distinct Pathogenesis and Host Responses during Infection of C. elegans by P. aeruginosa and S. aureus.* Plos Pathogens, 2010. **6**(7).

309. Mpoke, S.S. and J. Wolfe, *Differential staining of apoptotic nuclei in living cells: Application to macronuclear elimination in Tetrahymena.* Journal of Histochemistry & Cytochemistry, 1997. **45**(5): p. 675-683.

310. Ito, Y., et al., *Method of specific detection of apoptosis using formamide-induced DNA denaturation assay.* Journal of Histochemistry & Cytochemistry, 2006. **54**(6): p. 683-692.

311. Benedict, C., et al., *Gut protein uptake and mechanisms of meal-induced cortisol release.* Journal of Clinical Endocrinology & Metabolism, 2005. **90**(3): p. 1692-1696.

312. Kujala, P., et al., *Prion Uptake in the Gut: Identification of the First Uptake and Replication Sites.* Plos Pathogens, 2011. **7**(12).

313. Schroder, B.A., et al., *The proteome of lysosomes.* Proteomics, 2010. **10**(22): p. 4053-4076.

314. Zhang, H.Z., B. Chen, and J.F. Banfield, *Particle Size and pH Effects on Nanoparticle Dissolution.* Journal of Physical Chemistry C, 2010. **114**(35): p. 14876-14884.

315. Cho, W.S., et al., *Progressive severe lung injury by zinc oxide nanoparticles; the role of Zn2+ dissolution inside lysosomes.* Particle and Fibre Toxicology, 2011. **8**.

316. Gilbert, B., et al., *The Fate of ZnO Nanoparticles Administered to Human Bronchial Epithelial Cells.* ACS Nano, 2012. **6**(6): p. 4921-4930.

317. Vatamaniuk, O.K., et al., *CeHMT-1, a putative phytochelatin transporter, is required for cadmium tolerance in Caenorhabditis elegans.* Journal of Biological Chemistry, 2005. **280**(25): p. 23684-23690.

318. Arulvasu, C., et al., *Toxicity Effect of Silver Nanoparticles in Brine Shrimp Artemia.* Scientific World Journal, 2014.

319. Ribeiro, F., et al., *Silver nanoparticles and silver nitrate induce high toxicity to Pseudokirchneriella subcapitata, Daphnia magna and Danio rerio.* Sci Total Environ, 2014. **466-467**: p. 232-41.

320. Yang, Y., et al., *Impacts of silver nanoparticles on cellular and transcriptional activity of nitrogen-cycling bacteria.* Environmental Toxicology and Chemistry, 2013. **32**(7): p. 1488-1494.

321. Foldbjerg R, A.H., *Mechanisms of Silver Nanoparticle Toxicity.* Archives of basic & applied medicine, 2013. **1**: p. 5-15.

322. Mariane Matzke, K.J., Thomas Backhaus, *Toxicity of differently sized and coated silver nanoparticles to the bacterium Pseudomonas putida: risks for the aquatic environment?* PeerJ 2014.

323. Christopher Batchelor-McAuley, K.T., Christopher C. M. Neumann, Eduardo Laborda, Richard G, Compton, *Why are Silver Nanoparticles More Toxic Than Bulk Silver? Towards Understanding the Dissolution and Toxicity of Silver Nanoparticles.* International Journal of Electrochemical Science, 2014. **9**: p. 1132-1138.

324. Manke, A., L.Y. Wang, and Y. Rojanasakul, *Mechanisms of Nanoparticle-Induced Oxidative Stress and Toxicity.* Biomed Research International, 2013.

325. Zhang Linlin, K.T., *Dissolution of silver nanoparticles in presence of natural organic matter.* Advanced Materials Letters, 2014. **5**(1): p. 6-8.

326. Stevenson, L.M., et al., *Environmental Feedbacks and Engineered Nanoparticles: Mitigation of Silver Nanoparticle Toxicity to Chlamydomonas reinhardtii by Algal-Produced Organic Compounds.* Plos One, 2013. **8**(9).

327. Liu, W.E., et al., *Real-time in vivo detection of biomaterial-induced reactive oxygen species.* Biomaterials, 2011. **32**(7): p. 1796-1801.

328. Singh, R.P. and P. Ramarao, *Cellular uptake, intracellular trafficking and cytotoxicity of silver nanoparticles.* Toxicology Letters, 2012. **213**(2): p. 249-259.

329. Ekkapongpisit, M., et al., *Biocompatibility, endocytosis, and intracellular trafficking of mesoporous silica and polystyrene nanoparticles in ovarian cancer cells: effects of size and surface charge groups.* International Journal of Nanomedicine, 2012. **7**: p. 4147-4158.

330. Huang, F.R., et al., *Quantitative nanoparticle tracking: applications to nanomedicine.* Nanomedicine, 2011. **6**(4): p. 693-700.

331. Monteiro-Riviere, N.A., et al., *Protein binding modulates the cellular uptake of silver nanoparticles into human cells: Implications for in vitro to in vivo extrapolations?* Toxicology Letters, 2013. **220**(3): p. 286-293.

332. Soto-Alvaredo, J., M. Montes-Bayon, and J. Bettmer, *Speciation of Silver Nanoparticles and Silver(I) by Reversed-Phase Liquid Chromatography Coupled to ICPMS.* Analytical Chemistry, 2013. **85**(3): p. 1316-1321.

333. Chao, J.B., et al., *Speciation Analysis of Silver Nanoparticles and Silver Ions in Antibacterial Products and Environmental Waters via Cloud Point Extraction-Based Separation.* Analytical Chemistry, 2011. **83**(17): p. 6875-6882.

334. Benoit, R., K.J. Wilkinson, and S. Sauve, *Partitioning of silver and chemical speciation of free Ag in soils amended with nanoparticles.* Chemistry Central Journal, 2013. **7**.

335. Bone, A.J., et al., *Biotic and Abiotic Interactions in Aquatic Microcosms Determine Fate and Toxicity of Ag Nanoparticles: Part 2-Toxicity and Ag Speciation.* Environmental Science & Technology, 2012. **46**(13): p. 6925-6933.

336. Bovenkamp, G.L., et al., *X-Ray Absorption Near-Edge Structure (XANES) Spectroscopy Study of the Interaction of Silver Ions with Staphylococcus aureus, Listeria monocytogenes, and Escherichia coli.* Applied and Environmental Microbiology, 2013. **79**(20): p. 6385-6390.

337. Yang, W. and S. Hekimi, *A Mitochondrial Superoxide Signal Triggers Increased Longevity in Caenorhabditis elegans.* Plos Biology, 2010. **8**(12).

338. Gruber, J., et al., *Mitochondrial Changes in Ageing Caenorhabditis elegans - What Do We Learn from Superoxide Dismutase Knockouts?* Plos One, 2011. **6**(5).

339. Mukhopadhyay, P., et al., *Simultaneous detection of apoptosis and mitochondrial superoxide production in live cells by flow cytometry and confocal microscopy.* Nature Protocols, 2007. **2**(9): p. 2295-2301.

340. Kirkland, R.A., G.M. Saavedra, and J.L. Franklin, *Rapid activation of antioxidant defenses by nerve growth factor suppresses reactive oxygen species during neuronal apoptosis: Evidence for a role in cytochrome c redistribution.* Journal of Neuroscience, 2007. **27**(42): p. 11315-11326.

341. Wang, X.H., et al., *Imaging ROS signaling in cells and animals.* Journal of Molecular Medicine-Jmm, 2013. **91**(8): p. 917-927.

342. Meyer, J.N., *QPCR: a tool for analysis of mitochondrial and nuclear DNA damage in ecotoxicology.* Ecotoxicology, 2010. **19**(4): p. 804-811.

343. Hunter, S.E., et al., *The QPCR assay for analysis of mitochondrial DNA damage, repair, and relative copy number.* Methods, 2010. **51**(4): p. 444-451.

344. Bess, A.S., et al., *Mitochondrial dynamics and autophagy aid in removal of persistent mitochondrial DNA damage in Caenorhabditis elegans.* Nucleic Acids Research, 2012. **40**(16): p. 7916-7931.

345. Jeong-Min Ahn, H.-J.E., Xinyu Yang, Joel N. Meyer, Jinhee Choi, *Comparative toxicity of silver nanoparticles on oxidative stress and DNA damage in the nematode, Caenorhabditis elegans.* Chemosphere, 2014.

346. Balch, W.E., et al., *Adapting proteostasis for disease intervention.* Science, 2008. **319**(5865): p. 916-919.

347. Taylor, R.C. and A. Dillin, *XBP-1 Is a Cell-Nonautonomous Regulator of Stress Resistance and Longevity.* Cell, 2013. **153**(7): p. 1435-1447.

348. Shen, X.H., et al., *Complementary signaling pathways regulate the unfolded protein response and are required for C-elegans development.* Cell, 2001. **107**(7): p. 893-903.

349. Richardson, C.E., S. Kinkel, and D.H. Kim, *Physiological IRE-1-XBP-1 and PEK-1 Signaling in <italic>Caenorhabditis elegans</italic> Larval Development and Immunity.* PLoS Genet, 2011. **7**(11): p. e1002391.

350. Richardson, C.E., T. Kooistra, and D.H. Kim, *An essential role for XBP-1 in host protection against immune activation in C. elegans.* Nature, 2010. **463**(7284): p. 1092-1095.

351. Bischof, L.J., et al., *Activation of the Unfolded Protein Response Is Required for Defenses against Bacterial Pore-Forming Toxin In Vivo.* Plos Pathogens, 2008. **4**(10).

Biography

Xinyu (Candy) Yang was born in Yongzhou, Hunan Province, China on October 21st, 1986 to Gaoxiong Yang and Daoluan He. She received her Bachelor of Engineering degree in Environmental Engineering from Shanghai Jiaotong University in July 2007, and then got her Master of Science degree in Zoology with Jim Oris from Miami University of Ohi in July 2009.

Publications:

Xinyu Yang, Andreas Gondikas, Stella M. Marinakos, Melanie Auffan, Jie Liu, Heileen Hsu-Kim, Joel N. Meyer. The mechanism of silver nanoparticle toxicity is dependent on dissolved silver and surface coating in Caenorhabditis elegans, Environmental Science and Technology, 2011. 46(2): p. 1119-1127

Meyer, J.N., Lord, C.A., **Yang, X.Y**., Turner, E.A., Badireddy, A.R., Marinakos, S.M., Chilkoti, A., Wiesner, M.R., Auffan, M. 2010. Intracellular uptake and associated toxicity of silver nanoparticles in *Caenorhabditis elegans*, Aquatic Toxicology 100: 140-150.

X. Y. Yang., R. E. Edelmann., J. T. Oris. Suspended C60 nanoparticles protect against short-term UV and fluoranthene photo-induced toxicity, but cause long-term cellular damage in *Daphnia magna*. Aquatic Toxicology. 2010. 100: 202-210.

Xinyu Yang, Chuangjia Jiang, Heileen Hsu-Kim, Appala Raju Badireddy, Michael Dyksra, Mark Wiesner, David E. Hinton, Joel N. Meyer. Silver Nanoparticle behavior, uptake, and toxicity in *Caenorhabditis elegans*: Effects of natural organic matter. Environmental Science and Technology 2014. In press.

Jeong-Min Ahn, Hynn-Jeong Eom, **Xinyu Yang**, Joel N. Meyer, Jinhee Choi. Comparative toxicity of silver nanoparticles on Oxidative stress and DNA damage in the nematode, *Caenorhabditis elegans*. Chemosphere 2014, In press.

Jinhee Choi, Olga V. Tsyusko, Jason M. Unrine, Nivedita Chatterjee, Jeone-Min Ahn, **Xinyu Yang**, Brittany L. M. Thornton, Ian T. Ryde, Daniel Starnes, Joel N. Meyer. A micro-sized model for the in vivo studies of nanoparticle toxicity: what has *Caenorhabditis elegans* taught us? Environmental chemistry. Submitted.

Clement Levard, Ernest M. Hotze, Benjamin P. Colman, Amy L. Dale, Lisa Truong, **X. Y. Yang,** Audrey J. Bone, Gordon E. Brown, Jr., Robert L. Tanguay, Richard T. Di Giulio, Emily S. Bernhardt, Joel N. Meyer, Mark R. Wiesner, and Gregory V. Lowry. Sulfidation of Silver Nanoparticles: Natural Antidote to Their Toxicity. Environmental Science and Technology, 2013. 47 (23), 13440-13448.

Levard, C., **Yang, X**., Meyer, J. N., Lowry, G. V. Response to Comment on Levard et al., Environmental Science and Technology, 2013.

Xinyu Yang, Adam Schindler, Ross Taggart, Heileen Hsu-Kim, Daivd R. Sherwood, David E. Hinton, Joel N. Meyer. *In vivo* study of the role of endocytosis and lysosome function in silver nanoparticle uptake and toxicity in *Caenorhabditis elegans*. In preparation.

Audrey J. Bone, Cole W. Matson, Benjamin P. Colman, **Xinyu Yang**, Joel N. Meyer, Richard T. Di Giulio. Silver nanoparticle toxicity to early life stage Atlantic killifish

(Fundulus heteroclitus) in complex environmental media: A comparison of laboratory, mesocosm and microcosm studies. In preparation.

Honors and Awards:

2008 - Miami Summer 2008 Fellowship

2012 NCSOT Best Poster Presentation Award

2012 SETAC Student Travel Award

2013 Duke Nicholas School and Graduate School Travel Award